INTERNATIONAL JOURNAL OF
IJCOE
COASTAL, OFFSHORE AND ENVIRONMENTAL ENGINEERING

International Journal of Coastal, Offshore and Environmental Engineering (IJCOE)
Vol. 9 / Issue. 2 / May 2024

International Journal of Coastal, Offshore & Environmental Engineering
Since 2015
ISSN: 2980-8731 (online)

Volume 9 | Issue 2 |May 2024

IJCOE
Editor-in-Chief: Prof. Hamid S. Bahai

www.ijcoe.org

International Journal of Coastal, Offshore & Environmental Engineering
Since 2015
ISSN: 2980-8721 (online)

In The Name of God

Message from the Editor-in-Chief

The IJCOE journal office was established in 2015,and its first issue was published in 2016. TheIJCOE covers a wide range of research in thefields of oceanography & ocean technology, aswell as marine industries & marine engineering.The editorial board of IJCOE consists of nearly130 of the greatest scientists and researchersfrom over 30 countries worldwide, and thejournal's review board comprises 1,000 membersfrom all five continents. The membership andapplication process for joining the editorial andreview boards of this journal is ongoing. IJCOE isa research-academic quarterly journal that haspublication and distribution permissions fromthe Press Organization and permission topublish scientific-research articles from theMinistry of Science, Research, and Technology(MSRT) with an "A" rating. It also holds a "Q1"rating from the ISC institute with an impactfactor (IF) of approximately 0.43 and isconsidered a "core journal" (prestigious andoutstanding journal). IJCOE is an open-accessjournal and allows the download and receipt ofaccepted articles in full text for free. It respectsand adheres to copyright and COPE regulations.The journal's office operates 24/7, providingservices to researchers. In addition to publishinga regular quarterly journal, IJCOE has 16 specialissues on specific topics in preparation. It alsoprovides conditions for publishing specializedbooks, references, and handbooks. Moreover, itis ready to cooperate with the secretariats ofreputable international conferences to publishtheir selected and outstanding articles. IJCOEevaluates, appraises, and publishes books,articles, and the scientific achievements andfindings of esteemed researchers and scientistsworldwide who are innovating and conductingin-depth research in the "important and strategicfield of the maritime technology & Oceanengineering." It welcomes any form of jointcooperation with universities, research institutes,and related research centers at the national,regional, and international levels, and extends ahand for collaboration.

Classification of Editorial Board in IJCOE

Editor-in-Chief

Director-in-Chief

Deputy Editor

Executive Managers

English Text Editor

Technical Editor

International Editorial Board

National Editorial Board

Editorial Board Associate

Editorial Board Assistant

Guest Editorial Board

Advisory Board

Administrative Coordinator

Honorary Board Member

Methodology Advisor

Author Benefits

- Open Access
- Rapid Publication
- Thorough Peer-Review
- No Copyright Constraints
- Coverage by Leading Indexing Services
- Discounts On Article Processing Charges (APC)
- No Space Constraints, No restriction on the maximum length of the papers, number of figures or colors

INTERNATIONAL JOURNAL OF IJCOE COASTAL, OFFSHORE & ENVIRONMENTAL ENGINEERING

Aims of IJCOE

Hydrodynamics

Marine equipment

Structural mechanics

Ocean environmental predictions

Stochastic calculations Experimental

Automatic Control of Marine Systems

Scope of IJCOE

Marine Hazards

Ocean Acoustics

Naval Architecture

Ocean Engineering

Coastal Engineering

Marine Meteorology

Marine Earth Sciences

Underwater Technology

Marine Renewable Energy

Polar & Arctic Engineering

Marine Renewable Energy

Marine Geography & Geodesy

Marine Environmental Engineering

Automatic Control of Marine Systems

Hydro Physics & Physical Oceanography

Type of papers

- Case Studies
- Book Reviews
- Review Article
- Letters to the Editor
- Methodology Papers
- Editorials and Commentaries
- Response or Rejoinder Papers
- Perspective or Opinion Papers
- Conceptual or Theoretical Papers
- Meta-Analysis and Systematic Reviews
- Short Communications or Brief Reports
- Research Articles (Original Research Papers)

Scientific Research Journal

Ministry of Science, Research And Technology (MSRT)

Jurnal Ranking 2023: A

Ministry Of Science, Research And Technology (ISC)

Citation Impact 2022: 0.429

Quartile 2022 : Q1

Core Collection

IJCOE is a Member of

Cantact Us

Office 1 | Research Institute of Meteorology and Atmospheric Science

Address | Tehran, Shahid Kharrazi Highway, Pajoohesh Blvd, Research Institute of Meteorology and Atmospheric Science, Sand and Dust Storm International Research Center (SDS-IRC), No. 13, 1st floor.

Phone | +982144787652

Postal code | 13611-14977

website | www.rimac.ac.ir

Office 2 | Iranian National Institute for Oceanography and Atmospheric Science

Address | Tehran, Dr. Fatemi Gharbi St., Shahid Etemadzade St., No. 3, third floor.

Phone | +982166944873

Postal code | 13389 – 14118

website | www.inio.ac.ir

Email | Info@ijcoe.org

Website | www.ijcoe.org

Follow Us

www.ijcoe.org

INTERNATIONAL JOURNAL OF IJCOE COASTAL, OFFSHORE & ENVIRONMENTAL ENGINEERING

Volume & Issue:

Volume 9, Issue 2, May 2024

Number of Articles: 6

Content

Mehdi Nezhadnaderi, Kiyanoosh Guilaninezhad, Mohammad Hossein Vafaee, Babak Pordel Maragheh, Babak Fazli Malidareh, Ali Sheykhbahaei, Abolfazl Bagheri and Seyed Mohammad Mousavi

INTERNATIONAL JOURNAL OF
COASTAL, OFFSHORE & ENVIRONMENTAL ENGINEERING IJCOE Vol.9/No.2/Spring 2024 (1-18)

Available online at: www. Ijcoe.org

Zoning and Mapping Recreational Activities in Coastal Marine Protected Areas (Case Study: Mangrove Forests of Hara PA)

Parvaneh Sobhani[1], Afshin Danehkar [2*]

[1] *Department of Environmental Science, Natural Resources Faculty, University of Tehran, Karaj, Iran. sobhani.parvaneh@guest.ut.ac.ir.ORCID: https://orcid.org/0000-0001-9878-3768*
[2*] *Department of Environmental Science, Natural Resources Faculty, University of Tehran, Karaj, Iran. danehkar@ut.ac.ir. ORCID: https://orcid.org/0000-0003-0641-9286*

ARTICLE INFO

Article History:
Received: 1 Mar. 2024
Accepted: 15 May 2024

Keywords:
Recreational Activities
Zoning
prioritization,
Mangrove Forests,
Hara PA

ABSTRACT

Selecting appropriate activities and their distribution in natural areas is one of the most important issues in tourism management and planning in natural ecosystems. Accordingly, in the present study, while identifying suitable areas for recreational activities development that are demanded and can be developed in the mangrove forests of Hara Protected Area (PA), these activities were prioritized according to the capabilities of the natural areas and the effective criteria for their development. The criteria were selected based on previous documents and studies, as well as experts' viewpoints. These criteria were standardized in the numerical range of 0 to 1 in a linear path and then weighted using the ANP model. Then, for each criterion, a spatial map was prepared in Arc GIS software, and the Topsis method was used in Topsis Solver software to prioritize recreational activities. As the results revealed, the zoning of recreational activities in this area includes 4 options of how to combine the recreational activities demanded in the mangrove forests of Hara PA. Based on the ranking of activities, the highest priority is related to option 2, and the next priorities include options 3, 1, and 4, respectively. In general, measuring the proportionality of recreational activities in tourism destinations, especially in PAs that have legal prohibitions and potential biological and protective restrictions for human activities development, is essential and can lead to proper planning and management. Considering that the mangrove forests of Hara PA are among the valuable protected reserves of the southern coasts of the country, prioritizing recreational activities in suitable areas and outside the protection zones of the region can help to sustainably use the capacity of natural resources and the appropriate distribution of recreational activities in the area while protecting these natural habitats.

1. Introduction

Recreational and nature tourism activities are one of the tourism sectors that has grown significantly in recent years due to the expansion of environmental requirements in all human activities, so it accounts for 30-40% of the global tourism volume [15, 31]. Recreational activities can be an important economic activity, but in case of improper development and not properly managed, they can also lead to harmful impacts on the environment and economy of natural ecosystems [21, 40]. Therefore, according to the increasing importance of nature tourism in the world, it is necessary to provide fields for the development of recreational activities that are appropriate to the nature

of each activity, along with the ecological and socio-economic requirements of the region.

Nature tourism oversees sustainable recreational activities in connection with environmental considerations in natural environments and Protected Areas (PAs), which can help control the negative impacts of tourists on these valuable biological reserves [38]. In this regard, one of the most important topics discussed in the management and planning of tourism in natural areas is how to choose recreational activities that can be developed and demanded by tourists in these areas [32]. Experts in the field of nature tourism believe that any development in the nature tourism industry can only be achieved through proper management and planning of destination recreational activities, as well as people's cooperation in the field of sustainable nature tourism protection and development in these susceptible areas [37]. Therefore, the zones and areas that can develop nature tourism are selected [27]. In the following, recreational activities that are suitable and can be established in the selected areas are placed and designed, and finally, a sustainable management program is presented considering training, participation and monitoring of recreational activities [8]. In general, the zoning and prioritization of selected recreational activities that are appropriate to nature is one of the most important goals of management and planning for the development of sustainable nature tourism in natural ecosystems and pristine PAs.

The increasing demand for the development of recreational activities requires management measures to adapt these activities to nature and protect biodiversity while reducing the negative impacts of tourism on natural areas [4, 34]. Considering the importance of this issue in preserving and exploiting natural areas, some studies conducted in this direction were investigated. Franceschinis et al. (2022), studied the factors that determine the choice of recreational activities in PAs. The findings showed that each recreational activity has different impacts and capabilities on natural heritage to generate income, protect nature, and increase the quality of local communities' life, so the selection of activities should be made according to the location characteristics of the park. DaRugna et al. (2022), studied the heterogeneity of recreational activities in a park and protected area. Their results showed that the lack of coordination of recreational activities in PAs can have significant negative consequences for natural areas. Xi & Ma (2021), assessed tourism resources and countermeasures based on network connections and the TOPSIS model. The results demonstrate that the relative importance of proportionality measurement of tourism resources and its evaluation is very important, and evaluation and countermeasures of these resources based on network communication and TOPSIS model can be effective. In another study, Mahmoudi et al. (2018) planned the development of nature tourism in the "Anshan" tourist area in Khuzestan province. The obtained results showed that this area has a moderate capacity for recreational planning and placement of recreational activities in nature and rural tourism.

According to the studies, most of the studies have focused on the evaluation of the ecological potential and the location of recreational areas in natural ecosystems, and less attention has been paid to the zoning and prioritization of recreational activities in accordance with natural areas, especially in PAs and coastal ecosystems that have sensitivity and highly fragile against environmental changes. Accordingly, in the present study, recreational activities were zoned and prioritized in Hara PA with the aim of sustainable nature development tourism in this area.

Mangrove forests of Hara PA, as a land-sea ecosystem on the coasts of the country, have many attractions and landscapes for the development of nature tourism. Since this area is known as one of the areas under the protection of the environmental organization, it has biological sensitivities and high protection prohibitions for the development of tourism and recreational activities. Therefore, the development of nature tourism in these natural habitats should be done within the framework of the principles of sustainability and considering the biological capacities of the area. Based on this, in the present study, by identifying suitable zones for the development of recreational activities in Hara PA, each of these activities is prioritized according to the capabilities of the natural areas and effective criteria for their development. In this regard, the main research questions are: 1) What are the suitable zones for the implementation of recreational activities that are demanded and can be developed in the mangrove forests of Hara PA? 2) Which recreational activities have a higher priority for the development of nature tourism in this area?

2. Study Area

Hara PA with an area equal to 86258 ha in Hormozgan province and in the position of north latitude 26° 43' 47" to 27° 01' 02" and east longitude 55° 23' 46" to 55° 54' 01" (Figure. 1). Mangrove forests in this area, based on the habitat, include 3 delta types (Kal and Mehran river deltas), coastal (Qeshm island coast) and island types [34]. The predominant plant species in the tree area is Avicennia marina, and in terms of its animal species, we can mention 6 families and 16 species of terrestrial and aquatic mammals, as well as 111 species of birds from 33 families [17]. This area is known as one of the most demanding places for coastal nature tourism due to its many tourist attractions and high potential for the development of recreational activities.

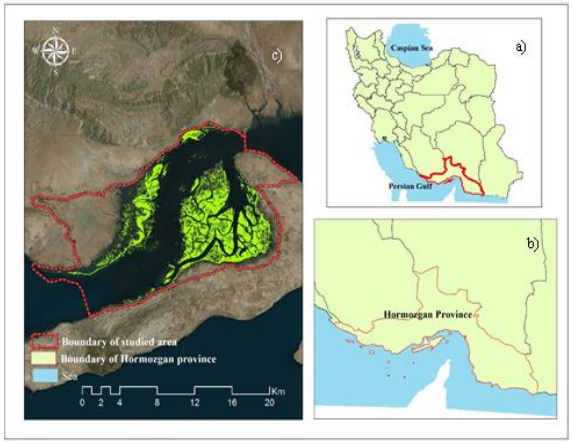

Figure. 1. Location of the studied area; a) Iran, b) Hormozgan province, c) Hara PA

3. Materials and methods

3.1. Methodology

To identify recreational activities that can be developed in Hara PA based on the expert's viewpoints and available documents [9, 25, 30], a list of recreational activities was prepared (Table 1). Then, 43 recreational activities were identified and given to tourists in the form of a questionnaire to determine their chosen activities and prioritize them in the numerical range of 1 to 10. According to Cochran's relationship, the sample size with the unknown population and with a confidence factor of 90%, according to Eq. 1 (Krebs, 1999), was determined to be equal to 96, and in this regard, by randomly distributing 100 questionnaires among the tourists, a survey was conducted and their demand was identified about the recreational activities available in this area.

$$n = \frac{z^2 pq}{d^2} \quad (1)$$

In the above equation, n: the number of required questionnaires, d: error rate (0.1), Z-statistic: 1.96, and p, q = 0.5. In the next step, the required activities were screened and selected according to Eq. 2. In this regard, Zi: weighted score of the activity, yi: the priority coefficient, xi: priority score, n_i: frequency of selecting the priority, and N: frequency of the requested activities. The basic selection of activities in this study is based on more than 10% of the total priorities, which have the most demand among recreational activities with an average of more than 100 (priorities 1 to 3). It should be mentioned that the final score of the activities is also standardized and reviewed according to the highest sum of the priority coefficients.

$$Z_i = \sum y_i n_i \times N \quad (2)$$

$$y_i = \frac{x_i}{\sum x_i}$$

Table 1. List of recreational activities suitable for development in the studied area

Recreational activities		
1) Pedal Boat (PEB)	16) Stand-Up Paddleboard (SUP)	30) Jet Boating (JEB)
2) Fan Boat (FBT)	17) Hovercraft (HOC)	31) Sailing Ships (SSH)
3) Flyfish Rides (FFR)	18) Banana Boat Rides (BBR)	32) Water Tricycle (WTR)
4) Rafting (RAF)	19) Body Glove Sea Shuttle) (BGS)	33) Kayak Ride (KYR)
5) Wind Surfing (WSU)	20) Jet Skis (JSK)	34) Kart Ride (KAR)
6) Skim Boarding (SKB)	21) Foil Surfing (FSU)	35) Kite Surfing (Kite Boarding) (KIS)
7) Zorbing (ZOR)	22) Parasailing (PAS)	36) Motor Kite (MOK)
8) Zipline (ZIP)	23) Visiting the Forest with a Balloon (VFB)	37) Glider Ride (GLR)
9) Atv's on the Beach (ATB)	24) Segway (SEG)	38) Bike Riding (BKR)
10) Beach Football (BFB)	25) Beach Volleyball (BVB)	39) Camel Riding on the Beach (CRB)
11) Watching Marine Wildlife (WMW)	26) Beach Paintball (BPT)	40) Bungee Jumping (BJU)
12) Walking in the Forest (WAF)	27) Watching Muddy Islands and Forest (WMF)	41) Watching Sports Competitions (WSC)
13) Visiting Villages near the Forest (VVF)	28) Picnic in Mangrove Fore st (PMF)	42) Camping in Mangrove Forest (CMF)
14) Traditional Fishing (TFI)	29) Photography in Mangrove Forest (PHM)	43) Sunbathing on the Beach (SUB)
15) Floating Gazebo (FGA)		

After examining the results of questioning to examine recreational activities, a series of spatial indicators were presented according to the land and coastal-sea nature of these activities. Therefore, according to relevant study records (Jahani et al. (2011); Akhondi (2014); Masnavi et al. (2013); Babazadeh (2014); Golchin et al. (2013); Mirkarimi et al. (2014); Shamshiri (2015); Sobhani (2022); Lotfikhah et al. (2017); Sharifian (2018); Mirzaei (2021); Markova et al. (2013); Danehkar et al. (2016); Asur et al. (2020); Misthos et al. (2019); Jahani (2019)), 13 indicators were used to estimate the spatial proportionality of recreational activities, including coastal slope, maximum elevation above sea level, beach material, wind intensity, precipitation intensity, speed of the water flow, maximum wave height, maximum water depth, best time for recreational activities (Tourism Climate Index), viewing angle, direction of view, maximum viewing distance, and landscape composition. Likewise, in the present study, the zoning of recreational activity demanded and developable in Hara PA was examined. Moreover, the spatial compatibility map of each of these activities was prepared based on the linear relationship of the combined spatial indicators. The codes related to the keywords of spatial indicators are also presented in Table 2.

Table 2. Spatial indicators codes (keywords) examined in recreational activities

Row	Spatial index	Code
1	Beach Material	BM
2	Coastal Slope	CS
3	Direction of View	DV
4	Elevation (above sea level)	EL
5	Landscape Composition	LC
6	Precipitation Intensity	PI
7	Viewing Angle	VA
8	View Distance	VD
9	Water Depth	WD
10	Speed of the Water Flow	WF
11	Wave Height	WH

12	Wind strength	WS

3.1.1. Prioritizing recreational activities

After zoning recreational activities, weighting and prioritization of these activities were conducted according to the series of selected criteria based on the viewpoints of 35 experts (Table 3) and similar studies and documents (Danehkar et al., 2019; Mirzaei, 2021, Lotfikhah et al., 2018). Likewise, in the process of identifying criteria, the environmental conditions of the studied area and other factors that can affect recreational activities development in this area were considered (Table 4).

Table 3. Characteristics of experts

Expertise	Number
Management and planning of coastal areas (coastal and wetland environment)	10
Environmental management and planning	7
Evaluation and land use planning	6
Environmental science and engineering	4
Management and planning of forest ecosystems (environmental assessment and planning)	8

Table 4. Criteria examined in the zoning of recreational activities

Criteria	Classes	Criteria	Classes
Existing sea	0-1000	Road access	0-100
infrastructure and	1000-2000	network (m)	100-200
ports (m)	<2000		<200
Distance from	0-1000	Distance from	0-1000
protective patches (m)	1000-2000	the city (m)	1000-2000
	<2000		<2000
Resident population	>1000	Location of	0-1000
(people)	1000-4000	settlements (m)	1000-2000
	<4000		<2000

In the following, the investigated criteria for prioritizing recreation areas in the numerical range of 0 to 1 were standardized according to the linear method according to Eq. 3 and 4. Then weight was assigned to each of the criteria using the ANP model. Finally, a spatial map was prepared for each criterion in ArcGIS software. In Eq. 3 and 4; $x_j^{Max} - x_j^{Min}$: the maximum and minimum value range of the desired indicators, x_j^{Max} : the maximum value assigned for the jth attribute, x_j^{Min} : the minimum value assigned for the jth attribute and Xij: the assigned value for the jth attribute and option i.

$$x_{ij} = \frac{x_{ij} - x_j^{Min}}{x_j^{Max} - x_j^{Min}} \quad (3)$$

$$x_{ij} = \frac{x_j^{Max} - x_{ij}}{x_j^{Max} - x_j^{Min}} \quad (4)$$

In addition, in the present study, the Topsis method was used in the Topsis Solver software to prioritize recreational activities, and the steps of this method are as follows (Chakraborty, 2022).

Step 1

Create an evaluation matrix consisting of "*m*" alternatives and "*n*" criteria, with the intersection of each alternative and criteria given as x_{ij}, hens, a matrix $\left(x_{ij}\right)_{m\times n}$.

Step 2

The matrix $\left(x_{ij}\right)_{m\times n}$ is then normalized to form the matrix

$R = \left(r_{ij}\right)_{m\times n}$, using the normalisation method

$$r_{ij} = \frac{x_{ij}}{\sqrt{\sum_{k=1}^{m} x_{kj}^2}}, i = 1,2,...,m,\ j = 1,2,...,n$$

Step 3

Calculate the weighted normalized decision matrix

$t_{ij=} r_{ij}.w_j,\ i = 1,2,...,m,\ j = 1,2,...,n$

Where $w_j = \dfrac{W_j}{\sum_{k=1}^{n} W_K}, \ j = 1,2,...,n$ so that $\sum_{i=1}^{n} w_i = 1$, and w_j is the original weight given to the indicator v_j, . $j = 1,2,...,n$

Step 4

Determine the worst alternative $\left(A_w\right)$ and the best alternative $\left(A_b\right)$:

$$A_w = \left\{ \left\langle \max(t_{ij} \mid i=1,2,...,m) j \in J- \right\rangle, \left\langle \min(t_{ij} \mid i=1,2,...,m) j \in J+ \right\rangle \right\} \equiv \left\{ t_{wj}, j=1,2,...,n \right\}$$

$$A_b = \left\{ \left\langle \max(t_{ij} \mid i=1,2,...,m) j \in J- \right\rangle, \left\langle \min(t_{ij} \mid i=1,2,...,m) j \in J+ \right\rangle \right\} \equiv \left\{ t_{bj}, j=1,2,...,n \right\}$$

Where,

$J+ = \{ j = 1,2,...,n, j \}$ associated with the criteria having a positive impact, and

$J- = \{ j = 1,2,...,n, j \}$ associated with the criteria having a negative impact.

Step 5

Calculate the L^2 - distance between the target alternative i and the worst condition A_w

$$d_{iw} = \sqrt{\sum_{j=1}^{n} \left(t_{ij} - t_{wj} \right)^2}, i = 1,2,...,m$$

and the distance between the alternative i and the best condition A_b

$$d_{ib} = \sqrt{\sum_{j=1}^{n} \left(t_{ij} - t_{wj} \right)^2}, i = 1,2,...,m$$

Where d_{iw} and d_{ib} are L^2-norm distances from the target alternative i to the worst and best conditions, respectively.

Step 6

Calculate the similarity to the worst condition:

$$s_{iw} = d_{iw} \Big/ \left(d_{iw} + d_{ib} \right), \quad 0 \le s_{iw} \le 1, \; i = 1,2,...,m$$

$s_{iw} = 1$ if and only if the alternative solution has the best condition; and

$s_{iw} = 0$ if and only if the alternative solution has the worst condition.

Step 7

Rank the alternatives according to $s_{iw} \; (i = 1,2,...,m)$

4. Results and Discussion

4.1. Identify recreational activities suitable for development in the area

The results showed that from 43 recreational activities in this area, 27 activities were selected (Table 5). In the next step, the screening and selection of demanded activities was done according to Eq 2. As the results demonstrate, 12 recreational activities with an average of more than 100 and based on the frequency of the first 3 selections (priority 1 to 3) had the most demand among tourists. In addition, the results show that among these activities, the highest standardized score is related to "visiting the forest with a balloon" (with a score of 69.55) and the lowest score is related to the activity "sunbathing on the beach" (with a score of 7.90). Likewise, the highest frequency in the first priority is allocated "walking in the forest" and "visiting villages near the forest" (n=16), in the second priority "visiting the forest with a balloon" (n=28), and finally, in the third priority, the highest frequency was assigned to "watching marine wildlife" (n=17). In this regard, the studies of Mirzaei (2021) and Sharifian (2018) showed that development of the tourism industry in any destination with different geographical and climatic conditions, requires the identification and selection of the most appropriate recreational activities that can be developed in the area.

Table 5. List of recreational activities identified in the area

Row	Recreational activities	xi	3	2	1	∑	Standardization	Weighted score	Standardized score
		yi	0.5	0.33	0.17				
1	Visiting the Forest with a Balloon	n	2	28	9	39	0.90	906.29	69.55
		xi.n	6	56	9	71			
		zi	1	9.24	1.53	11.77			
2	Watching Marine Wildlife	n	15	8	17	40	1	729.68	56
		xi.n	45	16	17	78			
		zi	57	2.64	2.89	13.03			
3	Walking in the Forest	n	16	7	0	23	0.79	597.98	45.89
		xi.n	48	14	0	62			
		zi	8	2.31	0	10.31			
4	Visiting Villages near the	n	16	3	0	19	0.69	431.52	33.12

	Forest	xi.n	48	6	0	54			
		zi	8	0.99	0	8.99			
		n	12	1	4	17	0.54	294.42	22.60
5	Jet Boating	xi.n	36	2	4	42			
		zi	6	0.33	0.68	1.01			
		n	4	10	2	19	0.43	276.36	21.21
6	Traditional Fishing	xi.n	12	20	2	34			
		zi	2	3.30	0.34	5.64			
7	Watching Muddy Islands and Forest	n	3	6	5	14	0.33	242.48	18.61
		xi.n	9	12	5	26			
		zi	1.50	1.98	0.85	4.33			
8	Camping in Mangrove Forest	n	4	6	5	15	0.37	241.5	18.53
		xi.n	12	12	5	29			
		zi	2	1.98	0.85	4.83			
9	Atv's on the Beach	n	0	8	7	15	0.29	187.67	14.40
		xi.n	0	16	7	23			
		zi	0	0.12	0	0.12			
10	Bike Riding	n	2	3	8	13	0.26	140.7	10.80
		xi.n	6	6	8	20			
		zi	1	0.99	1.36	3.35			
11	Photography in Mangrove Forest	n	5	0	7	12	0.28	125.46	9.63
		xi.n	15	0	7	22			
		zi	2.50	0	1.19	3.69			
12	Sunbathing on the Beach	n	1	7	3	11	0.25	102.92	7.90
		xi.n	3	14	3	20			
		zi	0.50	2.31	0.51	3.32			
13	Body Glove Sea Shuttle	n	0	8	1	9	0.22	95.54	7.33
		xi.n	0	16	1	17			
		zi	0	2.64	0.17	2.81			
14	Motor Kite	n	9	0	0	9	0.35	81	6.22
		xi.n	27	0	0	27			
		zi	4.50	0	0	4.50			
15	Sailing Ships	n	0	4	0	4	0.10	63.36	4.86
		xi.n	0	8	0	8			
		zi	0	1.32	0	1.32			
16	Zorbing	n	5	0	0	5	0.19	42.5	3.26
		xi.n	15	0	0	15			
		zi	2.50	0	0	2.50			
17	Zipline	n	3	0	1	4	0.13	26.72	2.05
		xi.n	9	0	1	10			
		zi	1.50	0	0.17	1.67			
18	Glider Ride	n	0	0	9	9	0.12	26.1	2

		xi.n	0	0	9	9			
		zi	0	0	1.53	1.53			
19	Water Tricycle	n	0	0	5	5	0.07	24.65	1.89
		xi.n	0	0	5	5			
		zi	0	0	0.85	0.85			
20	Camel Riding on the Beach	n	0	1	5	6	0.09	14.16	1.09
		xi.n	0	2	5	7			
		zi	0	0.33	0.85	1.18			
21	Rafting	n	3	0	0	3	0.12	12	0.92
		xi.n	9	0	0	9			
		zi	1.50	0	0	1.50			
22	Bungee Jumping	n	1	0	0	1	0.04	9.5	0.73
		xi.n	3	0	0	3			
		zi	0.50	0	0	0.50			
23	Segway	n	0	0	5	5	0.07	9.35	0.72
		xi.n	0	0	5	5			
		zi	0	0	0.85	0.85			
24	Fan Boat	n	0	4	0	4	0.10	7.92	0.61
		xi.n	0	8	0	8			
		zi	0	1.32	0	1.32			
25	Kart Ride	n	0	0	3	3	0.04	5.61	0.43
		xi.n	0	0	3	3			
		zi	0	0	0.51	0.51			
26	Pedal Boat	n	0	0	3	3	0.04	2.04	0.16
		xi.n	0	0	3	3			
		zi	0	0	0.51	0.51			
27	Beach Paintball	n	0	0	2	2	0.03	1.7	0.13
		xi.n	0	0	2	2			
		zi	0	0	0.34	0.34			

4.2. Investigating recreational activities according to location indicators

After identifying and determining the recreational activities demanded in the area, these activities were investigated according to the spatial indicators in Table 6. In this way, every recreational activity was examined and analyzed in a range of defined index values.

Table 6. Spatial indicators of proportionality of recreational activities demanded

Indicator / Activity	Landscape Composition	Maximum viewing distance (m)	Viewing Angle & Direction of View	Best time for recreational activities (TCI)	Maximum Water Depth (m)	Maximum Wave Height (m)	Speed of the Water Flow (m/s)	Precipitation Intensity (mm)	Wind intensity (Km/h)	Beach Material	Maximum Elevation above sea level (m)	Coastal Slope (%)

Visiting the Forest with a Balloon (VFB)	Various	<300[1]	–		Very good to excellent	–	–	–	No heavy rain	16<	–	–	5<
Watching Marine Wildlife (WMW)	Various	1500<	[3]East to South	110-180	[2]January-February	–	–	–	No heavy rain	–	–	–	–
Walking in the Forest (WAF)	Uniform	–	–		Very good to excellent	–	–	–	No heavy rain	30<	–	–	5<
Visiting Villages near the Forest (VVF)	Uniform	500<	[4]Northeast to South	45-180	Very good to excellent	–	–	–	No heavy rain	–	–	20<	–
Jet Boating (JEB)	–	–	East to South	110-180	Very good to excellent	5	1	1<	No heavy rain	30<	Sandy	–	5<
Traditional Fishing (TFI)	–	–	–		Very good to excellent	5	1	1<	No heavy rain	–	–	–	
Watching Muddy Islands and Forest (WMF)	Various	500<	East to South	110-180	Very good to excellent	–	1	–	No heavy rain	–	–	–	–
Camping in Mangrove Forest (CMF)	–	–	–		Very good to excellent	–	–	–	No heavy rain	–	Non-muddy	–	–
Atv's on the Beach (ATB)	–	–	–		Very good to excellent	–	–	–	No heavy rain	30<	Sandy	–	5<
Bike Riding (BKR)	–	–	–		Very good to excellent	–	–	–	No heavy rain	30<	Sandy	–	5<
Photography in Mangrove Forest (PHM)	Various	500<	[5]Northeast to West	45-270	Very good to excellent	–	–	–	No heavy rain	–	–	–	–
Sunbathing on the Beach (SUB)	–	–	–		Very good to excellent	–	–	–	No heavy rain	–	Sandy	–	–

[1] Vertical view based on the height above the sea level in the area

[2] As the weather cools down and birds migrate to this area

[3] Based on the existing birdwatching site in the area

[4] Based on the high concentration of historical and traditional villages in the northeastern and southern regions of the area

[5] Based on the distribution of mangrove habitats in the area

4.3. Recreational activities zoning

4.3.1. Suitable zones for visiting the forest with a balloon

Visiting the forest with a balloon is an activity that can be done in conditions with a beach slope of less than 5%, wind less than 16 km/h, no heavy rain, tourist climate (during the months of December, January, February, March and April) in very good and excellent conditions, vertical viewing distance less than 300 m and various landscape combinations are applicable. The linear model of this activity zoning is as follows and in Figure. 2, suitable zones for the implementation of this activity can be seen.

VFB=CS1+WS2+LC1

4.3.2. Suitable zones for watching marine wildlife

Watching sea animals and birds in this area, in the condition of no heavy rain, in the winter season and during the months of January and February (coinciding with the migration of birds to the area), the viewing angle 45 to 180 degrees, in the east to south direction, in the maximum visibility distance up to 1500 m, and with various landscape combinations for this activity is significant (Figure. 3).

WMW= (VA1, VA2, VA3, VA4) + (VD1, VD2, VD3) + LC1

4.3.3 Suitable zones for walking in the forest

Suitable conditions for the implementation of this activity include beach slope less than 5%, wind intensity less than 30 km/h, no heavy rain, tourism climate in very good to excellent conditions and various landscape combinations. Suitable areas for this activity are according to Figure. 4.

WAF=CS1 + (WS1, WS2) + LC2

4.3.4. Suitable zones for visiting villages near the forest

Visiting villages near the mangrove forests at a maximum height of less than 20 meters, no heavy rain, tourism climate in very good to excellent conditions, viewing angle 45 to 180 degrees (northeast to south viewing direction), distance visibility less than 500 m, and this activity is possible with the combination of a uniform landscape. Figure. 5 also shows the zoning map for the implementation of this recreational activity.

VVF= (EL1, EL2, EL3) + (VA1, VA2, VA3, VA4) +VD1, LC2

4.3.5. Suitable zones for traveling by Jet boating

To perform this recreational activity (Figure. 6), the slope of the beach must be less than 5% and sandy. Likewise, other requirements for using this activity include wind speed less than 30 km/h, no heavy rain, water flow speed less than 1 m/s, maximum wave height of 1 m, and maximum water depth of 5 m. The appropriate time for this activity is in the conditions of very good to excellent tourism climate and in the viewing angle of 110 to 180 degrees (east to south view direction).

JEB= CS1+BM1+(WS1, WS2) +WF1+(WH1, WH2) +(WD1, WD2, WD3) +(VA3, VA4)

4.3.6. Suitable zones for traditional fishing (hook fishing)

It is possible to perform this recreational activity in the condition of no heavy rain, the water flow speed is less than 1 m/s, the maximum wave height is 1 m, and the maximum water depth is 5 m. Furthermore, the favorable indicator of tourism climate for traditional fishing is very good to excellent. Figure. 7 also shows the zoning map for the implementation of this recreational activity.

TFI= WF1+(WH1, WH2) +(WD1, WD2, WD3)

4.3.7. Suitable zones for watching muddy islands and forest

Viewing muddy islands and mangrove forests should be done in conditions such as no heavy rain, maximum wave height of 1 m, tourism climate in very good to excellent conditions, viewing angle 110 to

180 degrees (east to south viewing direction), maximum viewing distance less than 500 m, and various landscape combinations for this activity is significant (Figure. 8).

WMF= (WH1, WH2) + (VA3, VA4) + VD1 + LC1

4.3.8. Suitable zones for camping in the mangrove forest

In terms of weather, camping in the mangrove forest is possible in the no heavy rain. Likewise, the beach material should be non-muddy type and the tourism climate should be in very good to excellent condition. It should be noted that due to the proximity to habitats, water areas, and the effects of tourists, as well as any possible danger, suitable zones for camping are considered at a distance of 100 m from the mentioned items (Figure. 9).

CMF= BM3

4.3.9. Suitable zones for traveling with an Atv's on the beach

It is possible to travel with an Atv's on the beach with a maximum slope of less than 5% and sandy material. Other requirements for doing this activity include wind intensity of less than 30 km/h, no heavy rain, and very good to excellent tourism climate (Figure. 10).

ATB= CS1 + BM1 + (WS1 + WS2)

4.3.10. Suitable zones for bike riding on the beach

Bike riding on the beach is applicable with a maximum slope of less than 5%, sandy beach material, wind intensity less than 30 km/h, no heavy rain, and very good to excellent tourism climate (Figure. 11).

BKR= CS1 +BM1 + (WS1+WS2)

4.3.11. Suitable zones for photography in the mangrove forest

The necessary conditions for photography in the mangrove forest include no heavy rain, a very good to excellent tourism climate, a viewing angle of 45 to 270 degrees (northwest to west viewing direction), a viewing distance of less than 500 m, and various landscape combinations (Figure. 12).

PHM= (VA2, VA3, VA4, VA5, VA6) + VD1 + LC1

4.3.12. Suitable zones for sunbathing on the beach

The conditions for the implementation of this activity include the sandy beach, no heavy rain, and the tourism climate is very good to excellent. Figure. 13 also shows the map of suitable and feasible zones for this recreational activity.

SUB=BM1

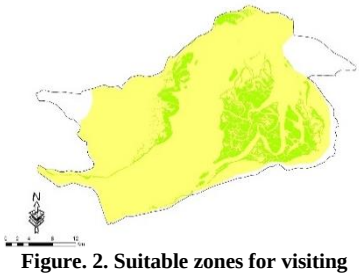

Figure. 2. Suitable zones for visiting the forest with a balloon

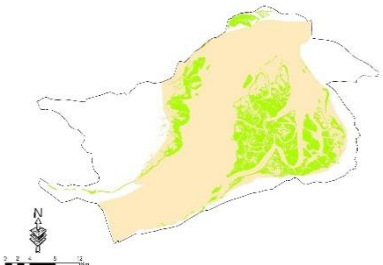

Figure. 3. Suitable zones for watching marine wildlife

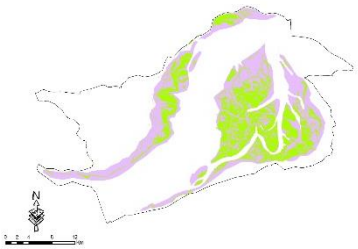

Figure. 4. Suitable zones for walking in the forest

Figure. 5. Suitable zones for visiting villages near the forest

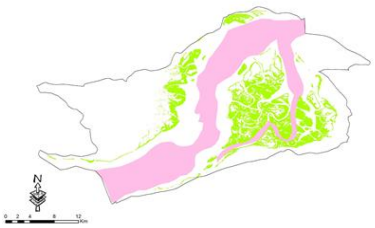

Figure. 6. Suitable zones for touring by jet boating

Figure. 7. Suitable zones for traditional fishing

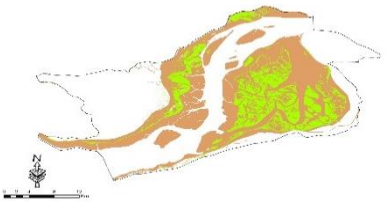

Figure. 8. Suitable zones for watching muddy islands and forest

Figure. 9. Suitable zones for camping in mangrove forest

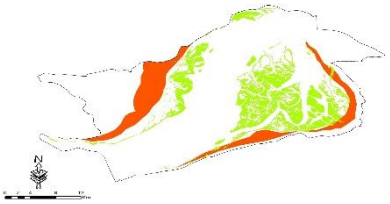

Figure. 10. Suitable zones for Atv's on the beach

Figure. 11. Suitable zones for bike riding

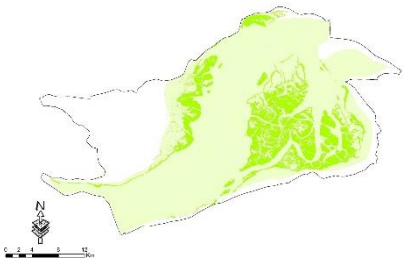

Figure. 12. Suitable zones for photography in mangrove forest

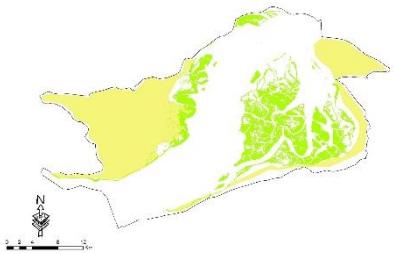

Figure. 13. Suitable zones for sunbathing on the beach

4.4. Zoning of recreational activities

After identifying the suitable zones for recreational activities development demanded in the area, the final map of the suitable recreational zones was compiled and prepared. Since the studied area is also known as a PA, the final map of the integration of recreational activities in this area was prepared by considering the position of the protection zones (1 and 2), and as a result, recreational activities corresponding to the protection spots were removed from the map (Figure. 14). This map includes 4 options for the state of dispersion of integrated recreational activities, which include the following according to Table 7:

• Option 1 includes zones with three recreational activities,

• Option 2 includes zones with four recreational activities,

• Option 3 includes zones with five recreational activities,

• Option 4 includes zones with seven recreational activities.

In this regard, the results of other studies such as Latfikhah (2018), Mirzaei (2021), and Danehkar (2019), which focused on the zoning of tourism activities in the southern regions of the country, indicate the similarity of geographical conditions and location, as well as the most effective spatial indicators in measuring the proportionality of recreational activities in this area.

Table 7. Combined recreational activities in the studied area

Option	Recreational activities
1	Walking in the forest, watching marine wildlife, visiting the forest with a balloon
2	Visiting villages near the forest, walking in the forest, watching marine wildlife, visiting the forest with a balloon
3	Photography in mangrove forest, traditional fishing, Jet boating, watching marine wildlife, visiting the forest with a balloon

4	Sunbathing on the beach, Atv's on the beach, camping in mangrove forest, watching muddy islands and forest, walking in the forest, watching marine wildlife, visiting the forest with a balloon

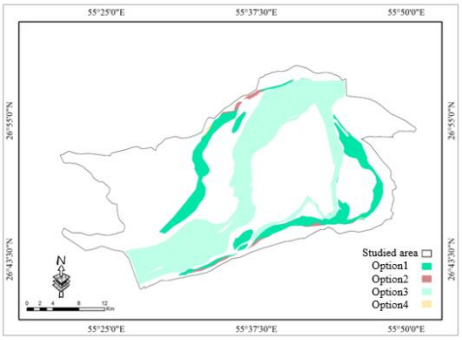

Figure. 14. Map of the combination of recreational activities in the studied area (including protection zones 1 and 2)

4.5 Weighing and prioritizing recreational activities

To prioritize demanded recreational activities in Hara PA, these activities were weighted and prioritized based on the suggested and selected criteria as follows. For this purpose, firstly, the standardization of the criteria was conducted (Table 8). As the results revealed, among the criteria, the access road network, distance from the city, the location of settlements, marine infrastructure and existing ports have a decreasing linear relationship, which means that by reducing these criteria, the distribution value and prioritization of recreational zones in the area increase. On the other hand, distance measures from protective patches and resident population have an increasing linear relationship. Thus, increasing the distance from protective patches (protection and safe zones of the area), as well as increasing the number of people living in the region, leads to an increase in the importance of recreational activities in these areas. Yaqubzadeh et al. (2020), also investigated the role of docks around mangrove habitats in Khamir port and Khor Azini. Their results showed that the existing docks and structures in these areas have increased widely in recent years, which have a great role and effects on the mangrove habitats in this area.

Table 8. Standardization classes of the studied criteria

Criteria	Classes	Function type	Standardized value of criteria	Criteria	Classes	Function type	Standardized value of criteria
Road access network (m)	0-100	Linear reduction	1	Existing sea infrastructure and ports (m)	0-1000	Linear reduction	1
	100-200		0.5		1000-2000		0.5
	<200		0		<2000		0
Distance from the city (m)	0-1000	Linear reduction	1	Distance from protective patches (m)	0-1000	Linear increase	0
	1000-2000		0.5		1000-2000		0.5
	<2000		0		<2000		1
Location of settlements	0-1000	Linear reduction	1	Resident population	>1000	Linear increase	0
	1000-2000		0.5		1000-4000		0.5

(m)	<2000	0	(people)	<4000	1

Following, the criteria were weighted using the ANP model and based on experts' viewpoints (Table 9). According to the obtained results, the highest weight is assigned to the criterion of marine infrastructure and existing ports (0.215), and the lowest weight is related to the criterion of distance from the city (0.104). Figure. 15 to 20 also show the spatial maps of studied criteria.

Table 9. The weighting coefficient of the studied criteria

Criteria	Criterion weight
Road access network	0.168
Distance from the city	0.104
Location of settlements	0.115
Existing sea infrastructure and ports	0.215
Distance from protective patches	0.187
Resident population	0.152

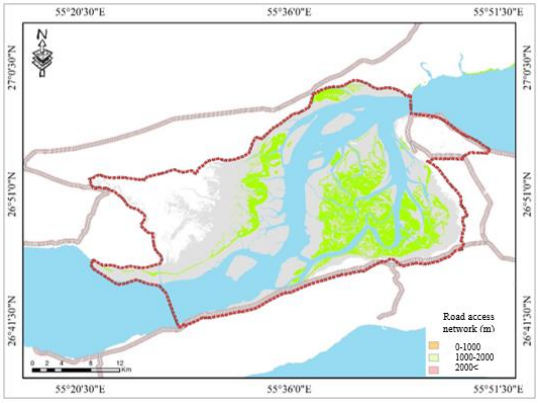

Figure. 15. Map of the road access network

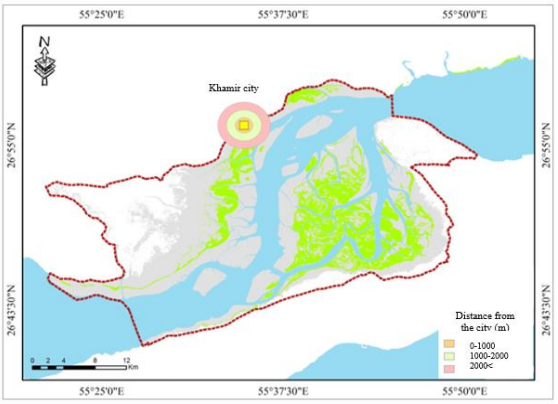

Figure. 16. Map of the distance from the city

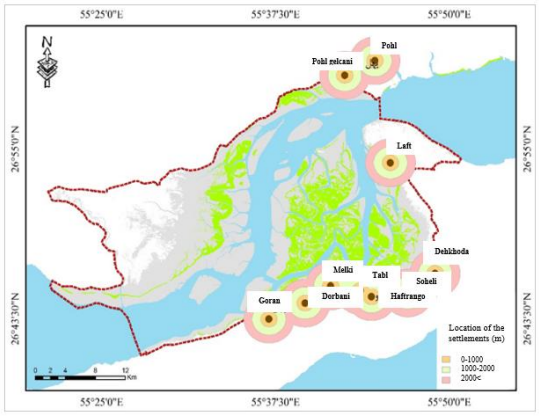

Figure. 17. Location map of the settlements

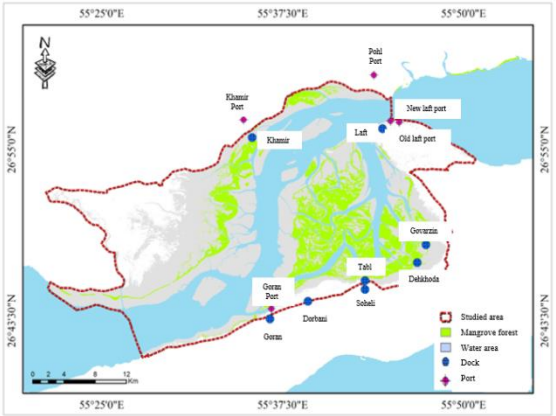

Figure. 18. Distribution map of existing sea infrastructure and ports

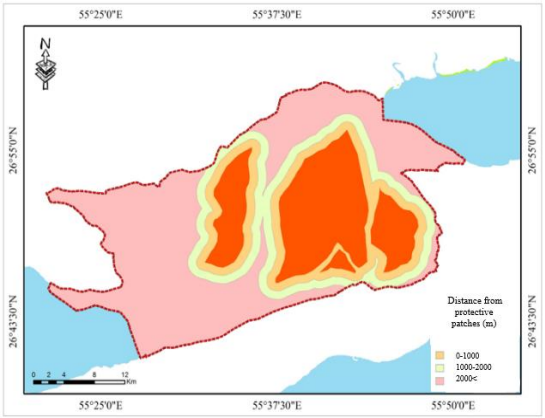

Figure.19. Map of the distance from protective patches

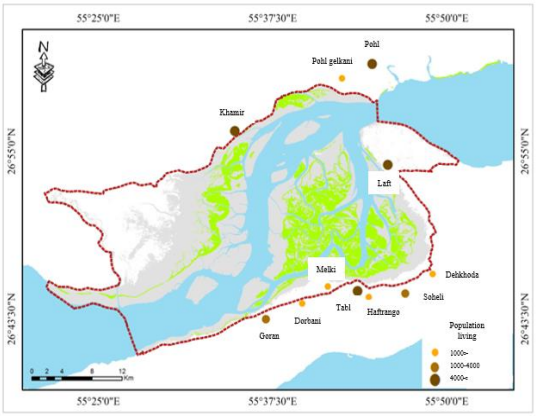

Figure. 20. Map of the population living in the area

In this study, the Topsis method was used in the Topsis Solver software to prioritize recreational activities (Tables 10 to 15). Based on the results obtained from the ranking of recreational activities, the highest priority is related to option 2, and the next priorities include options 3, 1, and 4, respectively (Table 16). In this regard, Mirzaei (2021), discussed the zoning and integration of tourism activities in the coastal cities of Hormozgan province. The results showed that Bandar Abbas city has the highest priority (in terms of favorable zones) for the development of recreational activities in this area. In another study, Sorkhaei et al. (2022), investigated the effective criteria in the development of sports and tourism activities in the coastal areas of Hormozgan. They stated that prioritizing the development of sports activities in this area requires the examination of economic-marketing criteria, infrastructure facilities, public relations and advertising, social-cultural, political-security, and management factors.

Table 10. Creating a decision matrix

Option	Road access network	Distance from the city	Location of settlements	Existing sea infrastructure and ports	Distance from protective patches	Resident population
1	1	2	3	5	4	2
2	2	1	4	5	5	3
3	1	2	3	4	5	4
4	4	1	3	5	2	4
Criterion type	–	–	–	–	+	+
Criterion weight	0.168	0.104	0.115	0.215	0.187	0.152

Table 11. Matrix normalization

Option	Road access network	Distance from the city	Location of settlements	Existing sea infrastructure and ports	Distance from protective patches	Resident population
1	0.21	0.63	0.45	0.52	0.47	0.29
2	0.42	0.31	0.61	0.52	0.59	0.44
3	0.21	0.63	0.45	0.41	0.59	0.59
4	0.85	0.31	0.45	0.52	0.23	0.59

Table 12. Determination of positive and negative ideal solution

Option	Road access network	Distance from the city	Location of settlements	Existing sea infrastructure and ports	Distance from protective patches	Resident population

+	0.035	0.032	0.051	0.088	0.110	0.089
–	0.14	0.065	0.07	0.111	0.043	0.044

Table 13. Determining the distance from the positive and negative ideal solution

Distance size	+	–
1	0.070	0.11
2	0.031	0.10
3	0.044	0.13
4	0.09	0.05

Table 14. Proximity to the positive and negative ideal solution and the ranking of the options

Option	Proximity factor	Rank
1	1.68	3
2	3.32	1
3	3.08	2
4	0.60	4

Table 15. Prioritization of recreational activities in the studied area

Priority	Options (combined recreational activities)
1	Visiting villages near the forest, walking in the forest, watching marine wildlife, visiting the forest with a balloon
2	Photography in mangrove forest, traditional fishing, Jet boating, watching marine wildlife, visiting the forest with a balloon
3	Walking in the forest, watching marine wildlife, visiting the forest with a balloon
4	Sunbathing on the beach, Atv's on the beach, camping in mangrove forest, watching muddy islands and forest, walking in the forest, watching marine wildlife, visiting the forest with a balloon

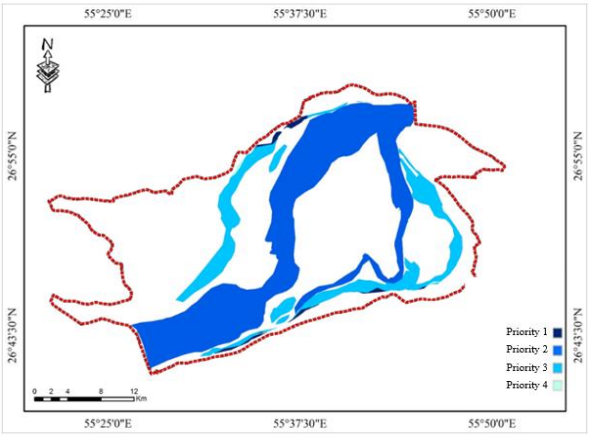

Figure. 21. Map of prioritizing recreational activities in the area

5. Conclusion

Selecting appropriate activities and their distribution in natural areas is one of the most important issues in tourism management and planning in natural ecosystems. Accordingly, the present study identified suitable zones for the development of recreational activities in Hara PA, each of these activities was prioritized according to the capabilities of the natural areas and effective criteria for their development.

As the results revealed, the zoning of recreational activities in this area includes 4 options of how to combine the recreational activities demanded in the mangrove forests of Hara PA. Based on the ranking of activities, the highest priority is related to option 2,

and the next priorities include options 3, 1, and 4, respectively. In general, measuring the proportionality of recreational activities in tourism destinations, especially in PAs that have legal prohibitions and potential biological and protective restrictions for human activities development (both physical and economic activities), is essential and can lead to proper planning and management. In fact, the successful development of a tourist destination can be based on effective planning and in compliance with the principles of sustainable development, and this goal is achieved when the development of suitable and developable recreational activities in the region is addressed. According to the results obtained, one of the most important factors in the development of sustainable nature tourism, as well as the possibility of using the power and tourist attractions in natural ecosystems, is the zoning and prioritization of recreational activities according to the environmental conditions of the region. Considering that the mangrove forests of Hara PA are among the valuable protected reserves of the southern coasts of the country, prioritizing recreational activities in suitable areas and outside the protection zones of the region can help to sustainably use the capacity of natural resources and the appropriate distribution of recreational activities in the area while protecting these natural habitats. In addition, for a more detailed investigation, it is suggested that the zoning of recreational activities in other mangrove habitats in southern Iran be investigated and analyzed with other methodologies in future research.

Acknowledgments

This article, taken from project number 4005972, has been completed with the cooperation and financial assistance of the Iran National Science Foundation Science deputy of presidency (INSF).

References

[1] Akhoondi, L., Danehkar, A., Arjmandi, R., & Shabanali Fami, H. (2014). Site Selection Appropriate Zones for Sport Tourism in Mountain Areas A Case Study: Karaj-Chalous Road. Journal of Natural Environment, 3 (3), 331-344.

[2] Asur, F., Sevimli Deniz, S., & Yazici, K. (2020). Visual Preferences Assessment of Landscape Character Types Using Data Mining Methods (Apriori Algorithm): The Case of Altınsaç and Inkoy (Van/Turkey). J. Agr. Sci. Tech 22 (1), 247-260.

[3] Babazadeh, S., Danehkar, A., & Taheri Sarteshnizi, F. (2014). Evaluation of tourism activities based on sustainable development (case study: Sisangan forest park). 21st National Geomatics Conference. Country Mapping Organization, Tehran, 1-10.

[4] Blanco-Cerradelo, L., Diéguez-Castrillón, M. I., Fraiz-Brea, J. A., & Gueimonde-Canto, A. (2022). Protected areas and tourism resources: Toward sustainable management. Land. 11 (11), 2059.

[5] Chakraborty, S. (2022). TOPSIS And Modified TOPSIS: A Comparative Analysis. Decision Analytics Journal, 2, 100021.

[6] Danehkar, A., & Mahmoudi, B.A. (2016). Design and management of forest parks. Institute of Scientific-Applied Higher Education. 293p.

[7] Danehkar, A., Karimi, S., Taheri Sartashnizi F., Davar, L., Jafari, Sh., Baghkhanipour, S., & Babazadeh, S. (2016). Ecological land capability evaluation in the Baliran pilot. Building a multiple-use forest management framework to conserve biodiversity in the Caspian Hyrcanian Forest Landscape. FRWO/UNDP/ GEF, 144p.

[8] Danehkar, A., Mahmoudi, B., & Torabi, A. (2016). Designing and Management of Forest Parks. Agricultural Research, Education & Extension Organization: Agricultural Education and Extension Institute.

[9] Danekar, A., Azizi Jalilian, M., Lotfikhah, S., Farozd, M., Davar, L., Samadi, B., Yaqoubzadeh, M., Mafigholami, D., Faizi, S., Mashhadi, M., Khatibi, A., Petrosian, H., Dadashzadeh Z., & Khodam Astanehossein. A.R. (2019). Action plan for the integrated management of the coastal zone of Bandar Khmeir city. Review plan of integrated management studies of coastal areas of Hormozgan province, Ports and Maritime Organization. Iran Structural Consulting Engineers. 382p.

[10] DaRugna, O.A., Kaemingk, M.K., Chizinski, Ch. K., & Pope, K. L. (2022). Heterogeneity of recreationists in a park and protected area. PLoS One. 17(5), e0268303.

[11] Eagles, P. F. J., McCool, S. F., & Haynes, C. D. A. 2002. Sustainable tourism in protected areas: Guidelines for planning and management. Gland, Switzerland and Cambridge, UK: IUCN.

[12] Franceschinis, C., Swait, J., Vij, A., & Thiene, M. (2022). Determinants of recreational activities choice in protected areas. Sustainability, 14 (1), 412.

[13] Gharibzadeh, M., Safania, A.M., Naghshbandi, S.S., & Abolfazl Farahani, A. 2023. Providing a model for the development of sports tours in the tourism industry. PLoS One, 18 (5), e0285457.

[14] Golchin, F., Naroyi, B., & Irani Behbahani, H. (2013). Investigation of user preferences based on visual quality assessment (case study: Mellat Zahedan Urban Forest Park). Environment, 39 (4), 193-203.

[15] Gumede, Th. K., Nzama, A. T., & Mdiniso, J. M. (2022). Evaluating the Effectiveness of the Strategies for

Sustaining Nature-Based Tourism amid Global Health Crises: A Global Perspective. Sustainable Built Environment, 1-29.
[16] Jahani A. (2019). Forest landscape aesthetic quality model (FLAQM): A comparative study on landscape modelling using regression analysis and artificial neural networks. J. For. Sci 65, 61-69.
[17] Kabuli, M., Aliabadian, M., Tohidifar, M., Hashemi, A.R., & Roselar, K. (2016). Iran bird atlas, first edition. 624p.
[18] Krebs, C.J. (1999). Ecological Methodology. Addison-Wesley Educational Publishers, Inc., Menlo Park, 620p.
[19] Lotfikhah, S., Frouzad, M., Yaqubzadeh, M., Danehkar, A., & Kordi, F. (2018). Coastal management plan (SMP) of Hormozgan province. Review plan for integrated management studies of coastal areas of Hormozgan province. Iran's structural consulting engineers. General Directorate of Coastal and Port Engineering, Vice-Chancellor of Infrastructure Development and Engineering. Ports and Maritime Organization. 177p.
[20] Mahmoudi, B.A., Payesh, K., & Heydari, Z. (2018). Planning the development of natural tourism in the model tourism area of Anshan in Khuzestan province. Scientific and specialized quarterly of tourism research and sustainable development. 1 (3), 37-44.
[21] Maldonado-Oré, E. M., & Custodio, M. (2020). Visitor environmental impact on protected natural areas: An evaluation of the Huaytapallana Regional Conservation Area in Peru. Journal of Outdoor Recreation and Tourism 31, 100298.
[22] Markova, M. (2013). Latgale upland church everyday landscape in development and growth of region and society. Proceedings of the Latvia University of Agriculture Landscape Architecture and Art, 3 (3), 83-89.
[23] Masnavi, M. R., Tasa, H., Kafi, M., & Dinarundi, M. (2012). Visual assessment of the landscape of the Qeshlaq Valley for the development of tourism. Journal of Environment, 39 (65), 133-144.
[24] Mirkarimi, S. H., Saidi, S., Mohammadzadeh, M., & Salman Mahini, A. R. (2014). Application of PCA method in evaluating the visual quality of landscape (case study: Ziarat area of Golestan province). Environment, 40 (2), 462-451.
[25] Mirzaei, A. (2021). Proportion measurement of territorial waters of Hormozgan province for marine tourism activities zoning. Master's thesis in the field of natural resources-environmental engineering. Agriculture and Natural Resources Campus, TehranUniv. of Natural Resources
[26] Misthos, L. M., Nakos, B., Krassanakis, V., & Menegaki, M. (2019).The effect of topography and elevation on viewsheds in mountain landscapes using geo visualization. International Journal of Cartography, 5 (1), 44-66.
[27] Ramyar, M., Asadi Amiri, T., Momeni, O., Ghasemi, M.J., & Zaheer, Z.U.R. (2020). Tourists' perspective on ecotourism infrastructures in Mazandaran province of Iran. J. of Humanities and Social Sciences Studies (JHSSS), 109-118.
[28] Shamshiri, S. (2015). Evaluation of the visual quality of the mirage of Goznehle Sanghar. Man and Environment, 13 (4), 27-41.
[29] Sharifi, N. (2021). Development of a comprehensive model for the purpose of zoning protected areas based on multi-criteria decision-making methods (case study: mangrove protected area). Doctoral dissertation in the field of environmental sciences. Faculty of Natural Resources and Environment - Islamic Azad University, Science and Research Unit. 150p.
[30] Sharifian, S. (2018). Selection of coastal tourism activities in Mazandaran province using multi-objective user allocation method (MOLA). Master's degree thesis. Faculty of Agriculture and Natural Resources, Faculty of Natural Resources, Tehran University of Natural Resources.
[31] Sobhani, P., & Danehkar, A. (2023a). Identifying Recreational Activities
and Investigating Location Indicators for Nature Tourism Development in Hara Protected Area, Tourism Management Studies, 18(61), 65-110.
[32] Sobhani, P., & Danehkar, A. (2023b). Zoning and prioritization of recreational activities in Khamir and Qeshm mangrove forests. Journal of Wood and Forest Science and Technology, 30(3), 87-114.
[33] Sobhani, P., & Danehkar, A. (2023c). Estimation of nature tourism carrying capacity in the mangrove forests of Khamir and Qeshm. Iranian Journal of Forest, 15(4), 377-392.
[34] Sobhani, P., & Danehkar, A. (2023d). Natural features and management areas of Khamir and Gheshm mangrove forests. Nature of Iranz. 8: 4-41. 8-16.
[35] Sobhani, P., Esmaeilzadeh, H., Sadeghi, S. M. M., Marcu, M.V., & Wolf, I.D. 2022. Evaluating Ecotourism Sustainability Indicators for Protected Areas in Tehran, Iran. Forests 13, 740.
[36] Sorkhai, F., Saibani, H.R., & Swadi, M. (2021). Developing a tourism destination management model with an emphasis on beach sports (case study: coastal cities of Hormozgan). J. of urban tourism. 9 (1), 18.
[37] Strickland-Munroa, J., & Moorea, S. (2013). Indigenous involvement and benefits from tourism in protected areas: a study of Purnululu National Park and Warmun Community, Australia. J. Sustain. Tourism, 21 (1), 26–41.
[38] Thapa, K., King, D., Banhalmi-Zakar, Z., & Diedrich, A. (2022). Nature-based tourism in protected areas: a systematic review of socio-economic benefits and costs to local people. International Journal of Sustainable Development & World Ecology, 29 (7), 625-640.
[39] Xie, W., & Ma, Y. (2021). Tourism Resource Evaluation and Countermeasures Based on Network Communication and TOPSIS Algorithm. Hindawi, Wireless Communications and Mobile Computing, 1-13.
[40] Yang, J., Xu, H., & Wang, X. (2022). Impact of tourism activities on the distribution and pollution of soil heavy metals in natural scenic spots on the northern slope of Tianshan Mountain. PLoS ONE 17 (7), e0267829.
[41] Yaqubzadeh, M., Salman Mahini, A.A., Moslehi, M., Danekar, A., & Mikayili Tabrizi, A.R. (2020). Investigating the role of dock on vegetative and reproductive characteristics of mangrove trees (Avicennia marina (Forssk.) Vierh). Iranian J. of Forest and Spruce Research. 28 (3), 244-256.

INTERNATIONAL JOURNAL OF
COASTAL, OFFSHORE & ENVIRONMENTAL ENGINEERING IJCOE Vol.9/No. 2/Spring 2024 (19-23)

Available online at: www. Ijcoe.org

THE EFFECT OF MONSOON ON THE IRANIAN COASTS IN THE GULF OF OMAN

Saeed Daneshmehr[1], Mohammad Reza Khalilabadi[2*], Mohammad Akbarnezhad Baie
[1] *Faculty of Naval Aviation, Malek Ashtar University of Technology*
[2] *Faculty of Naval Aviation, Malek Ashtar University of Technology*

ARTICLE INFO

Article History:
Received: 14 Jan. 2024
Accepted: 09 Mar. 2024

Keywords:
Monsoon
Monsoon Line
Gulf of Oman
Chabahar Bay
Pazm Bay

ABSTRACT

Monsoon is a very important meteorological phenomenon that affects a large part of the Indian Ocean every year. These effects sometimes extend to the seas and bays connected to this ocean, especially the Gulf of Oman, and have destructive effects on the economic activities of this area. Although the effects of monsoon on the coasts of Iran are much less than the coasts of the Arabian Sea, but local reports indicate that the monsoon usually affects two bays belonging to Iran, Chabahar Bay and sometimes Pazm Bay in the northeast of the Gulf of Oman. In this research, the monsoon phenomenon in the northwest of the Indian Ocean has been analyzed in order to investigate its effects on the waters of the Gulf of Oman. One of the important results of this study is the extraction of Monsoon Line. In this syudy, the monsoon line is defined as the boundary line of the monsoon. This line, if we call it the Monsoon line, indirectly connects Ras Al-Had to the west of Chabahar Bay and sometimes also includes Pazm Bay.

1. Introduction

Indian Ocean monsoon is a well-known phenomenon that strong monsoon winds periodically affect most of the western parts of the Indian Ocean. This phenomenon starts in late spring and continues until almost the end of summer.

Although the effects of monsoon on the coasts of Iran are much less than the coasts of the Arabian Sea, but local reports indicate that the monsoon usually affects two bays belonging to Iran (namely, Chabahar Bay and sometimes Pazm Bay), which are located in the northeast of the Gulf of Oman. But its effects are rarely reported in the west of Pezem Bay. It has even sometimes been observed that monsoon storms have entered to the inner regions of the Gulf of Oman. For example, in June 2007, Hurricane Gonu swept across large parts of the Gulf of Oman and even affected parts of the Iranian coast[1]–[3]. The Gulf of Oman is a deep waterway that connects the Persian Gulf to the Indian Ocean. Due to the importance of this water basin, many studies have been done, especially in the field of oceanography and ocean engineering in this region[4]–[16]. This study was conducted to determine the extent to which the effects of the Indian monsoon typically enter the Gulf of Oman, and what parts of the coast of Iran are affected.

2. 2. Material and Methods

In this research, the studied area is the Northwest Indian Ocean and the Gulf of Oman. The northwest region of the Indian Ocean experiences the monsoon phenomenon every year. In this study, atmospheric data related to the study area in the months of monsoon occurrence were extracted and analyzed. In order to investigate the effects of monsoon winds and the resulting waves, wind field, wave statistics and swell have been analyzed. The ECMWF database is used to achieve this goal. This database is a reliable source that has been used as a reference for many studies[17]–[21].

3. Results

Figure (1) shows the wind field in the northeastern Indian Ocean during the Monsoon period. Figure (2) shows the wave field in the northeastern Indian Ocean during the Monsoon period. As this figure shows, a definite boundary has been formed between the Monsoon area and the Gulf of Oman. This line, if we call it the Monsoon line, indirectly connects Ras Al-Had to the west of Chabahar Bay and sometimes also includes Pazm Bay (figure 3).

precipitation. These data are usually accessible from databases such as ECMWF or NOAA [8].

Although the effects of monsoon on the coasts of Iran are much less than the coasts of the Arabian Sea, but local reports indicate that the monsoon usually affects two bays belonging to Iran (namely, Chabahar Bay and sometimes Pazm Bay), which are located in the northeast of the Gulf of Oman. But its effects are rarely reported in the west of Pazm Bay. It has even sometimes been observed that monsoon storms have entered to the inner regions of the Gulf of Oman [9].

The Gulf of Oman, including Pazm Bay, is influenced by the southwest monsoon winds of India during the summer. This monsoon brings changes to the marine environment, impacting factors such as fisheries, plankton biodiversity, and larval fish assemblages in bays along the Gulf of Oman. The onset of the summer monsoon contributes to enhanced fisheries in coastal bays like Pazm Bay. It's important to note that studies have been conducted on the effects of monsoons on various aspects of marine life in different bays within the Gulf of Oman, highlighting the significant impact of these seasonal winds on the ecosystem [10] [11].

For example, in June 2007, Hurricane Gonu swept across large parts of the Gulf of Oman and even affected parts of the Iranian coast(10,16,17). The Gulf of Oman is a deep waterway that connects the Persian Gulf to the Indian Ocean. Due to the importance of this water basin, many studies have been done, especially in the field of oceanography and ocean engineering in this region(1,2,5–9,11–15,18). This study was conducted to determine the extent to which the effects of the Indian monsoon typically enter the Gulf of Oman, and what parts of the coast of Iran are affected.

2. Material and Methods

In this research, the studied area is the Northwest Indian Ocean and the Gulf of Oman. The northwest region of the Indian Ocean experiences the monsoon phenomenon every year. In this study, atmospheric data related to the study area in the months of monsoon occurrence were extracted and analyzed. In order to investigate the effects of monsoon winds and the resulting waves, wind field, wave statistics and swell have been analyzed. The ocean-atmosphere database is used to achieve this goal. This database is a reliable source that has been used as a reference for many studies(3,4,19).

To analyze the impact of the Indian monsoon on the waves in the Oman Sea, we can follow the steps below. In the following, the necessary materials and methods for our analysis are described in detail and a block diagram of the work steps is presented [12] [13].

2.1. Materials

The main materials used in this research can be categorized as follows [14] [15]:

a) Dataset:

For atmospheric and oceanic data analysis, there are several databases that can help you get accurate and comprehensive information. In the following, some valid databases are introduced:

- ECMWF (European Medium-Term Weather Forecast Center):
  - Weather data provider including forecasts and observations of pressure, temperature, humidity, precipitation, etc.
  - Wave and ocean data are also available in this database [16].
- NOAA (US National Oceanic and Atmospheric Administration):
  - Includes atmospheric and oceanic data, such as temperature, precipitation, ocean currents and hurricane statistics.
  - GHCN (Global Historical Climatology Network) database for historical climate data [17].
- NASA (United States National Aeronautics and Space Administration):
  - Providing climate and ocean data through projects such as MODIS (Moderate Resolution Imaging Spectroradiometer) and other space missions [18].
- Copernicus Climate Change Service (C3S):
  - This database contains a set of climatic and atmospheric data that includes forecasts and observations [19].
- World Ocean Database (WOD):
  - A global database of ocean observations, including temperature, salinity, oxygen and other parameters [10] [20].
- Global Historical Climatology Network (GHCN):
  - A collection of historical climate data including temperature and

precipitation from different stations around the world [21].

- Argo Project:
    - A global project that includes ocean depth observations through automatic floats [22].

These databases are useful sources for analyzing atmospheric and oceanic data [23]. Depending on the type of analysis we want to do, we can take advantage of these resources. In this research, due to some factors such as the amount of access to the data of the target area and accessibility, etc [24]., from the ECMWF dataset was used. access to the ECMWF database, in particular:

- wave data (significant wave height, wave period, wave direction)
- Atmospheric pressure data.

b) Software tools**:**

There are many tools and software for analyzing and displaying atmospheric-oceanic data, for example, these can be mentioned:

- Python or R for data analysis
- Libraries: NumPy, Pandas, Matplotlib for Python; dplyr, ggplot2 for R.
- GIS tools (such as QGIS) if spatial analysis is needed
- Statistical software (such as R or SciPy in Python) for regression analysis
- Ocean Data viewer packages such as ODV, Ferret, etc., in order to analyze and display atmospheric and oceanic data in terrestrial coordinates [25].

c) Hardware requirements:

A computer with enough processing power and memory to manage big data.

2.2. Methods

In order to analyze the corresponding atmospheric and oceanic data in the monsoon months, as well as to investigate its effects in the Gulf of Oman [26], the following steps and methods were followed:

a) data extraction:

- Extraction the relevant datasets from ECMWF for the study period that includes the Indian monsoon season (June to September).
- Ensuring that the data includes wave and atmospheric parameters [7].

b) Data preparation:

- Dataset cleaning by managing missing values and outliers.
- Converting data into a usable format (such as time series) [27].

c) Data analysis:

- Correlation analysis between monsoon low pressures and wave characteristics in Oman Sea.
- Using statistical methods such as regression analysis to determine the effect of monsoons on wave height and direction.
- Visualize data trends using graphs and charts [28].

d) Interpretation of the results:

- Interpreting statistical results to understand the relationship between Indian monsoon and wave activities in the Oman Sea.
- Discuss the findings in relation to the existing literature on ocean wave behavior and monsoon effects [29].

e) Documentation:

- Preparation of a report that explains the methods, results and interpretations in detail.
- Inclusion of visual representations of data analysis (graphs, charts) [30].

3. Results

In this study, atmospheric data related to the study area in the months of monsoon occurrence were extracted and analyzed. In order to investigate the effects of monsoon winds and the resulting waves, wind field, wave statistics and swell have been analyzed. To detect anomalies, we used various statistical and machine techniques. By applying these techniques, we can effectively detect anomalies in our datasets or systems.

Figure (1) shows the wind field in the northeastern Indian Ocean during the Monsoon period.

Figure (2) shows the wave field in the northeastern Indian Ocean during the Monsoon period. As this figure shows, a definite boundary has been formed between the Monsoon area and the Gulf of Oman. This line, if we call it the Monsoon line, indirectly connects Ras Al-Had to the west of Chabahar Bay and sometimes also includes Pazm Bay (figure 3).

Figures (4) and (5) show the local wave field and Swell field in Chabahar Bay during the Monsoon period, respectively. The average height of the local wave in this area is about 0.5 meters, while the height of the swell is about 2 meters. This significant difference shows that during the Monsoon period, Chabahar Bay was strongly influenced by the swell caused by the Monsoon.

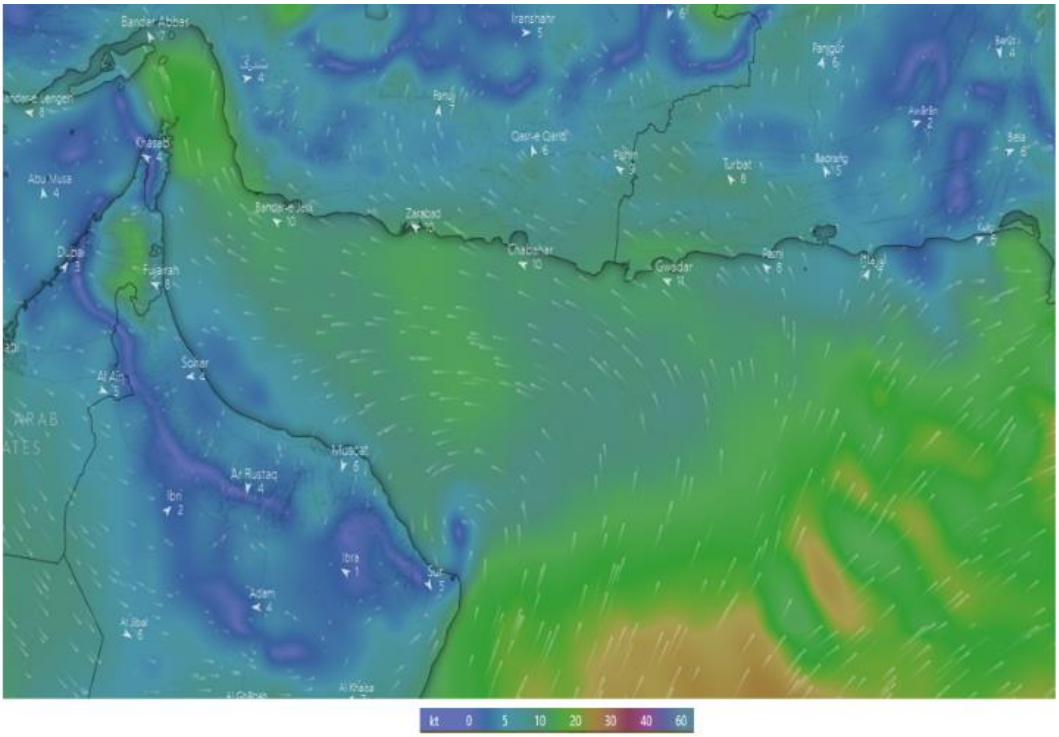

Figure 1. Wind field in the northeastern Indian Ocean during the Monsoon period.

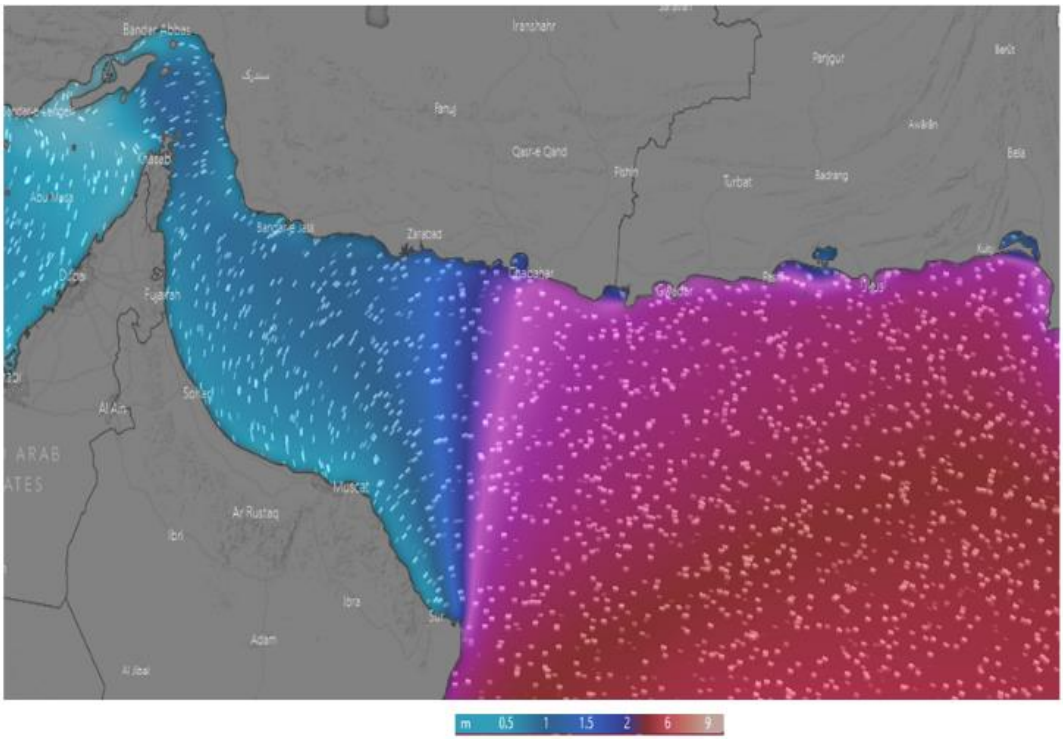

Figure 2. Wave field in the northeastern Indian Ocean during the Monsoon

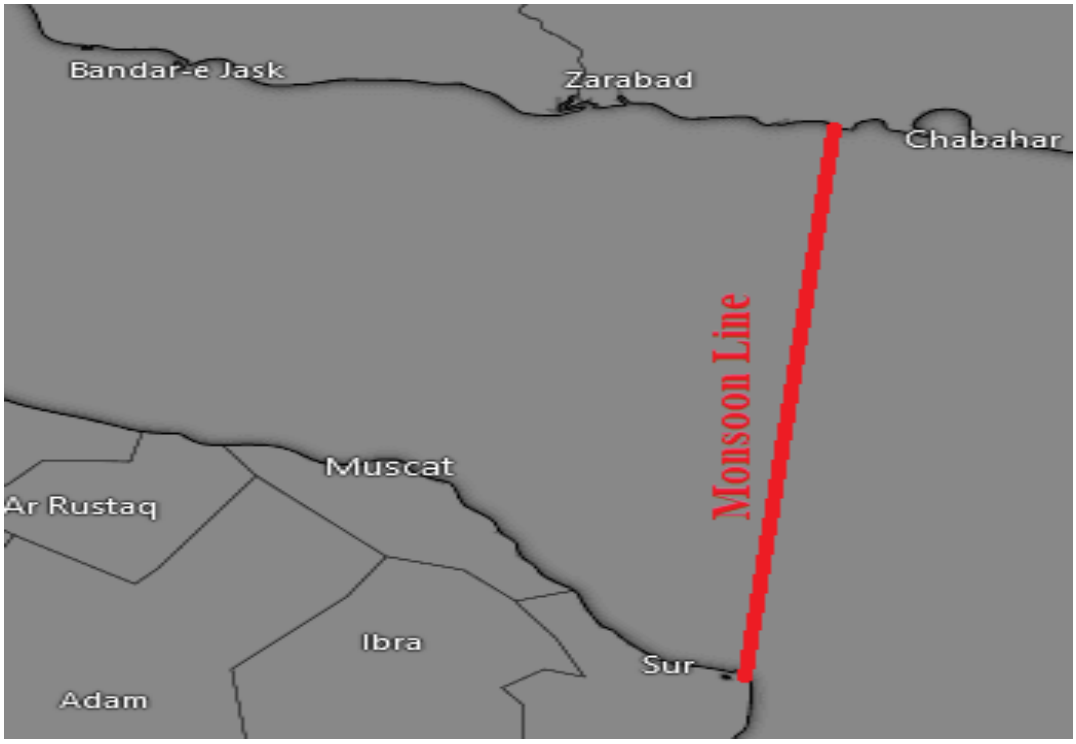

Figure 3. Monsoon Line

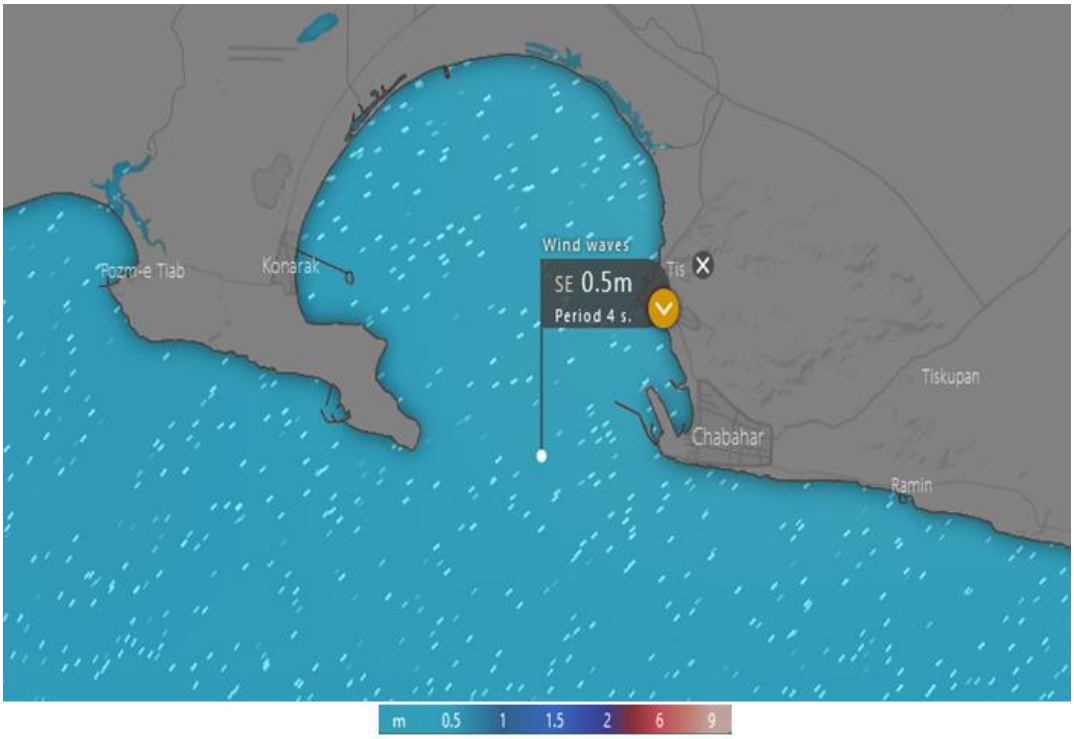

Figure 4. Local wave field in Chabahar Bay during the Monsoon period.

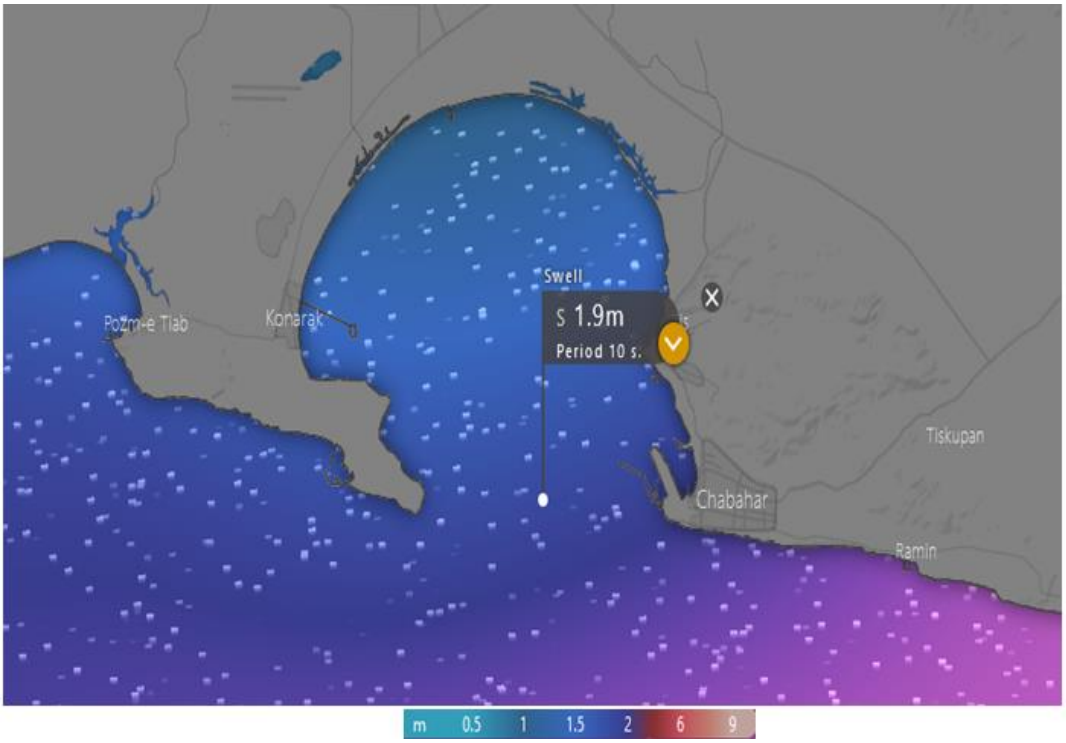

Figure 5. Swell in Chabahar Bay during the Monsoon period.

4. Conclusions

Strong monsoon winds usually affect the western part of the Indian Ocean during the monsoon months. It is rare for monsoon storms, such as Gonu cyclone, to enter the Gulf of Oman. But the study of wind and wave fields in this area shows that the waves that are formed due to monsoon winds and storms in the northwest of the Indian Ocean, enter the eastern part of the Gulf of Oman in the form of swell and affect parts of the coast of Iran. A definite boundary has been formed between the Monsoon area and the Gulf of Oman. This line, if we call it the Monsoon line, indirectly connects Ras Al-Had to the west of Chabahar Bay and sometimes also includes Pazm Bay.

References

[1] Wang, B., Jin, C., & Liu, J, "Global monsoon: Concept and dynamic response to anthropogenic warming," *Mausam*, vol. 74, no. 2, pp. 493-502, 2023.

[2] A. Ghorbani , M.R Khalilabadi, "Positioning using classification and regression: case study of Oman Sea," *International Journal of Coastal and Offshore Engineering*, vol. 4, no. 3, pp. 35-41, 2020.

[3] Zia, A., Rana, I. A., Arshad, H. S. H., Khalid, Z., & Nawaz, A, "Monsoon flood risks in urban areas of Pakistan: A way forward for risk reduction and adaptation planning," *Journal of Environmental Management*, vol. 336, p. 117652, 2023.

[4] Daneshmehr S,Khalilabadi M, "Study of sound speed profile and formation of sound channels in deep waters of North Indian Ocean," *Journal of the Iranian Society of Acoustic Sciences (formerly Acoustic Engineering)*, vol. 11, no. 2, pp. 27-32, 2024.

[5] M. Heidari , M.R Khalilabadi , A. Bidokhti, "Monthly sea level variations in the northern part of Persian Gulf," *Journal of Aqustic Ecology*, vol. 1, no. 3, pp. 10-20, 2012.

[6] Roy, S., Hazra, S., & Chanda, A, "Changing characteristics of meteorological drought and its impact on monsoon-rice production in sub-humid red and laterite zone of West Bengal, India," *Theoretical and Applied Climatology*, vol. 151, no. 3, pp. 1419-1433, 2023.

[7] Bremner, L., Cullen, B., Cane, J., & Geros, C, "Monsoon as method," *cultural geographies*, vol. 31, no. 2, pp. 249-270, 2024.

[8] Sun, X., Wang, H., & Mei, S, "Highway performance prediction model of International Roughness Index based on panel data analysis in subtropical monsoon climate," *Construction and Building Materials*, vol. 366, p. 130232, 2023.

[9] M.R Khalilabadi, "Internal wave generation in the gulf of Oman (Outflow of Persian Gulf)," *Indian Journal of Geo-Marine Sciences*, vol. 44, no. 3, pp. 519-527, 2015.

[10] Khalilabadi, M., Shahmirzaei, H., & Daneshmehr, S, "Underwater acoustic modeling in the Gulf of

Oman," *Journal of Acoustical Engineering Society of Iran*, vol. 10, no. 2, pp. 21-34, 2023.

[11] M.R Khalilabadi, M. Akbari Nasab, "Study of static stability and double diffusion in the Oman Sea," *Iranian Journal of Marine Science and Technology*, vol. 18, no. 71, pp. 11-19, 2014.

[12] M.R Khalilabadi, M. Peimani, N. Kharestani, "Simulation of the effect of the holey-sock drogue on the drifter performance," *Journal of Oceanography*, vol. 13, no. 50, pp. 107-116, 2022.

[13] Zhou, X., Zhan, T., Tan, N., Tu, L., Smol, J. P., Jiang, S., ... & Shen, Y, "Inconsistent patterns of Holocene rainfall changes at the East Asian monsoon margin compared to the core monsoon region," *Quaternary Science Reviews*, vol. 301, p. 107952, 2023.

[14] M.R Khalilabadi, P. Alamdarloo, "Modeling marine currents in the gulf of Oman using the Mike3D model," *Journal of Environmental Science Studies*, vol. 5, no. 1, pp. 2404-2412, 2020.

[15] Lenka, S., Gouda, K. C., Devi, R., & Joseph, C. M, "Dynamics of Indian summer monsoon in different phases," *Climate Dynamics*, vol. 62, no. 1, pp. 473-495, 2024.

[16] Borne, M., Knippertz, P., Weissmann, M., Martin, A., Rennie, M., & Cress, A, "Impact of Aeolus wind lidar observations on the representation of the West African monsoon circulation in the ECMWF and DWD forecasting systems," *Quarterly Journal of the Royal Meteorological Society*, vol. 149, no. 752, pp. 933-958, 2023.

[17] Sooraj, K. P., Aswale, A. M., Swapna, P., Terray, P., & Sandeep, N. S, "Modulations in the Indian summer monsoon–ENSO teleconnections by the North Tropical Atlantic," *Climate Dynamics*, vol. 61, no. 9, pp. 4603-4622, 2023.

[18] Tan, M. L., Armanuos, A. M., Ahmadianfar, I., Demir, V., Heddam, S., Al-Areeq, A. M., ... & Yaseen, Z. M, "Evaluation of NASA POWER and ERA5-Land for estimating tropical precipitation and temperature extremes," *Journal of Hydrology*, vol. 624, p. 129940, 2023.

[19] Kowal, K. M., Slater, L. J., Lopez, A. G., & Van Loon, A. F, "A comparison of seasonal rainfall forecasts over Central America using dynamic and hybrid approaches from Copernicus Climate Change Service seasonal forecasting system and the North American Multimodel Ensemble," *International Journal of Climatology*, vol. 43, no. 5, 2023.

[20] Nguyen-Le, D, "Climatology of the global summer monsoon rainy seasons: Revisited from a high-resolution satellite climate data record," *Atmospheric Research*, vol. 289, p. 106749, 2023.

[21] Applequist, S., Durre, I., & Vose, R, "The Global Historical Climatology Network Monthly Precipitation Dataset, Version 4," *Scientific Data*, vol. 11, no. 1, p. 633, 2024.

[22] Jha, R. K., & Bhaskar, T. U, "Generation and Assessment of ARGO Sea Surface Temperature Climatology for the Indian Ocean Region," *Oceanologia*, vol. 65, no. 2, pp. 343-357, 2023.

[23] M.R Khalilabadi,H Shahmirzaee,S Daneshmehr, "Propagation of ultrasonic radiation in the presence of seabed topography in the North Indian Ocean," *Journal of Oceanography*, vol. 14, no. 54, pp. 87-99, 2023.

[24] M.R Khalilabadi, "2D Modeling of Wave Propagation in Shallow Water by the Method of Characteristics," *Archives of Acoustics*, vol. 47, no. 3, p. 407–412, 2022.

[25] Sahu, N., Das, P., Ratna, S. B., Saini, A., Mallick, S. K., Kumar, A., & Mohapatra, M, "A bibliometric analysis for Indian summer monsoon variability," *Spatial Information Research*, pp. 1-17, 2024.

[26] M.R Khalilabadi,O. Mahpeykar, "Numerical modelling the effect of wind on Water Level and Evaporation Rate in the Persian Gulf," *International Journal of coastal and offshore engineering*, vol. 6, no. 1, pp. 47-53, 2021.

[27] Rajeevan, M., Mohapatra, M., Unnikrishnan, C. K., Geetha, B., Balachandran, S., Sreejith, O. P., ... & Sagar, K, "Northeast Monsoon of South Asia," *Meteorological monograph*, pp. 1-216, 2023.

[28] Ahmad, M. M., & Haider, M. T. U, "Design of Smart Irrigation System in Sone Command Area Bihar for Paddy Crop," *In Information Systems for Intelligent Systems: Proceedings of ISBM 2022*, pp. 25-36, 2023.

[29] Liu, Z., Zhang, Z., Cheng, D., Duan, Z., & Ni, J, " Spatial influence of the Asian Summer Monsoon on pollen assemblages of the Tibetan Plateau and its potential implication for the interpretation of fossil pollen records," *Palaeoclimatology, Palaeoecology*, vol. 625, p. 111690, 2023.

[30] Thacker, M., Kumaran, K. P. N., Hamilton, P. B., & Karthick, B, "Appraisal of Asian monsoon variability in the Indian subcontinent and East Asia through the Quaternary using diatom records," *Earth-Science Reviews*, p. 104622, 2023.

INTERNATIONAL JOURNAL OF
COASTAL & OFFSHORE ENGINEERING
IJCOE Vol.9/No. 2/Spring 2024 (26-37)

Available online at: www. Ijcoe.org

3D Hydrodynamic Numerical Modeling of Gorgan Bay

Seyed Mostafa Siadatmousavi[1*], Alireza Eftekhari[2]

[1] Associate Professor, Iran University of Science and Technology; siadatmousavi@iust.ac.ir*
[2] MSc Student, Iran University of Science and Technology; eftalireza@proton.me

ARTICLE INFO

Article History:
Received: 21 Jan 2023
Accepted: 15 Mar. 2024

Keywords:
Numerical Modeling
Current Speed
Temperature
Air Pressure
Rivers

ABSTRACT

Gorgan Bay (GB) is a semi-enclosed basin located southeast of the Caspian Sea (CS), Iran. The bay was registered as a biosphere reserve in 1976 and had an international focus on conservation. GB severely suffers from low water quality and water level. A hydrodynamic model was used to determine its general circulation, differences in temperature, water elevation, and current speed. This investigation includes the study of current vectors' profiles and analyzing the effects of rivers and air pressure in the circulation of this water body. The average current speed was determined to be 0.1 m/s through the bay. The lowest and highest temperatures were investigated and were -0.53°C and +36.57°C, respectively. The general circulation is mostly counter-clockwise. Water elevation and temperature inside GB always follow a seasonal sinusoidal pattern. This paper neglects the effects of rivers on GB hydrodynamics due to their insignificance discharge. Also, the air pressure has a profound effect on the water level. Current vectors showed that while current speed inside this water body has decreased in the past decade, the temperature increased by almost 7°C.

1. Introduction

Gorgan Bay (GB) is a shallow water body located southeast of the CS. It is partially separated from the sea by Miankaleh Peninsula, an elongated barrier system. The bay currently has two connections to the sea through two narrow channels: Chapaghli and Ashuradeh. GB is about 60 km along the bay axis with a maximum width of about 12 km, with an average depth of about 1.8m [1].

As shown in Figure 1, the bay is relatively isolated from the sea and is characterized by significantly low wave energy [2]. The water level fluctuations of the tide in GB are negligible [3]. Therefore, tidal impacts on physical processes can be ignored, compared to the effects of wind and density gradients in GB [4,5].

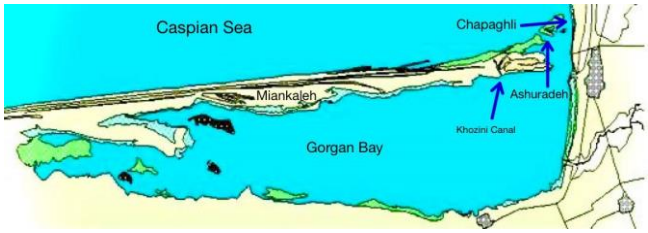

Figure 1. Gorgan Bay [26]

As one of Iran's protected environments, GB is a habitat for migratory birds and the primary habitat for sturgeon fish. GB is the only Iranian bay on the southern shores of the CS that was registered as a biosphere reserve in the Ramsar Convention in 1976.

GB receives fresh water from a number of rivers and small streams that originate in the humid northern slopes of the Alborz Mountain range towards the south. This bay is mostly affected by processes within the basin. The water balance GB is affected by the infiltration of CS water, precipitation, evaporation and a smaller amount of freshwater from the river [9].

Due to the severe influence of CS on the physical properties of GB, decreasing water-level of CS has significantly increased the time residence of the water body, and also resulted in eutrophication. Based on the studies, the continuation of the warming trend of the climate governing the CS in the next century can cause the water level of the CS to decrease by 5 m in the next 75 years [6]. Sharbaty [7], while predicting the impact of the long-term process of lowering the water level of the CS on the life of GB, forecasted by the time that the water level of CS reaches -27.6 m, there is no connection to the CS. Population growth around the bay and industrial and agricultural development has also resulted in discharging wastewater into the bay, which decreased the water quality of this basin and raised some serious concerns regarding the future of this sanctuary [1].

Therefore, there is international concern about GB and the appropriate decisions to restore this water body. One of the significant prerequisites in comprehensive studies on water bodies is performing hydrodynamic research. Hydrodynamic modeling is a powerful tool for describing the flow in water basins. The hydrodynamic modeling has become a part of computational fluid dynamics with the development of technology in numerical models and advanced computing systems [8]. Among The hydrodynamic phenomena in the GB, the wind essentially has an essential role in creating the wave-driven currents, sediment transport, and morphological processes in this basin.

Other than the wind, other factors should be considered when creating the three-dimensional hydrodynamic model MIKE 3 FM Flow Model. This numerical modeling system considers the effects of bed topography, drag forces, river inflows, climatic changes in the water level, and the fluctuation of water discharge in open boundaries. Also, it can determine water levels and layered currents to successfully simulate the estuary, bay, and coastal areas. The MIKE 3 model uses the implicit method with variable direction to temporally and spatially integrate the continuity and equations of motions.
This study uses the ECMWF-ERA5 database to force the MIKE model with the required atmospheric data. To analyze the characteristics of the bay, 18 points, each in 4 layers, were examined. These points are divided into six categories. West, middle, east, mouth, boundary, and deepest part of the bay were studied. The model ran three times under three different scenarios to assess the importance of river and air pressure on the hydrodynamics of the GB as follows:
1) the comprehensive analysis of GB under real conditions.
2) The same as (1) but without the input of its main eight rivers.
3) The same as (1) but without air pressure variations.

2. Materials and Methods

The largest Bay on southern shore of the CS has an area of approximately 400 km^2, an average length of 60 km, and an average width of 12 km. The GB geographical coordinates are from 36.5 to 37 N and from 53,4 to 54.1 E. This Bay is separated from the CS by the Miankaleh Peninsula. Although the length of this peninsula is about 60 km and its average width is 2 km, these numbers change over time due to the Caspian Sea's sea-level rapid fluctuations [11]. The bay stretches from east to west as shown in Figure 1. A narrow and long margin of Miankaleh separates the bay from the sea. Its maximum depth is around 5 m in the southeast and its minimum depth is about 1 m in the western region. GB was connected to the sea by four canals consisting of 3 Ashuradeh islands and the Miankaleh peninsula. However, today there is only one canal between the Bandartorkman and the tip of the peninsula, the small island of Ashuradeh. The rest of the canals in the sea have dried up, the islands of Ashuradeh are connected to the Miankaleh Peninsula, and there is no more islands [12].

2.1 Hydrodynamic Modeling

Mike 3 is a 3D model developed by the Danish Hydraulic Institute (DHI). This model uses the intercellular finite volume method to discretize the governing equations of processes; such as continuity, momentum, and transfer-diffusion equations. These equations are discretized using flexible triangular cells, as shown in Figure 2. The hydrodynamic module of the model is based on the numerical solution of the Navier-Stokes equations, taking into account the Boussinesq assumptions and hydrostatic pressure for an incompressible fluid [14].
The parameters used in the hydrodynamic relations are presented in Table (1).

$$\frac{\partial u}{\partial x}+\frac{\partial v}{\partial y}+\frac{\partial w}{\partial z}=S \tag{1}$$

$$\begin{aligned}\frac{\partial u}{\partial t}+\frac{\partial u^2}{\partial x}+\frac{\partial vu}{\partial y}+\frac{\partial wu}{\partial z} &= fv-g\frac{\partial \eta}{\partial x}-\frac{1}{\rho}\frac{\partial P_a}{\partial x}\\ &-\frac{g}{\rho}\int_z^{\eta}\frac{\partial \rho}{\partial x}dz-\frac{1}{\rho h}\left(\frac{\partial s_{xx}}{\partial x}+\frac{\partial s_{xy}}{\partial y}\right)+F_u\\ &+\frac{\partial}{\partial z}\left(v_t\frac{\partial u}{\partial z}\right)+u_sS\end{aligned} \tag{2}$$

$$\begin{aligned}\frac{\partial v}{\partial t}+\frac{\partial v^2}{\partial x}+\frac{\partial uv}{\partial y}+\frac{\partial vw}{\partial z} &= fu-g\frac{\partial \eta}{\partial y}-\frac{1}{\rho}\frac{\partial P_a}{\partial y}\\ &-\frac{g}{\rho}\int_z^{\eta}\frac{\partial \rho}{\partial y}dz-\frac{1}{\rho h}\left(\frac{\partial s_{yx}}{\partial x}+\frac{\partial s_{yy}}{\partial y}\right)+F_u\\ &+\frac{\partial}{\partial z}\left(v_t\frac{\partial u}{\partial z}\right)+v_sS\end{aligned} \tag{3}$$

2.2 Model Setup

This study uses the Iranian National Institute for Oceanography field data of 5 RCM instruments to calibrate the model. The ECMWF-ERA5 database was used to implement the MIKE model with data along with important river inputs, bed resistance, atmospheric radiation data, and sea level air pressure changes. The bathymetry map is one of the most critical inputs of hydrodynamic models because there needs to be more precision in modeling the geometric boundaries to simulate the desired phenomenon correctly. The Iranian National Institute provided the bathymetric data for simulations.

Table 1. Parameters used to present model equations

Parameter symbol	Parameter definition	Parameter symbol	Parameter definition
$h = \eta + d$	Total water depth	Z,y,x	Cartesian coordinates
w,v,u	Flow velocities in order z,y,x	η	Water level elevation
$f = 2\Omega sin\phi$	Coriolis force	D	Constant water depth
ρ	Water density	G	Earth's gravitational acceleration
$S_{xx}, S_{xy}, S_{yx}, S_{yy}$	Reflective stress tensors	V_t	Vertical vortex viscosity
P_a	Atmospheric pressure	ρ_0	Water reference density
u_s, v_s	The velocity of water flowing from a point source	S	Discharge Springs

The measurement file was completed in the Mesh Generator-MIKE ZERO environment. The selection of the computing network should be done according to the accuracy and cost of computing so that the results are independent of the computing network. A grid with a large size causes wrong results, and a grid with a minimal size causes the volume of calculations to increase tremendously. After making a series of volumetric files and testing the accuracy of their results, the file presented in Figure 2 was selected as the optimal computing grid [8].

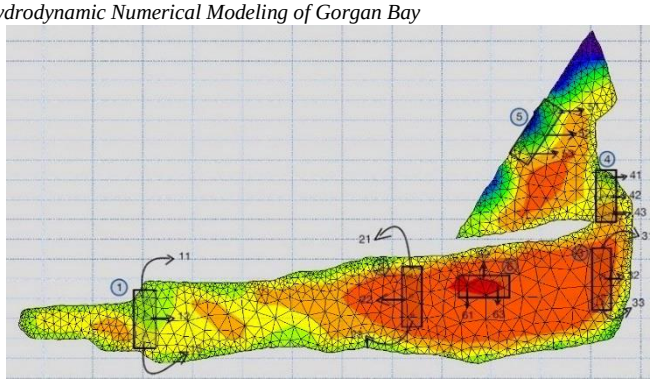

Figure 2. The mesh file and 18 points selected for the study

Wind force has been used as a variable in space and time as an essential factor in shaping the currents of the Bay and gathered from the ECMWF data center to investigate the current patterns of GB. In addition, the inflow discharge of 8 rivers to GB (Qarasu, Baghu, Gaz, Sar Kalaneh, Nokandeh, Golugah, Rostam Kala, and Behshahr) has been incorporated. The boundary conditions of water level fluctuations were enforced to the boundary using outputs of a large-scale calibrated FVCOM model [10].

To include the effects of solar radiation, the data of air temperature, relative humidity, and 2m surface temperature of GB from the data of the ECMWF-ER5 database, which have sufficient accuracy in performing numerical modeling, have been used. Latent heat, sensible heat, short and long wave radiation are all numerically entered into the model according to Valizadeh [10].

A four-layered 30 seconds time steps Mike 3 FM model was performed to simulate a three-dimensional pattern due to wind, bottom topography, precipitation, evaporation, air pressure, and principal rivers leading to GB. Three years of the simulation were performed to investigate such effects on the hydrodynamics of GB. Four sigma layers were employed as more layers only increased the cost of calculations and did not have a significant effect on the accuracy of the results. Barotropic pressure modeling and vortex viscosity are considered with the Smagorinsky formulations with a constant value of 0.28. Also, bed resistance roughness was set at 0.05 m.

2.3 Calibration, Validation, and Stability

The calibration process was performed by comparing the Iranian Institute for Oceanography field measurements of the measured points with the model output. In Table (2) and Figure (3), the names and locations of five measuring stations by the National Institute of Oceanography are evident. From August 10, 2019, to August 25, 2019, the temperature and current speed at these points were measured and recorded by the National Institute of Oceanography. Pearson's correlation coefficient was used to study model output and field data accuracy. For a statistical population, the correlation coefficient of the population is defined as follows:

$$\rho_{(X,Y)} = x = \frac{\mathrm{cov(X,Y)}}{\sigma_X \sigma(Y)} = \frac{E[(X-\mu_x)(Y-\mu_Y)}{\sigma_X\ \sigma_Y} \quad (4)$$

Figure 3. Locations of RCMs

Table 2. Stations, position, and depth of RCMs

Installation Depth (m)	Installation Position		Stations
	Longitude	Latitude	
1,1	54° 2.355'E	36° 53.919'N	RCM9-1
1.5	54° 2.212'E	36° 53.952'N	RCM9-2
1.8	54° 1.918'E	36° 54.022'N	RCM9-3
2.4	54° 1.536'E	36° 54.113'N	RCM9-4
2.5	54° 1.322'E	36° 54.163'N	RCM9-5

where cov is the covariance, σ_X is the standard deviation of variable X, μ_X is the mean of variable X, and E is the mathematical expectation. According to this method, model output and field data's correlation coefficient is 0.72. Figure (4) shows the temperature measured in the middle of the mouth at a depth of 1.8 m by the device installed at this depth in a period of 2 weeks compared with the modeling data.

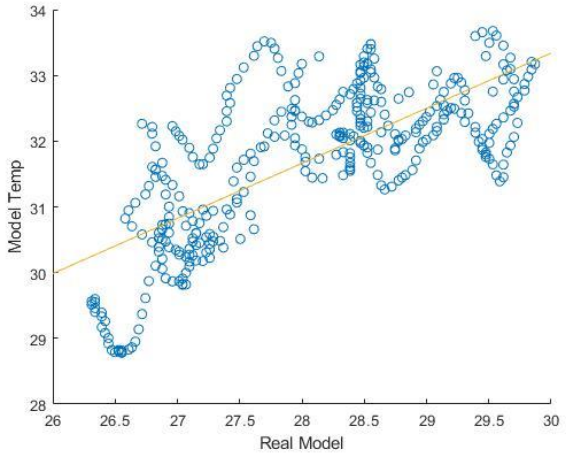

Figure 4. Calibration of Model and in situ data

3. Results and Discussion

3.1 Temperature

As shown in Figure 2, 18 points, each in 4 layers, were examined to analyze the Bay's temperature. These points are divided into six categories. 1. West, 2. Middle, 3. East, 4. Mouth, 5. Boundary, and 6. The deepest part of the Bay was studied. Each of these sections was studied separately and compared with each other. For better identification, these points are coded so that the first digit from the left represents the studied profile, and the next two digits are the location of the discussed point and the layer where the point is studied, respectively.

As shown in Figure 5, the temperature fluctuations were studied across the entire Bay. The temperature inside the Bay has changed sinusoidal in all places and all layers during different seasons. The study of temperature changes revealed that the lowest temperature reaches -0.05°C, and at the highest temperature, it reaches +36.5°C. It should be noted that with all existing similarities, the average temperature of the entire Bay is 20.4°C, and also, due to the heat received from the sun, the average temperature in the surface layer experiences a higher temperature than the average temperature in the bottom layer of GB.

Another issue that should be mentioned is the visible temperature difference at different points on the surface and bottom of GB in the same period. In the winter season, we experience a temperature difference of more than 12°C on the surface of the western part of the bay and the model border. This temperature difference can also be seen with a slight decrease at the entrance of the bay, so that in the hot season, on average the surface and bottom of the GB in the western part experience a lower temperature than the eastern areas. This temperature difference, although insignificant, can also be seen from the north to the south of the Bay; so, as we move from the northern coasts (Miankaleh) to the southern coasts, we will see an increase in temperature.

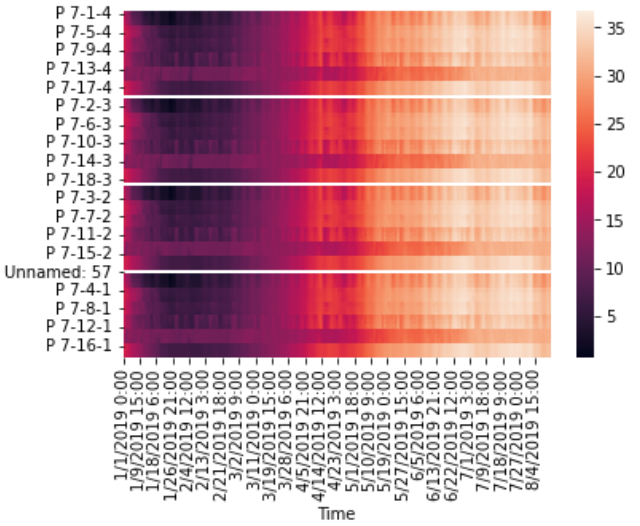

Figure 5. Temperature at different points inside GB

3.1.1 Western section of the Bay

In the western part of the bay, which is more affected by changes in temperature and water level of GB due to its distance from the mouth of the bay, its depth, and also due to the topography of the region, the temperature has similar behavior in all layers. The research results indicate that the water temperature in

GB is greatly influenced by the seasonal temperature fluctuations of the bay.

The temperature on the northern coast of the western side of GB experiences a temperature difference of 1°C on average in all seasons of the year. The average temperature is relatively high from 11 June to 9 September in all layers, and the temperature of 35.6°C is the highest temperature calculated in the layer near the bottom of the bay. The lowest temperature was measured as -0.53°C in the surface layer on the northern shores of the western part of GB. In all layers, as we move from the northern coasts to the southern coasts, it gets hotter, as well as the middle of the bay in the western part, which experiences its lowest temperature in the bottom layer of the bay.

Also, the temperature gradually decreases from the surface to the bottom of the Bay.

3.1.2 Middle section of the Bay

The temperature changes in the layers are noticeable in the middle part of the Bay since the most significant depth of the Bay is located there. GB receives fresh water from several rivers and small streams that originate in the humid northern slopes of the Alborz Mountain range towards the south [18]. In the summer season, we see the highest temperature on the southern coasts, and in the winter season, we see the lowest temperature. Most temperature fluctuations occur on the southern coasts of GB. Unlike the western part of the bay, in the deep part of the bay (middle), the distance between the temperatures in different layers is more different as the depth increases. In the middle part, the temperature changes fluctuated between 2.56 and 36.62°C; Thus, GB is very much affected by seasonal temperature fluctuations in the Bay. Like the western part of the Bay, the maximum and minimum temperatures occur in July and January, respectively. The average temperature in this profile is 20.7°C, and it should be kept in mind that as the winter season approaches, the temperature will decrease as one moves from the northern coast to the southern coast. This process of change will be repeated in all layers.

3.1.3 Eastern section of the Bay

The eastern part of GB is the closest point to the mouth of the Bay and the rivers that flow into it. Various permanent and seasonal rivers flow into the Bay from the southern and eastern parts of the Alborz Mountain range, including the Qarasu and Gorganrod rivers in the northeast of the Bay, with an average discharge and annual sediment of about 0.5 million cubic meters and 3.5 million tons are the most important of them. GB, in January and March seasons, experiences relatively lower temperatures in all layers compared to the western and central part of the Bay, but the behavior of those places, like other parts of the interior of the Bay, is seasonally fluctuating. Its maximum and minimum, like in other places, happened in July and December.

Another noteworthy point in the eastern part of the Bay is its temperature behavior. The eastern areas near the mouth of the Bay feel lower temperatures in summer than the middle-eastern and the southeast part of the Bay. Also, they are the warmest point among profiles 1 and 2 in the winter season. By moving from the northeast to the southeast, the minimum temperature decreases. With a temperature of 2.4°C, the minimum temperature in the surface layer southeast of the Bay occurs in profile 3.

3.1.4 Mouth of the Bay

Temperature changes in the winter season are not more significant in any place inside GB than outside its mouth. Ashuradeh mouth - Bandar Turkman, located in the northeast of GB (approximately 400 m wide, 3 km long, 1.5 m average depth), where intense water exchange with GB takes place, witnesses a minimum temperature range of 2.56 and a maximum of 35.96°C. In winter, there is a temperature difference of more than 8°C in just over two days.

In the research conducted in the past by Ranjbar and Hajizadeh [3], they also witnessed seasonal temperature fluctuations in the GB and reported the maximum and minimum temperatures in the seasons of July and December. The temperature range of the bay in this research was at a minimum temperature similar to the current research, but the highest temperature recorded in their research was 29.2°C, which is lower than the current study, which may be due to the difference in the years in which the modeling was done. This finding indicates the warming of the bay over time, which is considered a climate risk and may eventually lead to the destruction of the bay.

3.1.5 Boundary of the Model

The highest minimum among all points in GB was recorded at model's boundary. The lowest temperature is 7.7°C, and the highest temperature is 32.4°C, which is the lowest among other parts of the Bay. In the bottom layer of GB, we see a temperature range of 9.91 to 31.83°C at point 511 near the model boundary. The border points of the model have the lowest temperature in the summer season and the highest temperature in the winter season.

3.1.6 The comparison of temperature of the Mouth and the Farthest Part from the Mouth

Six points have been identified in the mouth of GB and the western areas of GB, which are further away from the mouth. The minimum temperature of the mouth of the Bay is 2°C warmer than the temperature of the western parts of GB. The study shows that the mouth and the west of the Bay experience the exact temperature of 35°C in summer. However, these two

points will feel a temperature difference of nearly 10°C in winter. The mouth of the Bay experiences a much higher temperature. The temperature difference in the mouth of the Bay and the western areas reaches its maximum value from 10 December to 10 March. This difference of nearly 10°C is continuously repeated in all layers. It is worth noting that in most of the modeling time, the mouth of GB feels a higher temperature than the western region of the Bay.

3.2 Water Level

The pattern of water level changes in GB, which is shown in Fig (6), is similar in the western, central, eastern, and deep parts, with few differences, and most fluctuations in the water level occur at the mouth of the bay and the boundary of the model in the CS. It is known that water level fluctuations in GB have a seasonal behavior such that from April to mid-August, the trend of surface water fluctuations in the Bay increases, and from mid-August to mid-February, a decreasing trend occurs, but with high fluctuations.

Fluctuations of the water level in the western part with an average, a minimum, and a maximum of 0.02, 0.04, and 0.22 m, respectively. From the western part of the Bay to the middle, there is an increase in depth and the height of surface fluctuations; So, in the middle part of the Bay, average and minimum fluctuations are 0.03 and 0.22 m, respectively. Fluctuations in the eastern part of the Bay behave similarly to the western part and maintain their average of 0.02 m. There is a sinusoidal behavior in the water height at the boundary of the model so that in the second six months of the year, it has a downward behavior, and in the first six months of the year, it has an upward behavior. It is worth mentioning that the deepest area of GB shows a maximum height fluctuation of 1.19 m.

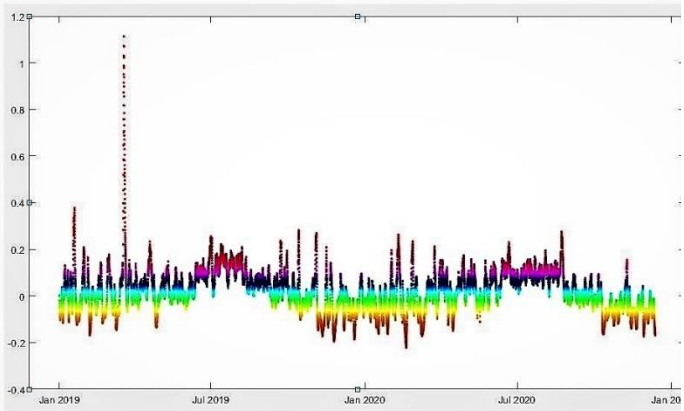

Figure 6. Time series of water level of GB

3.3 Current Speed

As shown in Figure 2, the speed of surface currents was studied at 18 points across GB in four layers. The speed of the currents is shown in Fig (7). At the mouth and the boundary of the model, currents were more substantial than others. Based on the modeling results, the surface layer of water and the bottom layer of GB have a noticeable difference in the speed of currents.

3.3.1 Western Part

The current speed near the southern shores of the Bay in the surface layer is lower than that of the northern shores. From north to south in the western part of the Bay, there was a downward trend in the speed of currents, and the average speed in the northern and southern parts was 0.03 and 0.02 m/s, respectively.

In the layer near the bottom of the GB, the speed of currents in all western parts is more uniform, and they experience lesser fluctuations, unlike the surface layer of the Bay. The average speed in this part is 0.015 m/s, and the maximum speed is 0.01 m/s, slightly higher in the southern part than in the northern part.

3.3.2 Middle Part

The speed on the northern coast in the central part is higher than on the southern coast of this part. The maximum speed is 0.16 m/s in the northern part and 0.1 m/s in the southern coasts, and the average speed of the differential currents is 0.06 m/s. A noticeable difference can be seen between the layer near the sea floor and the surface layer. The speed in the surface layer is higher on the southern coasts than on the northern coasts, but the highest speed occurs in the center of this section. It is worth mentioning that from the bottom of the north to the south of this section, the speed is 0.02 m/s.

3.3.3 Eastern Part

In this section, the difference in the speed of currents in the northern and southern parts was 0.02 m/s. The average speed close to the mouth of the Bay, the central part, and the southern part are 0.34 m/s, 0.19 m/s, and 0.11 m/s, respectively. Like point 314, this layer has the highest speed; after that, the center and south of the Bay experience faster speed respectively. This section's maximum speed currents is 0.23 m/s in the northern part.

3.3.4 Mouth of the Bay

The speed increases from the north of this area to the south. At point 414, the average speed was 0.74 m/s, and the maximum speed was 0.79 m/s. Meanwhile, at point 434, the average and maximum speed, the highest value in the whole bay, are 0.12 and 1.1 m/s, respectively. In the bottom layer, in each region, speed decreases, but the increasing trend of flow speed remains the same from 414 to 434. So the average at point 414 is equal to 0.051 m/s and at point 434 is equal to 0.088 m/s.

3.3.5 Boundary of the Model

In the surface layer at the model's boundary, we see homogeneous velocity fluctuations, the maximum of which is 0.44 in the center of this section, and the average is 0.09 m/s. In the bottom layer, the flow velocity fluctuations have the same trend as the surface layer; the only difference is that they have a difference of 0.1 m/s with the surface layer at all points.

3.3.6 Deepest part of GB

The bay's mid-bottom was studied in this section, which is the deepest part. Its center's maximum and average speeds are 0.1 and 0.017 m/s, respectively.

3.4Study of flow vectors

This study has been done in twelve seasons, the results of the first three have been ignored so that the model is stable and the results are reliable.

3.4.1 Spring

In April, the intensity of currents at the mouth of the bay is very high, and in fact, the highest intensity of currents in GB has been witnessed in this place. Also, currents from west to east can be seen on the northern and southern coasts, considering that the density and intensity of these currents are more visible on the northern coasts than on the southern ones. An eddy current is formed in the center of the bay and the shallow western part.

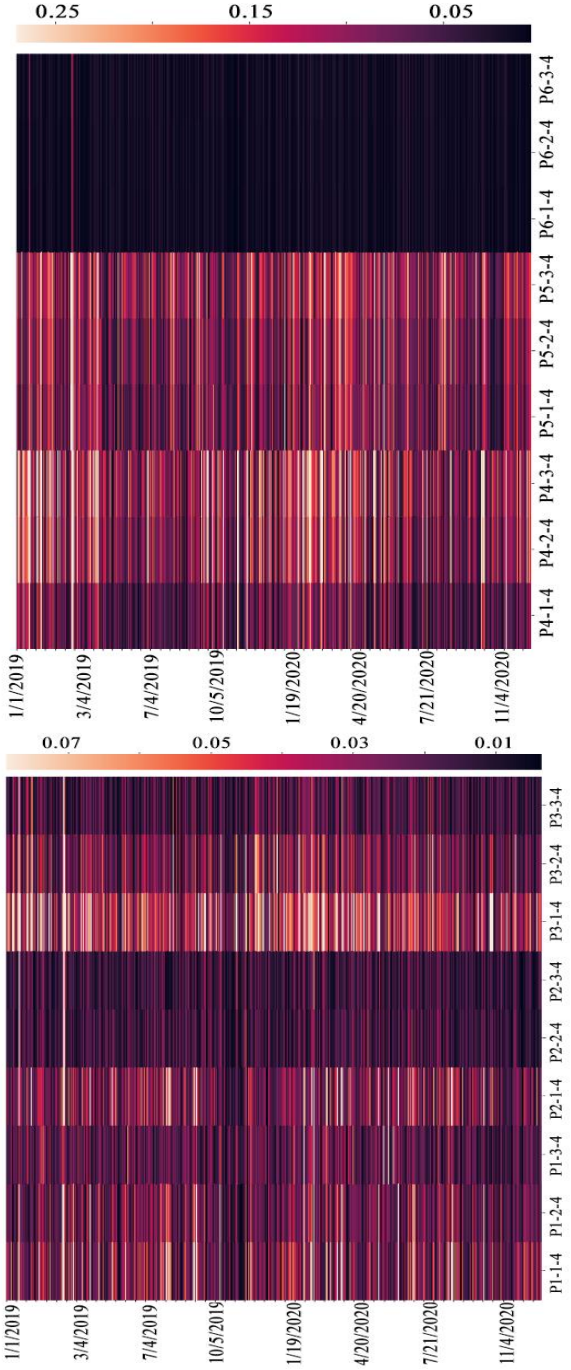

Figure 7 Surface currents of GB – Surface layer of every profiles from north to south coasts

Notably, the model results show the difference in the water level inside and outside GB. The model shows a difference of three centimeters inside the bay compared to its outside. From mid-May to mid-June, we see an increase in the water level in the bay. This increase in level leads to a difference in the level inside the bay so that the right side of the bay is more than one centimeter higher than the western part. The water level continues to rise until the end of the season, but this water level difference can still be seen inside the bay.

The current vectors show that the density and intensity of the current are higher on the northern coasts than on the southern coasts. It also indicates a current from the entrance into GB, and eddy currents are seen in the middle and west of it.

3.4.2 Summer

In the surface layer of the bay, there is a trend from west to east. In this layer, the north shores experience more current than the south shores, and a vortex forms near the mouth of the bay. In this layer, during the summer, the intensity of currents in the shallow part is less and remains constant in the deep part. In the deep part of the bay, there is a counter-clockwise eddy all summer long. The intensity of the currents in the bottom layer, on the north and south coasts, decreases during the summer.

The trend of increasing the water level inside GB continues in July and reaches the most considerable difference in the water level inside the bay in the summer season. During the whole summer, the difference in the level of the eastern and western parts inside GB is quite evident. In July, the currents on the northern coasts are more than on the southern coasts, the density of currents is witnessed at the mouth of the bay, and the eddy currents are visible in the central and western parts of the bay.

In August, the speed of the currents in the north and south coasts and the mouth of the bay reach their lowest level. However, still, the difference in the balance in the eastern and western parts of the bay is seen. From mid-September to mid-October, there is a decrease in the GB's water level, and the currents in the north and south coasts and the mouth of the bay experience a significant increase compared to last month.

3.4.3 Autumn

The currents become more robust and denser as we move toward the mouth of the bay. The currents on the north and south coasts are from west to east. In addition, to counterclockwise eddies, currents from west to east can be seen in the middle of the bay. As November and December are approaching, this time, it is the west of the Bay that has a higher average level than the east. The currents have lost their speed,

density, and intensity in the coasts and mouth of the bay.

3.4.4 Winter

In the winter season, we see a change in the average water level so that in January, the western part of the bay has a higher level than the eastern part. However, this trend changed in March, and this is the right part of the bay, which has a higher average level than the western part. Regarding the currents, as the end of winter approaches, the speed of the currents in all parts is increasing.

3.5 Profiles of flow vectors

This study has been done in four seasons; the results of the first three months of the model have been ignored so that the model is stable and the results are reliable.

3.5.1 Spring

Currents in April in the surface layer and the bottom layer follow a similar trend most of the time. In the surface layer, the flow vectors move toward the opening. The flow density at the opening and boundary of the model is very high. In the bottom layer, the speed of currents in the deep part of the bay is negligible. In May, most of the currents in the surface layer were towards the inside of the bay; the intensity of the currents in this layer near the north and south coasts was higher than the bottom layer.

In the surface layer, a series of currents move from the southern coast to the northern coast, and we also see counterclockwise eddy currents in the deep part of the bay. In June, in the surface layer in the deep part of the bay, currents are from east to west, but on the northern and southern coasts, these currents are along the coasts from west to east. In the bottom layer, counterclockwise eddies occur in the deep part of the bay.

3.5.2 Summer

In the surface layer of the bay, there is a trend from west to east. In this layer, the north shores experience more current than the south shores, and a vortex form near the mouth of the bay. In this layer, during the summer, the intensity of currents in the shallow part is less and remains constant in the deep part. In the deep part of the bay, there is a counter-clockwise eddy all summer long. The intensity of the currents in the bottom layer, on the north and south coasts, decreases during the summer.

3.5.3 Autumn

In the surface layer, counterclockwise eddy currents are formed in the deep part of the bay in October. The currents in the crater are strong, and over time, their intensity decreases during the fall. Currents on the north and south coasts are from west to east. In this layer, in November, the main currents are from west to east, and of course, these currents are insignificant, such as the currents near the north and south coasts. In December and early January, currents move from the mouth into the bay, and a vortex can be seen in the shallow part of the bay, which is located in the west of the bay, during autumn. In the bottom layer, the current on the southern coast is negligible. In this layer, the deep part of the bay has a small current towards the mouth of the bay during autumn, except in November, when eddy currents are seen in the deep part of the bay again.

3.5.4 Winter

In the winter season, two currents occur in two different directions in the surface layer and bottom of GB. The flow in the surface layer is from the mouth to the inside of the bay during winter. Since the middle of January, there have been currents on the northern coasts, but they are not seen on the southern coasts. These currents are insignificant in the deep part of the bay. Moving towards February, the currents become much more potent and can be seen in the mouth, north, and south coasts, as well as in the deep part of the bay. Just like the surface layer of the bottom layer, a similar trend is created for currents during winter; currents move from the bay's sides to the outside.

3.6 Effects of main rivers

GB receives fresh water from several rivers and small streams that originate in the northern wet slopes of the Alborz Mountain range to the south. The construction of dams and the use of freshwater resources in agriculture worsens the bay's condition because of the decrease in the water output of the Gorgan River, Qarasu, and other rivers, as well as the drainages leading to the southern part of the bay. In the last two decades, the rapid drop of the sea level by 150 cm has created unexpected water exchange conditions between the sea and the bay by the existing waterways.

It is evident that the level inside the bay has no significant relationship with the rivers and only depends on its topography and the currents entering its mouth. A model run without considering rivers showed that currents in winter and summer near the northern and southern shores of the Bay cause slight changes in the water circulation pattern. Regarding the velocity vectors, it should be mentioned that only in the layer close to the bottom of GB did minor changes occur on the northern coasts from mid-December to mid-January. These changes can be seen on the southern coasts from mid-August to mid-September.

3.7 Effects of air pressure

In the equations of motion, pressure changes can cause flow changes and create flows on a large scale. It is gathered that the water level inside GB depends on the pressure parameter and the differences are evident in almost all year seasons. Also, velocity vectors affect the pressure parameter near the northern and southern coasts of the Bay from mid-May to mid-June. The lack of pressure has affected the average velocity of currents; So, in the winter season, the

intensity of the velocity vectors in the surface and bottom layer of the bay is less than in no-pressure state. In addition, the absence of pressure in May and June in the bottom layer of the areas near the coast has reduced the intensity of the current vectors.

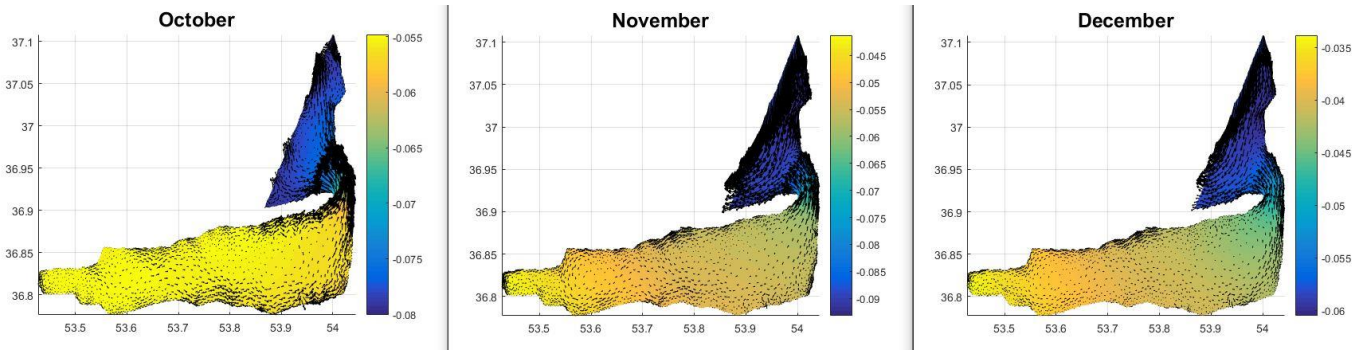

Figure 8. Currents vectors and Water Level in Autumn

4. Conclusions

A bay is a geomorphic and sedimentary basin with a distribution controlled by the geological setting, climate, hydrology of the rivers, eustatic conditions, and the hydrodynamics of waves and longshore currents [19]. Transitional waters such as bays are often exposed to a wide range of stresses associated with the dense human population inhabited by coastal regions. [20] [21] In this research, GB, one of the thirteen biospheres inside the borders of Iran, was studied. This bay was registered as a biosphere reserve in 1976, and there is an international view on its protection [22].

This research studied the fluctuation of hydrodynamic objectives, such as water surface elevation and current speed, under three scenarios to provide findings that can make available important information on adapting suitable decisions relating to the management and restoration of water bodies. The water circulation inside this basin is counterclockwise and a function of wind-induced currents in all the layers. In shallower areas, the transportation of water masses was eastward. In deeper areas, there was westward transportation. Therefore, the circulation of water in GB was composed of gyres. These findings were in agreement with previous studies' findings [3].

The average current speed inside the bay is 0.1 m/s, which is lower than previous studies conducted because water exchange between GB and the Caspian Sea has reached an all-time low. The water circulation inside this basin is counterclockwise and a function of wind-induced currents in all the layers. In shallower areas, the transportation of water masses was eastward. In deeper areas, there was westward transportation. Therefore, the circulation of water in GB was composed of gyres. These findings were in agreement with the findings of previous studies [8, 23,3].

The prevailing wind direction is southwest, which, together with the bathymetry of the bed, is why there is not enough time for water to escape into the deeper areas in the center of the bay. As said in studies of Kheirabadi [4] and Ranjbar and Hajizadeh Zaker [5], GB is highly affected by three factors: a) the Caspian Sea, B) Wind forcing, and C) Geophysical factors in physical terms.

In figures 8 and 9, the background color shows the water level in GB. The water level fluctuates inside and outside of GB and in the eastern and western parts of the bay throughout the year. Its cause is the overflowing of rivers that mostly flow into it from the bay's east, southeast, and south sides. According to Figure (9), it is worth noting that the currents at the bay's entrance are much higher than in other parts of it. Also, from west to east, strong wind-induced currents are seen near the northern and southern coasts, and the average speed of the current on the northern and southern coasts is higher than in its interior areas. Even though the currents in the surface layer and bottom are similar for most of the year, we see a difference in the flow direction in the winter season.

The bay receives freshwater input from 10 small rivers and precipitation; discharge of all rivers into the bay is about 1.3 m^3/s, and the precipitation rate is 30.7 cm/year for the bay. 62% of the freshwater inputs are from the Qareh Sou River, with a flow of 800 L/s. [1] With that said, rivers have not had a significant effect on the flow vectors, and the currents in winter and summer near the north and south coasts of the Bay cause slight changes in the water circulation pattern.

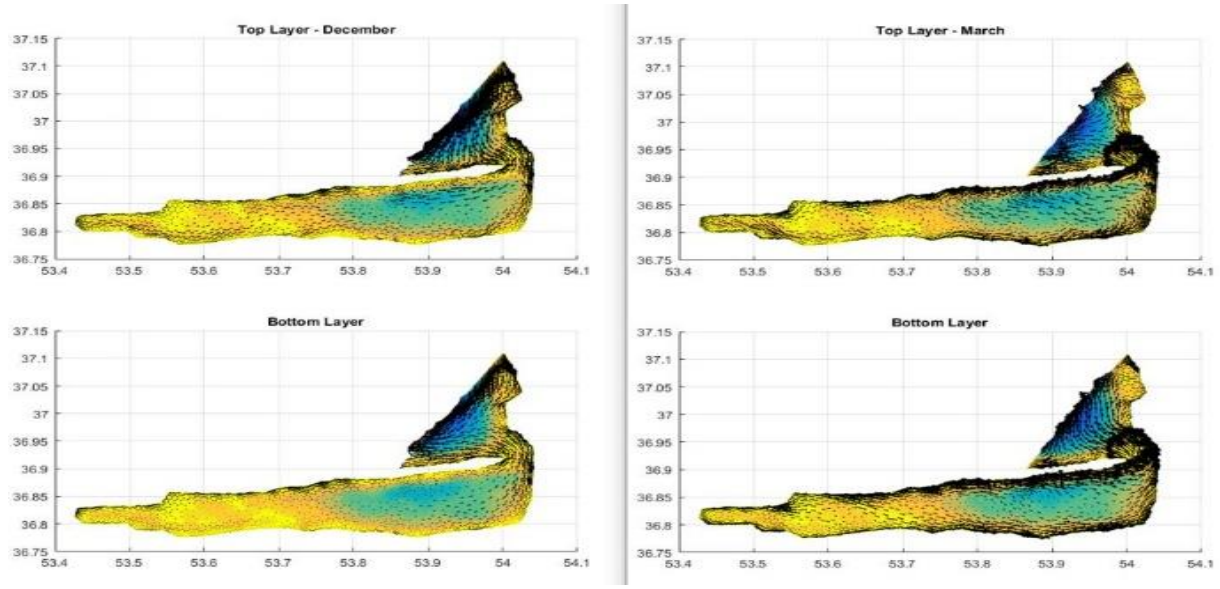

Figure 9. Currents vectors and depth in GB

The water level inside GB is influenced by several factors. One is the water level of the CS and the topography of the bottom of the GB. This study clearly shows that the water level inside GB also depends on the pressure parameter. The lack of pressure has affected the average velocity of currents.

The temperature inside the bay has changed sinusoidally in all places and all layers during different seasons, caused by the seasonal variability of atmospheric fluxes. This result directly correlates with the studies of Ranjbar and Hajizadeh Zaker [3]. The temperature on the northern coasts of the western side of GB experiences a temperature difference of 1 degree on average in all seasons of the year with other places in the west of the bay. Unlike the western part of the Bay, in the deep part of the Bay (middle), the distance between the temperatures in different layers is more different as we go deeper into GB's depth. The minimum temperature in the surface layer of water southeast of the bay occurs in profile 3, with a temperature of 2.4°C.

Temperature changes in the winter season are not more significant in any place inside GB than outside its mouth. The temperature in the coastal areas of GB is the highest, with 36.35°C in July and August. It reaches zero degrees in January on the southern coast, which is its lowest value. In former studies, the maximum temperature inside the bay was estimated at around 29-30°C. However, this paper indicates that the temperature inside the water body has accelerated over the past decade and shows a maximum degree of 36.57°C. This paper finds these effects directly putting GB under stress because of climate change..

Several suggestions are given below for future investigations on the restoration of GB:

1. The restoration of GB requires solutions compatible with the existing ecological and hydro morphological conditions and includes the scenario of long-term reduction of the Caspian Sea water level until the end of the 21st century.
2. According to the results of past studies in this regard and the topography and hydrography maps of the coast, finding the most suitable place to construct the canal can be very important.
3. The reduction of water self-purification in the GB due to the decrease in water volume and disconnection from the CS can also be investigated. Poor water quality has seriously affected the ecotourism and fishing industries on which people depend for their livelihood. As a result, building water quality models for the bay can help improve the residents' quality of life.
4. Predicting the effects of water level reduction on the degree of drought in the international wetlands of Gorgan, Gamishan and Miankaleh under the possible scenarios of water level reduction through computer simulation and using the output results of the model for appropriate planning for the development of vegetation in dry coastal areas to prevent dust. The region helps inland coastal communities such as birds to create ecological nests and increase the population.
5. Estimating the time required for the complete drying of GB and Miankaleh Wetland after being separated from the CS under a set of

climatic and hydrological factors governing the basin.

5. References

[1] Ranjbar, M.H., Alaee, M.J. and Nazarali, M., 2019. A modeling study of the impact of increasing water exchange rate on water quality of a semi-enclosed bay. Ecological Engineering, 136, pp.177-184.

[2] Bastami K, Bagheri H, Haghparast S, Soltani F, Hamzehpoor A, Bastami M (2012) Geochemical and geo-statistical assessment of selected heavy metals in the surface sediments of Gorgan Bay, Iran. Mar Pollut Bull 64:2877–2884

[3] Ranjbar, M.H. and Hadjizadeh Zaker, N., 2018. Numerical modeling of general circulation, thermohaline structure, and residence time in Gorgan Bay, Iran. Ocean Dynamics, 68(1), pp.35-46.

[4] Kosarev A (2005) Physico-geographical conditions of the Caspian Sea. In: The handbook of environmental chemistry. Springer

[5] Kitazawa D, Yang J (2012) Numerical analysis of water circulation and thermohaline structures in the Caspian Sea. J Mar Sci Technol 17: 168–180.

[6] Khairabadi, Hassan and Mohammad Vali Samani, Jamal and Nouri, Ruholah and Ranjbar, Hassan, 2014, 3D simulation of Gorgan Bay hydrodynamics by MIKE3 model FM١٤ث Iranian Hydraulics Conference،Zahedan،https://civilica.com/doc/437909

[7] , Qanqormeh Abdul Azim, Sharbati Saeed,predicting the effect of the long-term trend of lowering the Caspian Sea water level on the life of Gorgan Bay.

[8] Khairabadi, Hassan and Mohammad Wali Samani, Jamal and Nouri, Rooh Elah and Ranjbar, Hassan, 2014، ٣D simulation of Gorgan Bay hydrodynamics by MIKE3 FM model, 14th Iranian Hydraulics Conference, Zahedan, https://civilica.com/doc/437909S. Sharbaty, S. Hosseini, V. Taghizadeh, M.R. Imanpour and S. Gorgin, Two-dimensional modeling in Gorgan Bay Currents influence by sea level changes and wind pattern changes, Proceeding of first Conference of Caspian sea ecology, Sari, Iran, 2010. (In Persian)

[9] Dr. Valizadeh, .(2019). Ph.D. Thesis, 3D Numerical Modeling of Circulation of Caspian Sea

[10] khoshravan, H. (2021). Caspian rapid Sea level fluctuation and intensity of displacement of the shorelines in the Gorgan Bay and Miankaleh coast', International Journal of Coastal and Offshore Engineering, 6(4), pp. 24-32.)

[11] PourSufi, .(2015). Ministry of Jihad Agriculture Agricultural Research, Education and Promotion Organization. Iran Fisheries Science Research Institute - Inland Water Aquatic Reserve Research Center.

[12] Ranjber, H. (1392) ،Investigating the absorption capacity of Gorgan Bay in relation to the input of plant nutrients using numerical modeling, Master's Thesis, Graduate School of Environmental Studies, University of Tehran

[13] DHI. (2007), User Manual Mike3 Flow Model FM, Hydrodynamic Module

[14]. (Payandeh, A., Hadjizadeh Zaker, N., & Niksokhan, M. (2014). Numerical assessment of the nutrient assimilative capacity of Khur-e-Musa in the Persian Gulf. Environmental Monitoring and Assessment, 187, 1–14.).

[15] (Ranjbar, M. H., & Hadjizadeh Zaker, N. (2014). Numerical simulation of currents in Gorgan Bay by PMO dynamics & MIKE 21 FM. Proceedings of 11th International Conference on Coasts, ports and Marine Structures (ICOPMAS), Iran, Tehran.),

[16] Marine Ecological Geography: Theory and Experience - Fashchuk, D.Y.9783642174445-Environmental Science and Engineering https://books.google.com/books?id=B576PjBg0WYC- 2011 Springer Berlin Heidelberg

[17]. Sharbaty, Saeed. "Simulation of wind-driven waves in the Gorgan Bay." Canadian Journal on Computing in Mathematics, Natural Sciences, Engineering and Medicine 3.2 (2012): 40-44

[18] Taheri, M., et al., 2012. Spatial distribution and biodiversity of macrofauna in the southeast of the Caspian Sea, Gorgan Bay in relation to environmental conditions. Ocean Sci. J. Korean Ocean Research and Development Institute and The Korean society of Oceanography 47 (2), 113–122. https://doi.org/10.1007/s12601-012-0012-8.

[19] Cloern, J.E., and A.D. Jassby. 2008. Complex seasonal patterns of primary producers at the land-sea interface. Ecology Letters 11 (12): 1294–1303. https://doi.org/10.1111/j.1461-0248.2008.01244.x.

[20] O'Boyle, S., R.Wilkes, G. McDermott, S. Ní Longphuirt, and C. Murray. 2015. Factors affecting the accumulation of phytoplankton biomass in Irish estuaries and nearshore coastal waters: A conceptual model. Estuarine, Coastal and Shelf Science 155: 75–88. https://doi.org/10.1016/j.ecss.2015.01.007.

[21] Darvishsefat, A., 2006. Atlas of protected areas of Iran. Assistance of ecology and biodiversity. Iranian Environmental Protection.

[22] Kheirabadi, H., et al., 2018. A reduced-order model for the regeneration of surface currents in Gorgan Bay, Iran. J. Hydroinform. 20 (6), 1419–1435. https://doi.org/10. 2166/hydro.2018.149.

[23] Kouhanestani, Z.M., et al., 2018. Assessment of spatiotemporal phytoplankton composition in relation to environmental conditions of Gorgan Bay, Iran. Estuaries Coasts. Springer US 1–17. https://doi.org/10.1007/s12237-018-0451-2.

[24] Sharbaty, S., 2012. 3-D simulation flow pattern in the Gorgan Bay in during summer. International Journal of Engineering Research and Applications (IJERA), 2(3), pp.700-707.

[26] Sharbaty, Saeed. (2012). Two Dimensional Simulation of Seasonal Flow Patterns in the Gorgan Bay. 2. 4382-4391.

INTERNATIONAL JOURNAL OF
COASTAL, OFFSHORE & ENVIRONMENTAL ENGINEERING IJCOE Vol.9/No. 2/Spring 2024 (38-52)

Available online at: www. Ijcoe.org

Optimization of Empty Container Operations by Demand Prediction and Simulation (Case Study: Shahid Rajaee Port)

Seyede Masoome Sadaghi[1*], Iman Shivafar[2], Mohammad Rastad[3]

[1*] *Assistant Professor; Road, Housing & Urban Development Research Center, S.sadaghi@bhrc.ac.ir*

[2] *Port Logistics Expert, Freelance Consultant, Iman.2948@gmail.com*

[3] *Port and Marine Expert, Freelance Consultant, Rastad25@gmail.com*

ARTICLE INFO

Article History:
Received:13 July 2023
Accepted :15 May 2024

Keywords:
Empty containers
Deep learning
Simulation
Optimization

ABSTRACT

With the increasing trend of containerization in large ports, empty container provision and management have become a major logistics service at ports. Every day, a large number of empty containers should be available to be sent to different logistics yards for stuffing and export purposes. The empty container demand forecast can highly improve the time and resource management by both terminal operators and port authorities. In this paper, Shahid Rajaee Port, as the largest and most important commercial port in Iran is investigated. A private terminal operator is the main provider and responsible party for the majority of empty container operations. The optimization process of empty container operations using machine learning and artificial intelligence methods is investigated in this paper. Given the possibility of predicting the demand for empty containers, it is possible to reduce the daily operation volume through advanced planning and consider necessary measures regarding the appropriate spatial distribution of empty containers before the demand arises. A simulation software is also used for different managerial scenarios. The results show that by sending half of the monthly predicted demand of only six out of 75 depot yards as well as the container yard in off-peak times, the total empty container delivery time can decrease up to 30 %. Besides that, planning a schedule for an asynchronous call of trucks to pick up the requested empty containers has proved to reduce the queue lengths and average waiting times up to 90%.

1. Introduction

In Shahid Rajaee port, empty containers are provided to shipping companies in off-deck depot yards as well as container vessels waiting to load empty containers at berths. The management of distribution and delivery of empty containers is carried out after the demand is determined. The process is important because any disruption can cause delays in delivering empty containers resulting in customers' dissatisfaction and even negative impact on the country's export process. An exclusive yard for the storage of empty containers (ECT), is located in the western part of Shahid Rajaee port on a land area of 11.5 hectares, with a static capacity of approximately 17,000 TEU of empty containers based on the layout model and operational constraints. Currently, it is mainly used for storage of 20-foot containers. 40-foot containers, which account for less than 10% of the empty container operations, are stored in another yard in case of emergency situations or insufficient storage space.

Due to the high demand from numerous customers, the management of distribution and delivery/receipt of empty containers is accompanied by many complexities, which, during peak demand, result in queuing and reduced operational efficiency at the port. This issue becomes even more complicated during times when the demand for exporting empty containers by vessels exists since the volume of demand from vessels at the quay is very high and

can lead to improving the performance of this cycle during peak demand and daily operational activities.

2. Related Works

Research in the field of artificial intelligence in container operations management include different issues such as transportation planning and scheduling, optimizing transportation capacity at ports, predicting future demands, resources management, etc. In most studies conducted, artificial intelligence and machine learning have been utilized to provide optimization algorithms for operational management processes. By analyzing historical data related to the transportation of empty containers, machine learning algorithms can identify patterns and predict future needs based on them. This prediction can assist ports in optimizing resource allocation and transportation capacity, thus preventing the need for excess empty containers or addressing their shortage. According to the conducted surveys, many prominent companies in the shipping industry, including Maersk, MSC, and CMA-CMG, as well as companies involved in port operations and logistics chains such as DPworld, directly and indirectly utilize artificial intelligence (AI) in their maritime and port services.

As an example, Nile Dutch Africa Line BV (NileDutch), a large shipping company specializing in container and break-bulk shipping between West Africa and the rest of the world, has utilized AI, machine learning and intelligent algorithms for empty container handling and relocation in collaboration with Transmetrics, a leading provider of predictive optimization and AI tools for logistics. The two partners jointly developed a predictive asset management software to streamline empty container flows which provides daily rolling AI-driven forecasts for the next 10-12 weeks based on the historical data and the external factors influencing the demand. The system also suggests the most optimal and actionable plan for empty repositioning, storage, repair & maintenance for the next 12 weeks, which takes into account all the related costs (including grading, stevedoring, gate costs, etc.). [1]

In 2019, Liu Yuan investigated the effect of machine learning in predicting empty container volumes, using five machine algorithms on the Los Angeles Port and Long Beach Port datasets. The best machine learning algorithms for predicting the volume of empty containers are introduced and compared with existing empirical methods and mathematical statistics methods. He has concluded that machine learning needs to combine multiple models or select more high-correlation feature quantities to improve performance on such prediction problems. [2]

In 2020, Shankar et al. used long short-term memory (LSTM) networks to forecast container throughput of the Port of Singapore. The LSTM model performance was compared with seven different time-series forecasting methods, including autoregressive integrated moving average (ARIMA). The results showed that LSTM outperformed all other benchmark methods. [3]

In 2022, a number of multivariate predictive models based on deep learning were developed to forecast container throughput in the port of Barcelona. The models' performances were assessed to identify the best model architecture and set of hyper parameters. A comparative analysis of the out-of-sample accuracy of some models in predicting the container traffic volume was carried out. [4]

In 2022, two novel approaches based on machine learning and probabilistic techniques were introduced to predict the future weekly availability of empty containers for more than 280 locations worldwide. A data set of more than 100 million events with different stages of container transportation process were used. Both models were based on a two-step forecast logic in which the expected location of a container was first predicted and the timestamp for arriving at that location was estimated afterwards. Artificial neural networks and mixture density networks were used in the machine learning model for the containers' movement forecast. The comparative assessment of the model results versus the actual availability of containers indicated the outperformance of the neural network approach over other approaches concerning every evaluation metric. [5]

Seaport resilience analysis and throughput forecast has been conducted for Busan port in 2022, using a deep learning approach. The mentioned research deals with data analytics for analyzing port resilience and a new paradigm for productivity forecasting that utilizes a hybrid deep learning method. Nonlinear analytical methods have shown that throughput demand at Busan port has a complex behavior due to business fluctuations and uncertainties. A combination of long short-term memory (LSTM) and random forest (RF) approaches have been utilized for port throughput forecasting. The LSTM networks have shown high effectiveness in time-series forecasting tasks and RF is proposed as a complementary method to mitigate residual errors from the LSTM scheme. [6]

The literature review has shown that system simulation tools can be very effective in operational optimization of ports and terminals. Container terminal simulation offers several advantages including performance evaluation, resource allocation optimization, reducing equipment idle times, minimizing vessels and trucks waiting times and improving overall operational efficiency. As an example, in 2015, a simulation of the internal transport system of empty container terminals was conducted using SIMIO software at Delft University of technology. The objective of the study was to determine the most suitable transport system for internal traffic within the terminals. [7]

In 2016, the optimal layout for a container terminal in Sri Lanka was selected using simulation. Considering that container movements within the terminal incur

costs and time, choosing an appropriate layout for the containers can lead to cost and time reduction in terminal operations [8].

Another study regarding the optimization of empty container operations is the simulation of the empty container transfer process between the quay and the terminal at the Tanger Med port in Morocco, which was carried out in 2017. In this study, the design of transfer operations and the simulation of empty containers, considering related activities at the container terminal, were proposed. The simulation was performed using ARENA software for a one-week time frame. The main idea of the modeling was to propose methods for allocating empty containers to storage locations based on vessel destination, movement time, and container type [9].

In 2018, another study was conducted to simulate and analyze container movements using ARENA software. In this study, the terminal's cranes, quay, internal transportation vehicles, and operators were examined. The results of this research provided a new simulation model for a developed terminal dataset, in which the terminal's utilization, waiting time, and resource counts were determined [10].

Another study on optimizing operations at container terminals was the analysis of container dwell time at the Surabaya terminal in the Tanjung Perk port in Indonesia in 2020. This study utilized ARENA software for discrete event simulation to model the terminal's operations and employed the RCA (Root Cause Analysis) method to analyze pre-simulation data. The resulting simulation model was an interpretation of a real system that combined logic and mathematics [11].

Prediction of empty container demands using LSTM method has been conducted for Shahid Rajaee port in 2024 in which the total demand of 72 terminals has been predicted for one month based on 22 months' available data. The predicted result for the representative month demand has shown only 0.3 percent deviation from the real demand value [12], [13].

3. Material and Method

In this section, the available dataset and the methodology for data interpretations are described.

3.1. Available Data Set

In the present paper, AI-based methods have been used to improve the spatial and temporal management of empty container allocation to the off-deck depot yards in Shahid Rajaee Port. The monthly demand of the empty container is predicted based on the demand history which is available on a daily basis for 25 months from August 15, 2021 to September 22, 2023 [14]. The data set includes the number, type, size, loading date, transportation agent, and destination depot yards of empty containers. Based on the initial analysis of the available data during the mentioned time period, out of approximately 245000 allocated empty containers, 93% were 20-foot and 7% were 40-foot. Therefore, the majority of the empty container movements between depot yards are related to the transfer of 20-foot containers. Consequently, the present study focuses on the operations of empty 20-foot containers. The daily and monthly 20-foot empty container allocations to off-deck depot yards and deck container yard (CY) is shown in Figure 1 and Figure 2 respectively. As shown in the Figures, the demands from vessels at CY are occasional but large which led to high total demands for empty containers at the empty container Terminal (ECT) at certain times. Empty containers are sent to various off-deck depots at Shahid Rajaee Port. The monthly average demands of 75 off-deck depots (named T1 to T75) and CY are shown in **Error! Reference source not found.** which indicate that the majority of demands are dedicated to a limited number of depots, and the demands of others are relatively low.

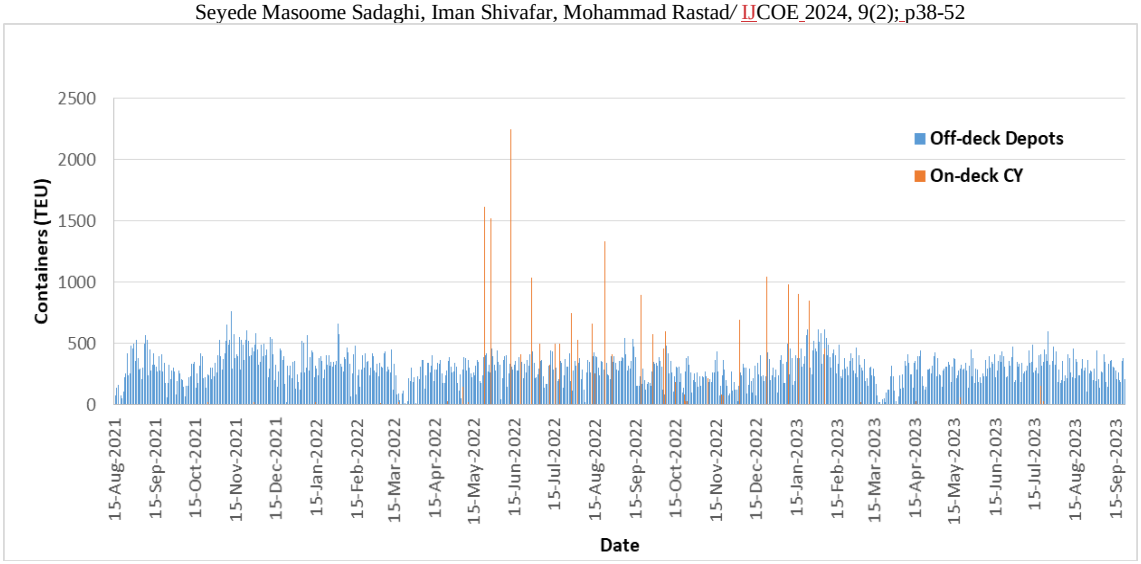

Figure 1. Daily 20' empty container allocations to off-deck depots and on-deck container yard (CY)

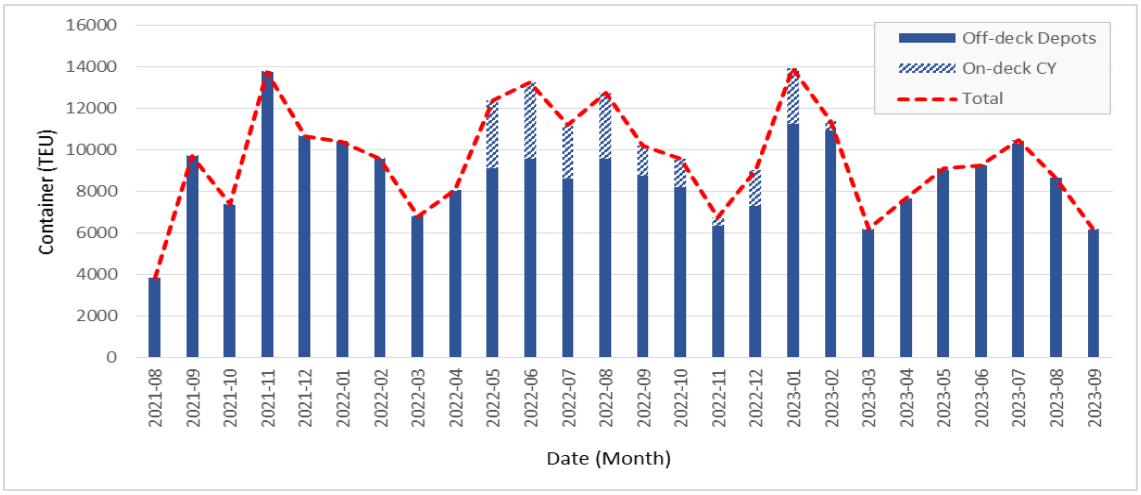

Figure 2. Monthly 20' empty container allocations to off-deck depots and CY

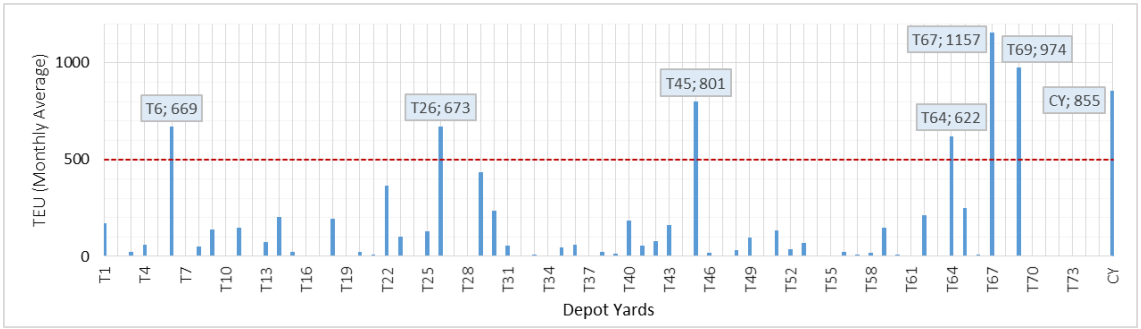

Figure 3. Monthly average demand of off-deck depots and CY

The management of empty container allocation during peak times can be improved by handling the high demand of main requesting depots. In the present study, CY and six main depots with an average monthly demand of more than 500 TEU have been selected for further investigations. The demand prediction is a prerequisite for implementing management measures to reduce the volume of daily operations and provide regular services to customers.

3.2. Methodology

With the advancement of deep learning, new models have been developed for time series prediction, among which Recurrent Neural Networks (RNNs) are considered to be one of the most effective approaches due to their feedback connections that allow information to be circulated within the network, creating a form of memory. However, the RNNs have some limitations in capturing long term dependencies for which, variations of RNNs such as Long-Short Term Memory (LSTM) and Gated Recurrent Unit (GRU) have been developed. The gating mechanism incorporated in these variations, control the flow of

information and determine which data in the sequence is important to be retained and which data should be discarded. The LSTM consists of numerous memory blocks known as cells. The data flow into and out of the cells is controlled by input, output and forget gates. For a time series (X_t), the first cell uses the initial state of the network and the first time step of the sequence to compute the first output and the updated cell state. The state of the layer at each time step consists of the hidden (output) state (h_t) and the cell state (c_t). At time step *t*, the block uses the current state of the network (c_{t-1}, h_{t-1}) and the next time step of the sequence to compute the output (h_t) and the updated cell state (c_t).

The cell state contains information learned from the previous time steps. At each time step, the layer adds information to or removes information from the cell state. The layer controls these updates using *gates*. The input gate (i) controls the cell state update, forget gate (f) controls the cell state reset, cell candidate (g) adds/removes information to/from cell state and output gate (o) controls the cell state added to the hidden state. Figure 4 illustrates how the gates forget, update and output the cell and hidden states at time step *t*.

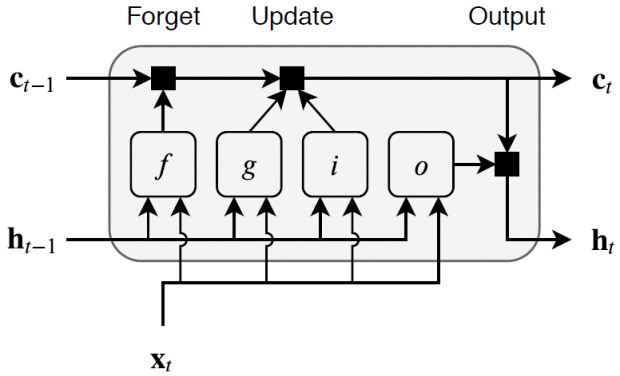

Figure 4. Data flow in LSTM at time step t

The cell state and the hidden state at time step *t* (c_t, h_t) are given by:

$$c_t = f_t \odot c_{t-1} + i_t \odot g_t \quad (1)$$

$$h_t = o_t \odot \sigma_c(c_t) \quad (2)$$

In the above equations, $\odot$ denotes the element-wise multiplication of vectors and σ_c denotes the state activation function for which hyperbolic tangent function ($tanh$) has been used. The gate functions at time step (t) are described by the following formulas:

$$i_t = \sigma_g(W_i \boldsymbol{x}_t + R_i \boldsymbol{h}_{t-1} + b_i) \quad \text{(Input gate)} \quad (3)$$

$$f_t = \sigma_g(W_f \boldsymbol{x}_t + R_f \boldsymbol{h}_{t-1} + b_f) \quad \text{(Forget gate)} \quad (4)$$

$$g_t = \sigma_c(W_g \boldsymbol{x}_t + R_g \boldsymbol{h}_{t-1} + b_g) \quad \text{(Cell candidate)} \quad (5)$$

$$o_t = \sigma_g(W_o \boldsymbol{x}_t + R_o \boldsymbol{h}_{t-1} + b_o) \quad \text{(Output gate)} \quad (6)$$

In these calculations, σ_g denotes the gate activation function for which the sigmoid function given by $\sigma(x) = (1 + e^{-x})^{-1}$ has been used.

The matrices W, R, and b are concatenations of the input weights, the recurrent weights, and the bias of each component, respectively.

This is the structure in which, the network passes important information along the sequence chain to obtain long-term dependencies and mitigate gradient related issues. The LSTM method has been employed to forecast the monthly demands of main depots based on the available datasets. Once the estimated demands for the upcoming month at main depots are determined, it is possible to send a portion of empty containers to the main depots ahead of schedule. Some of these depots even have stripped containers which are normally sent back to ECT while they can be kept if the predictions confirm the requisite. To assess the effectiveness of the proposed scenarios, ARENA software has been used for simulating the operational allocation process.

4. Demand Prediction

In the present study, 25 months of data is available. The initial 24 months of demand data for six main depots have been used for network training and testing. The training process of the network is done on 90 percent of data for adjusting the hyper-parameters to achieve acceptable validation results and the rest of data is used for testing. After training and testing the network, the demand for the 25th month is predicted and compared to the actual values as shown in Figure 5.

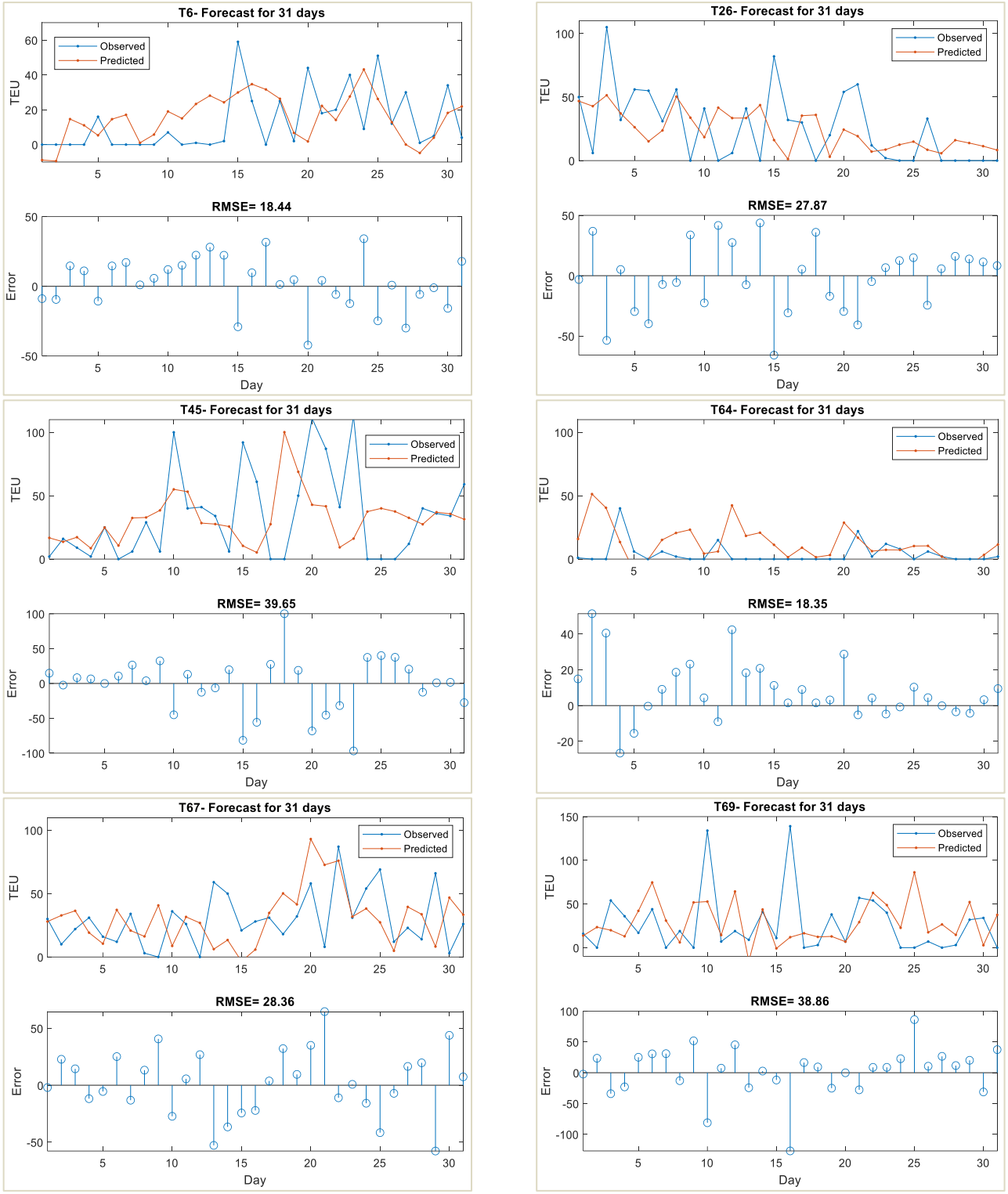

Figure5. Predicted daily demands of 25th month versus actual values for six main depots

As it can be seen in Figure 5, the daily predictions do not always demonstrate perfect alignments with actual demands which might be due to the insufficient length of the input data or the fact that the variation does not follow a regular trend and is very susceptible to different local parameters. However, the sum of daily predicted values for a month can be used as an estimation for the upcoming month's demand. The sum of daily predicted values for the last month is compared to the actual demands in Table 1 which indicates that the predictions are acceptable for most of the selected depots. However, the error is significant in case of T64 depot which could be due to its specific and coincidental circumstances. It is obvious that with the increase in the length of input data in the future, the accuracy of predictions will increase.

Table 1. The predicted versus actual demands for 25th month in six main depots

Depot ID	Actual Demand	Predicted Demand	Error (TEU)	Error (%)
T6	405	477	72	18
T26	804	741	-63	-8
T45	1052	987	-65	-6
T64	124	385	261	210

T67	910	963	53	6
T69	821	896	75	9

5. Simulation of Empty Container Distribution

Knowing the approximate demand of main depots, it is possible to send a portion of demand ahead of the schedule during off-peak times, or utilize stripped empty containers available at the demanding depots. To assess the effectiveness of this approach, ARENA software is used for simulating the operational empty container allocation process in September 2023. Three scenarios have been considered for the simulation as explained below:

i. In the first scenario, the normal condition based on the actual demands of September 2023 is simulated.

ii. An abrupt increase in the CY demand is added to the normal condition. Total demand of 2000 TEU is considered for CY.

iii. In this case, it is assumed that half of the predicted demand for six main depots and CY are pre-sent during off-peak times. The rest of the demand for these depots are kept in the simulation.

Figure 6 shows that a limited number of depots allocate the significant volume of the demand and the share of other depots is negligible. In September 2023, 99.4 % of the total demand was allocated by 30 depots out of 75 depots. In the simulation process, these 30 depots are considered. The distance from ECT to demanding depots and their monthly demands in different simulation scenarios are shown in Table 2.

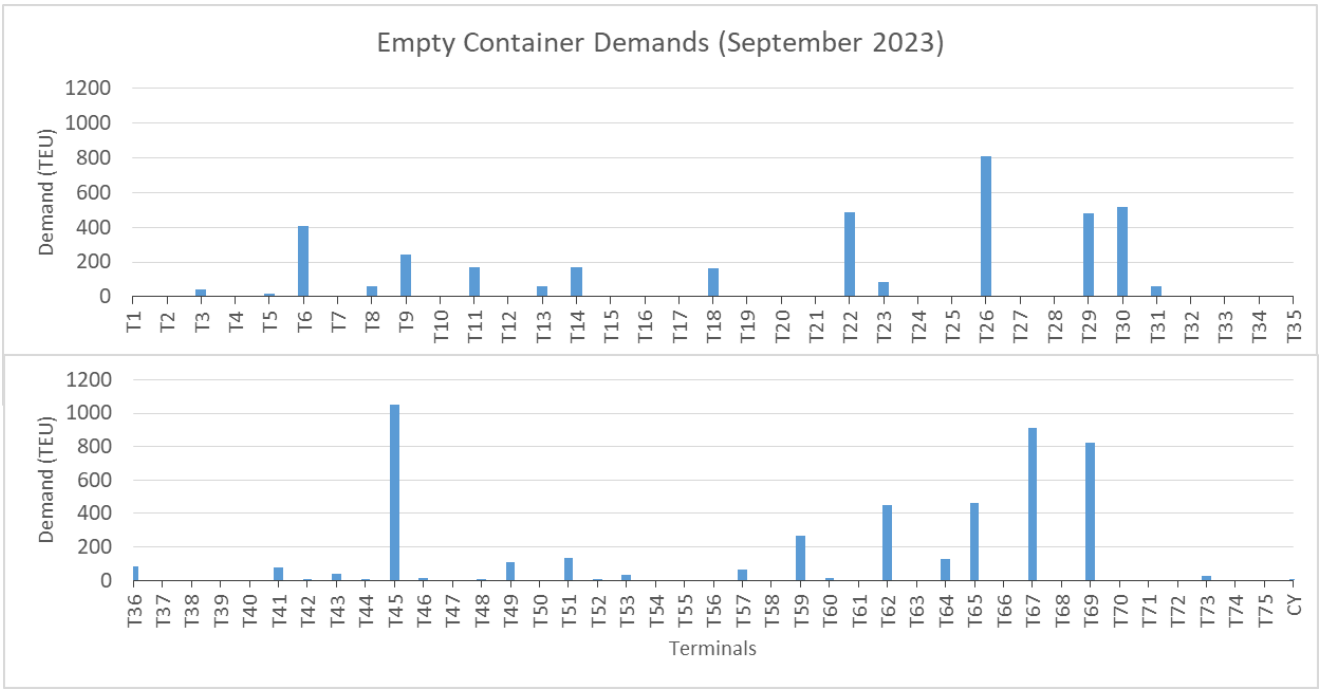

Figure 6. Depots' empty container demands in September 2023

Table 2. Depots' demands in in September 2023 in three simulation cases [12]

Depot	Distance from ECT (m)	Demand (TEU)		
		Scenario 1	Scenario 2	Scenario 3
T3	3000	40	40	40
T5	3000	20	20	20
T6	4000	405	405	167
T8	3000	58	58	58
T9	4000	245	245	245
T11	3300	172	172	172
T13	3000	60	60	60
T14	1500	169	169	169
T18	2400	161	161	161
T22	1700	483	483	483
T23	3000	84	84	84
T26	3400	804	804	434
T29	3400	477	477	477
T30	2000	513	513	513
T31	3000	62	62	62
T36	3000	85	85	85
T41	3000	74	74	74
T43	3000	37	37	37
T45	3700	1052	1052	559
T49	2000	108	108	108

Depot	Distance from ECT (m)	Demand (TEU)		
		Scenario 1	Scenario 2	Scenario 3
T51	1300	136	136	136
T53	3000	31	31	31
T57	3000	64	64	64
T59	2700	263	263	263
T62	300	448	448	448
T64	3700	124	124	0
T65	2300	463	463	463
T67	1200	910	910	429
T69	1700	821	821	373
T73	3000	25	25	25
CY	2500	4	2000	1000
Total	-	8398	10394	7240

In the simulation process, it is assumed that enough empty containers are always available at ECT. Based on the registered and approved monthly demand of requesting depots, their exclusive trucks are called to refer to ECT for picking up the empty containers but for sending empty containers to the CY, ECT trucks are used. Each truck has the possibility to move two TEU at the same time, so in the simulation, each input entity is equivalent to two TEU. Hence, the number of entities entering the system is considered to be half of the demand. It is assumed that two staff members at ETC are in charge of executive operations, who carry out the load-on services of empty containers onto trucks during 12 working hours per day (day shift). The time required to load each truck is assumed to follow a triangular distribution with minimum, maximum and average of 2, 10 and 6 minutes respectively. The number of trucks sent by each depot is different. Based on field surveys, each depot uses an average of five trucks to transport empty containers. The number of ECT trucks for sending empty containers to the CY is 14. The speed of trucks in the port area varies between 20 and 60 km/h, which depends on the travel time and the amount of traffic on the internal roads. In this study, the traffic information of the area was not available and the approximate speed of the trucks was assumed to be 40 km/h. In the destination depots and CY, two personnel are considered to unload the trucks, who perform the executive operations with a triangular distribution similar to the loading stage. The operational steps of empty containers distribution and the simulation model are shown in Figure 7 and Figure 8 respectively.

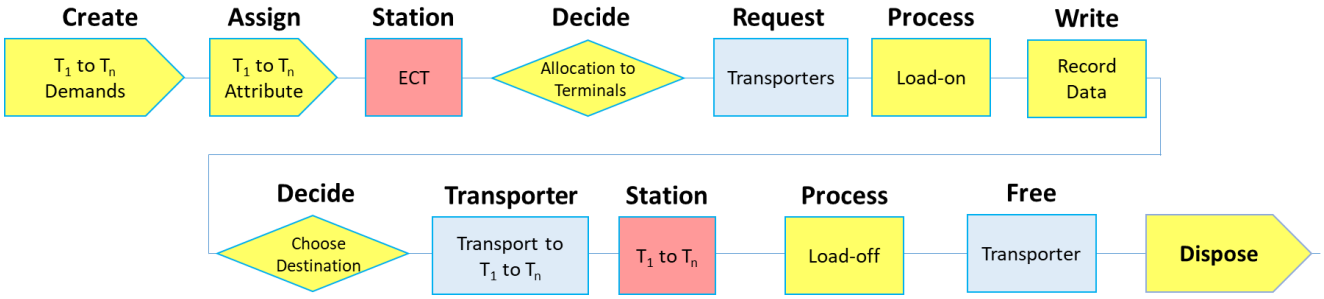

Figure 7. Operational steps of empty containers distribution

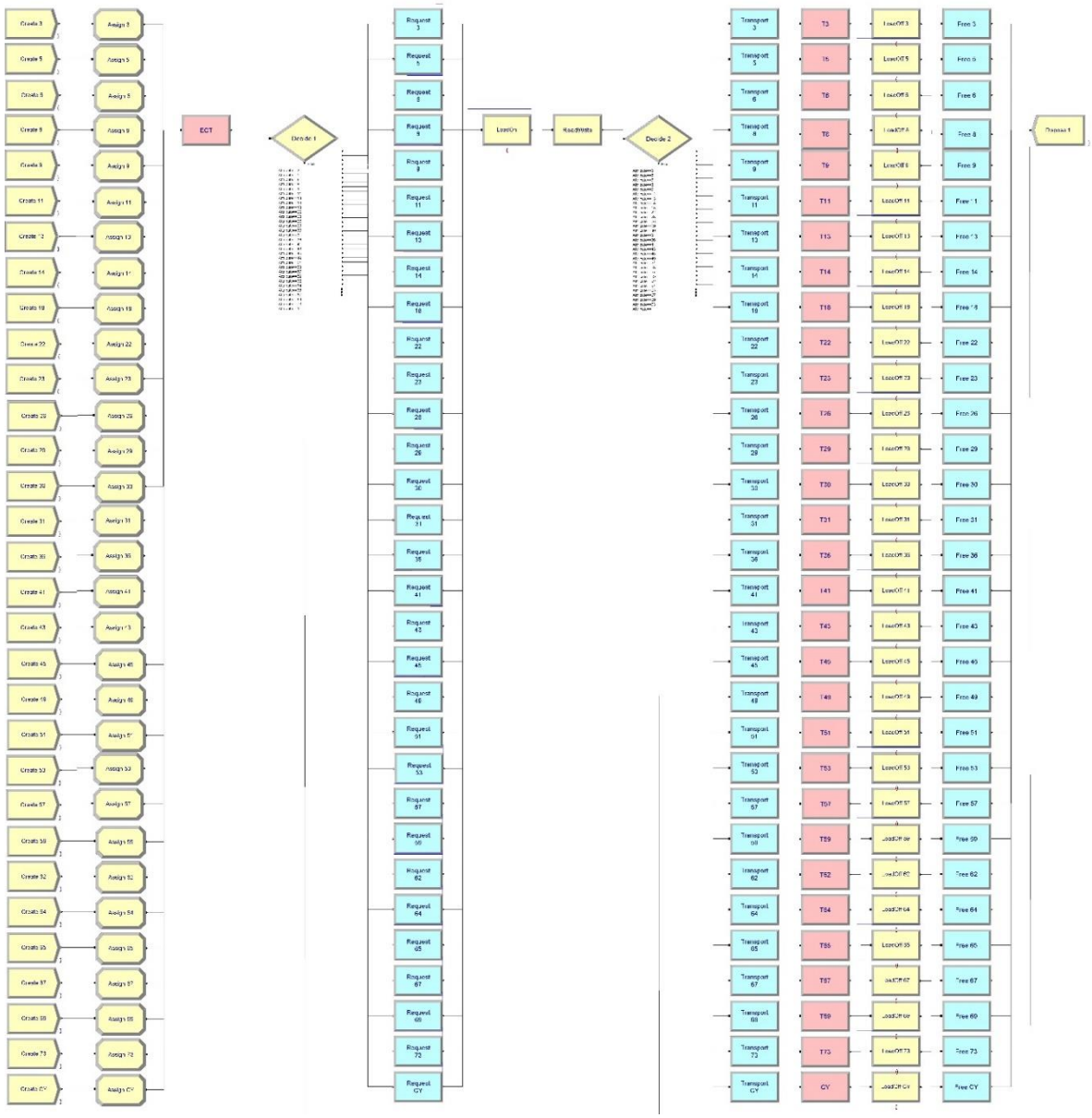

Figure 8. ARENA simulation model for empty containers distribution

In the first scenario regarding the normal condition in September 2023, the total actual demand is 8398 TEU for which 4199 entities have entered the system. Considering that two executive agents at each depot can load-on two trucks simultaneously and each truck requires a minimum loading time of two minutes, the whole distribution time cannot take less than 70 hours. However, considering that the time required to load on each truck is assumed to follow a triangular distribution with an average of 6 minutes, the optimal average operational time would be around 210 hours.

In the initial modeling, the number of allocated transporters (trucks) to each demanding depot was considered unity. The average time for delivering all the entities to the destination depots was approximately 288 hours (24 working days). As mentioned previously, based on field surveys, each depot yard uses an average of five trucks to transport empty containers and 14 trucks are usually used by ECT to deliver empty containers to the CY. So, in the next step, the number of available transporters increased to the mentioned values. The results show that the total time required to deliver all the empty containers reduces to 213 hours (18 working days). Further increase in the number of trucks did not have a meaningful effect on the total operational time. The only consequence would be an increase in traffic and queue length at ECT for load-on process. It can be concluded that the number of trucks used by the depots for delivering empty containers is almost optimum.

In the second scenario, an abrupt increase in the demand from the CY is added to the normal condition. The CY demand (which was actually 4 TEU in the desired month) is increased to 2000 TEU and consequently the total demand in this condition reaches 10394 TEU (5197 input entities).

The total time required to deliver all the empty containers in this case has increased from 213 hours (18 working days) to 262 hours (22 working days).

In the third scenario, it is assumed that half of the predicted demand for six main depot yards (section 4) is sent ahead of schedule during off-peak times. The

rest of the demands for these depots are kept in the simulation. It is also assumed that half of the CY demand (1000 TEU) is pre-sent and only 1000 TEU is considered as CY demand. Consequently, the total empty containers to be sent have reduced from 10394 TEU to 7240 TEU (30% reduction). These results show that the total delivery time has also decreased from 262 hrs. (22 working days) to 183 hrs. (16 working days). The main results of the simulations are presented in Table 3.

Table 3. Main simulation results

Item	Scenario			Unit
	1	2	3	
Total Simulation Time	212.6	261.9	183.3	hours
Total Wait Time (Maximum)	212.5	261.8	183.2	hours
Total Transfer Time (Maximum)	0.1	0.1	0.1	hours
Load On Wait Time Per Entity (Maximum)	7.58	8.07	7.86	hours
Load On Wait Time Per Entity (Average)	3.21	3.70	4.23	hours
Load On Queue Waiting Time (Maximum)	7.48	8.01	7.76	hours
Load On Queue Waiting Time (Average)	3.11	3.6	4.13	hours
Load On Queue Number Waiting (Maximum)	148	161	156	Number
Load On Queue Number Waiting (Average)	62	71	82	Number
Load Off Wait Time Per Entity (Maximum)	0.23	0.25	0.25	hours
Load Off Queue Waiting Time (Maximum)	0.08	0.15	0.15	hours
Load Off Queue Number Waiting (Maximum)	2	3	3	Number
Load Off Queue Number Waiting (Average)	0	0	0	Number

The results indicate that the maximum transfer times in all scenarios are negligible compared to the waiting time at load-on queue. Hence, increasing the number of trucks or the assumed velocity does not affect the results considerably. This is important from the viewpoint of resource allocation management and traffic control measures. It is also remarkable that the waiting time in load-on process is considerable at ECT where all the trucks sent by requesting depots shall pass through a shared queue. On the contrary, the load-off processes at different depot yards do not lead to significant queues or noticeable waiting times. Although the entire distribution and transportation operations can be completed within a month, the length of the load-on queue and the associated average waiting times are significantly high in all the scenarios indicating the importance and necessity of management measures.

The daily variation of load-on queue length and average waiting time for different scenarios are shown in Figure 9 and Figure 10. The trends show that in case all the requesting depots send their trucks simultaneously to pick up the empty containers, a long queue is formed at ECT at the beginning of the month and the average waiting time of trucks in the load-on queue reaches 4 to 5 hours.

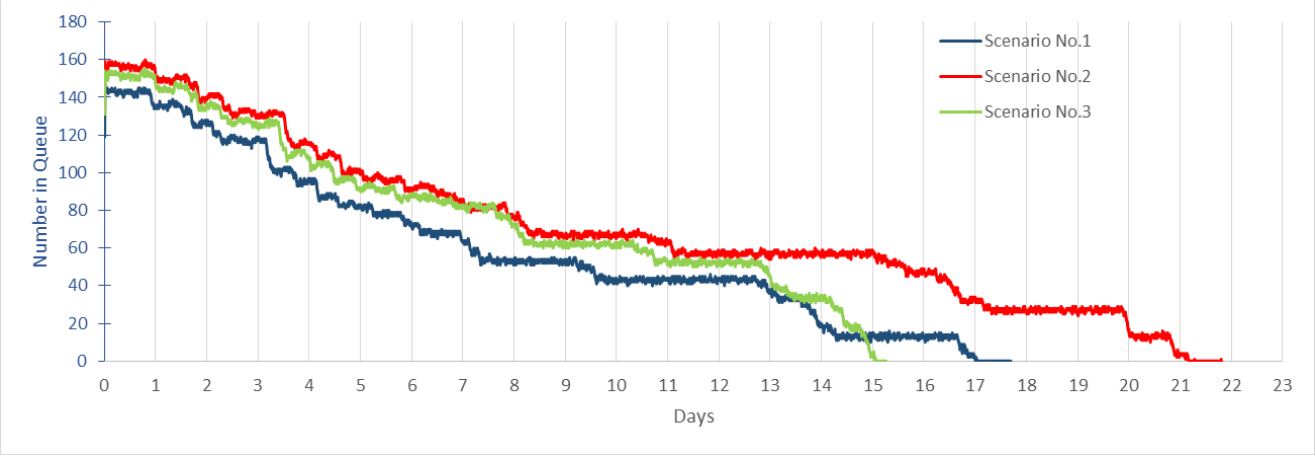

Figure 9. Daily load-on queue length for different scenarios

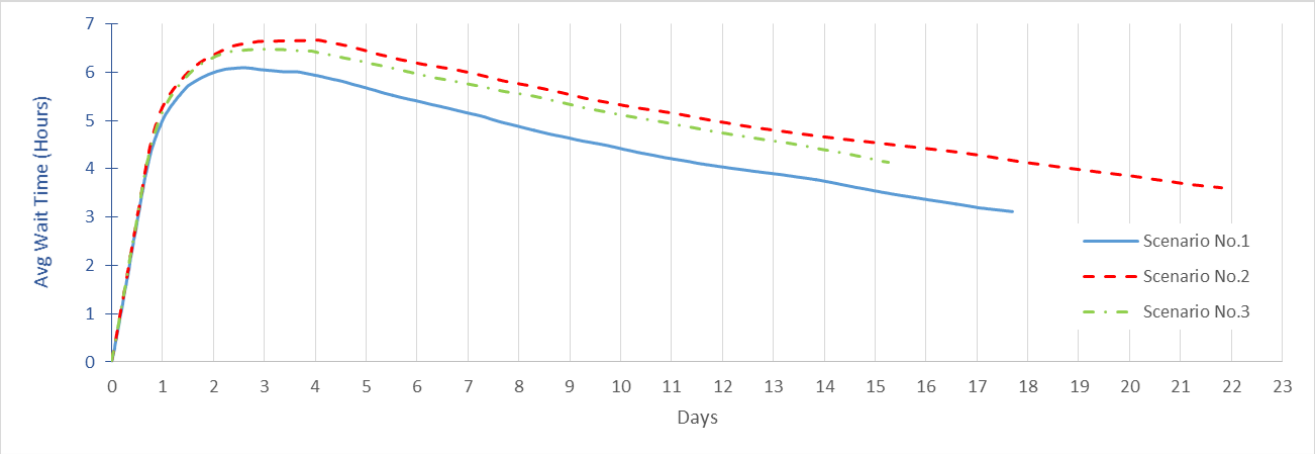

Figure 10. Average waiting time in load-on queue for different scenarios

One solution for reducing the queue length and waiting time is the asynchronous calling of the trucks from different depots on a pre-scheduled plan. Such schedules can be planned and checked through simulations. As an example, an asynchronous schedule is planned for the first scenario and the resulting queue length and waiting times are compared to the case of simultaneous call of trucks. As it can be seen in Figure 11 and Figure 12, while the entire operational time has remained 18 days, the max number in load-on queue has decreased from 147 to 13 (91% reduction) and waiting times has decreased from 6 to 0.5 hrs. (92% reduction). Although this approach is found to be very useful, it should be applied with caution and based on operation simulations since blind scheduling may result in extension of the overall operational duration.

The results including the similar scheduling for the second and the third scenarios are shown in Figure 13 to Figure 16 and Table 4.

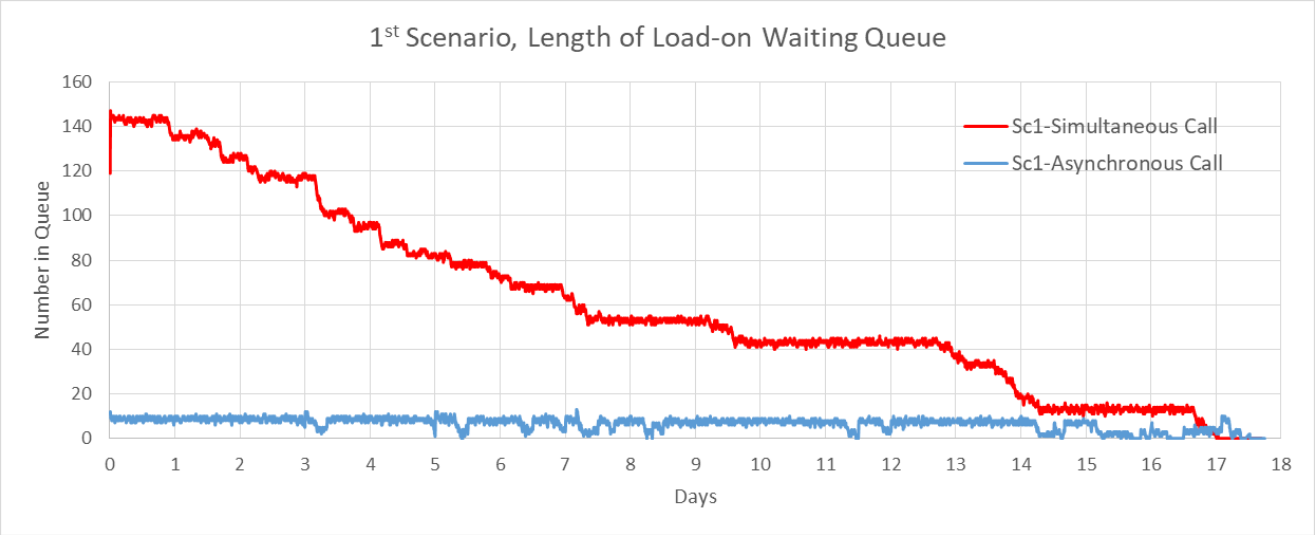

Figure 11. First scenario queue length, simultaneous versus asynchronous call of trucks

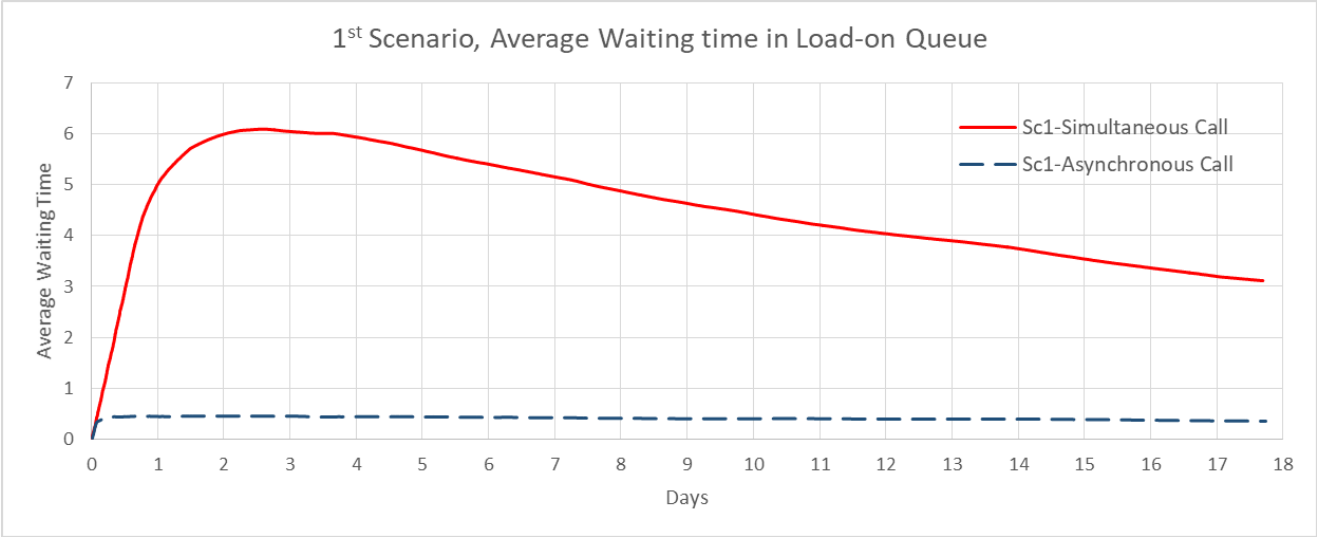

Figure 12. First scenario average waiting time, simultaneous versus asynchronous call of trucks

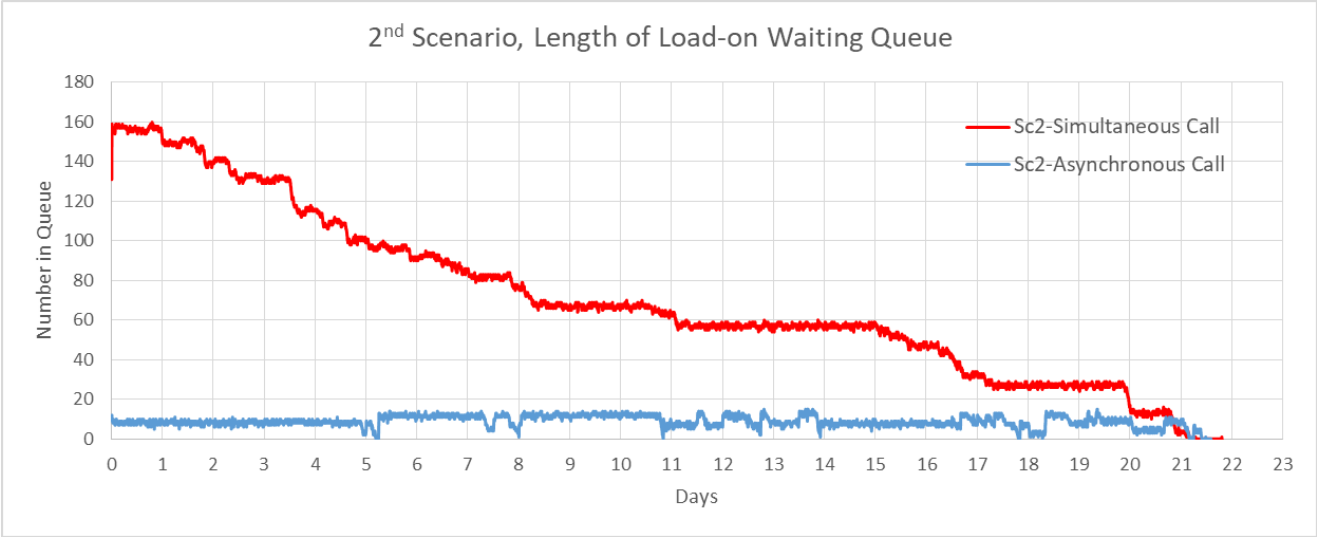

Figure 13. Second scenario queue length, simultaneous versus asynchronous call of trucks

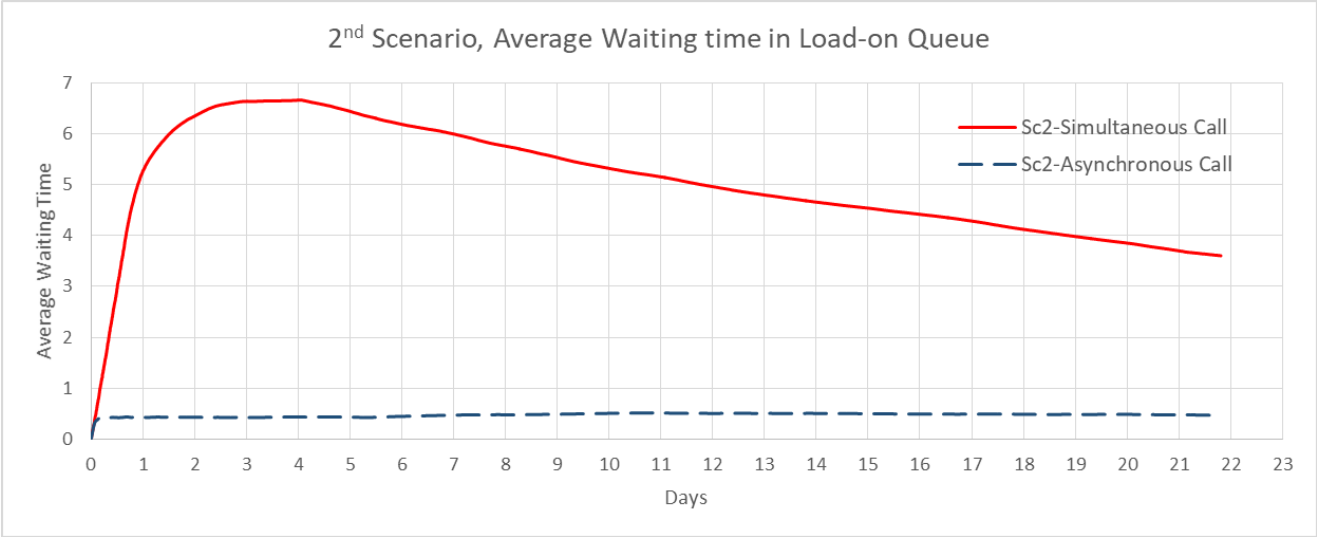

Figure 14. Second scenario average waiting time, simultaneous versus asynchronous call of trucks

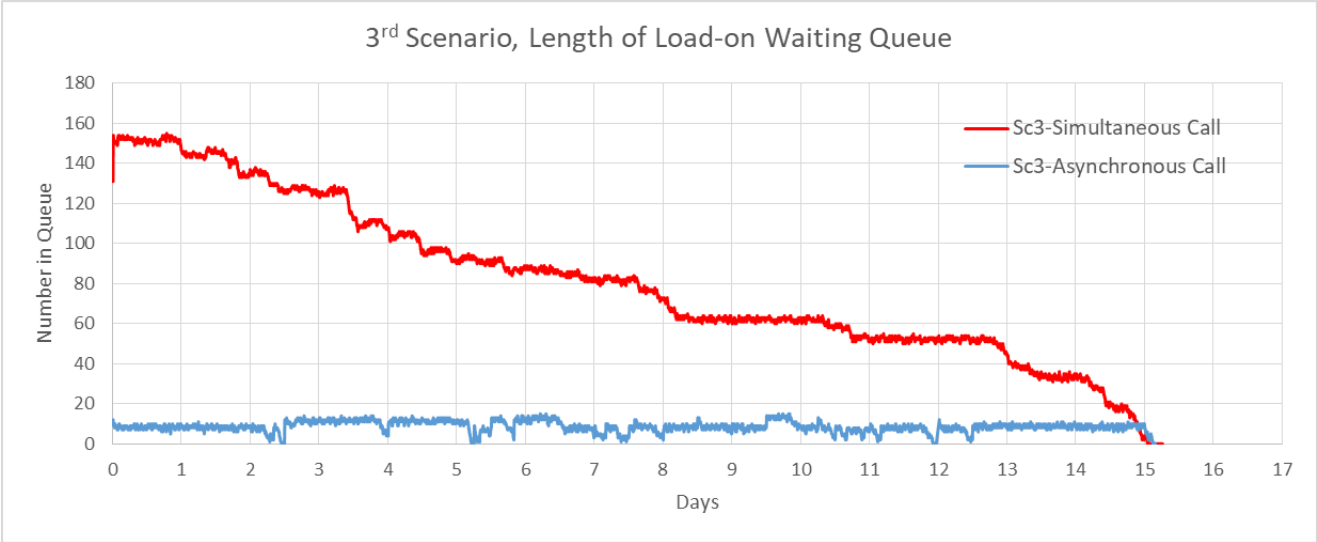

Figure 15. Third scenario queue length, simultaneous versus asynchronous call of trucks

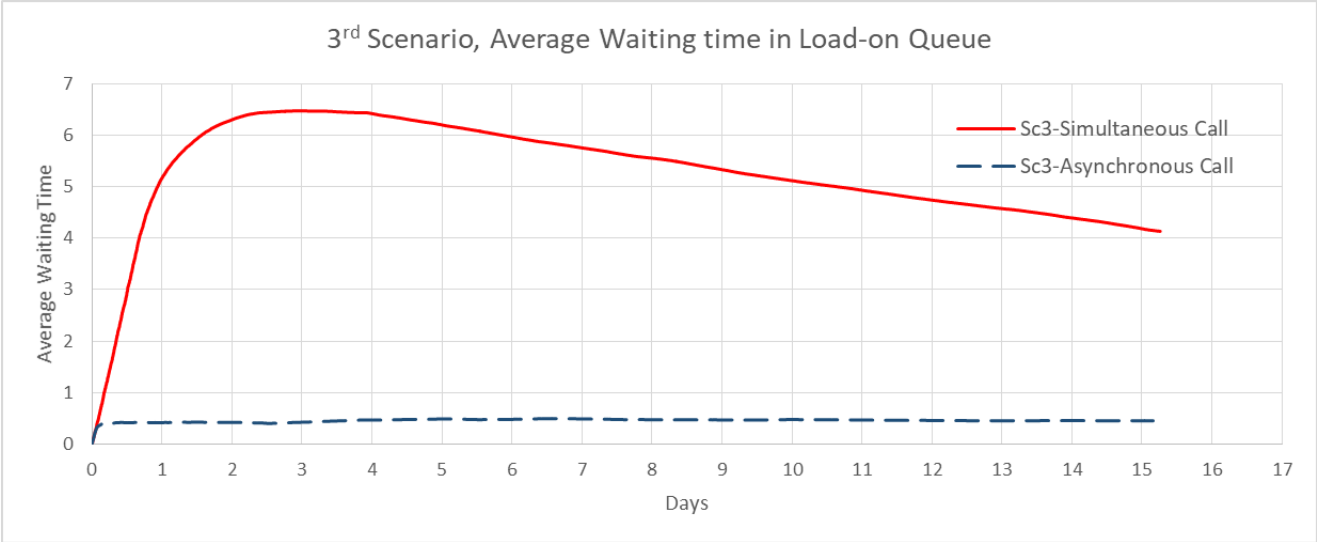

Figure 16. Third scenario average waiting time, simultaneous versus asynchronous call of trucks

Table 4. Load-on queue condition, simultaneous versus asynchronous call of trucks

Item	Call of Trucks	Scenario		
		1	2	3
Total Load-On Queue Time (hrs)	Simultaneous	212	262	183
	Asynchronous	213	259	182
	Difference %	***0.5***	***-1.1***	***-0.5***
Max Number in Load-On Queue (Number)	Simultaneous	147	160	155
	Asynchronous	13	15	15
	Difference %	***-91.2***	***-90.6***	***-90.3***
Peak of Average Waiting Time in Load-On Queue (hrs)	Simultaneous	6.1	6.7	6.5
	Asynchronous	0.5	0.5	0.5
	Difference %	***-91.8***	***-92.5***	***-92.3***

It is observed that while the entire operational time is kept almost constant, the scheduling of truck calls has led to a considerable decrease (around 90%) in queue lengths and average waiting times.

6. Conclusion

In this paper, the optimization process of empty container operations in Shahid Rajaee Port of Iran has been investigated using machine learning and simulation tools. Management of empty containers delivery to demanding depot yards and vessels is rather complex in this port, especially when high demands arise from container yard for loading empty containers on vessels. The demand history was available on a daily basis for 25 months. Although the empty containers are sent to almost 75 demanding depots, the records show

that the majority of demand was dedicated to a limited number of them. Six main depots with an average monthly demand of more than 500 TEU as well as container yard have been selected for demand prediction using Long-short-term-memory neural network. The daily predictions did not always demonstrate perfect alignments with actual demands due to insufficient data, but the sum of daily predicted values gave a good estimation for a month. Knowing the approximate demand of main depots, it is possible to send a portion of monthly demand ahead of the schedule during off-peak times, or utilize stripped empty containers available at the demanding depot. To assess the effectiveness of this approach, the operational empty container allocation process in September 2023 was simulated. The normal condition based on the actual demands was first simulated. Then, an abrupt increase in the CY demand was added to the total demand. Eventually, half of the predicted demand for six main depots and the CY was subtracted from the model assuming that it was sent to the depots ahead of schedule during off-peak hours. The simulations revealed that the load-on process at ECT is the operational bottleneck. The transfer time and load-off operations at destination depots do not have a significant effect on the total operational duration. Early demand prediction of only six depots as well as the CY and providing half of the predicted demand ahead of the schedule can reduce the total operational time up to 30%. However, such remedies do not have any positive effect on reducing the maximum queue length or average waiting times. The simulation results have shown that the depots' trucks should not be called simultaneously upon demand confirmation at ECT. Planning a schedule for asynchronous call of trucks to pick up the requested empty containers can reduce the queue length and average waiting time up to 90%. Although an asynchronous call of trucks has been found to be highly effective in reducing the queue length, it cannot be used randomly and without a precise plan since it may lead to the extension of the overall operational duration.

7. References

[1] Transmetrics. (n.d.). Case Study: Predictive Empty Container Management for NileDutch. Retrieved 9 2023, from https://www.transmetrics.ai/case-study/predictive-empty-container-management-niledutch/#cs2

[2] Yuan, L. (2019). Machine Learning Approach to Forecasting Empty Container Volumes. Karlskrona, Sweden: Faculty of Computing, Blekinge Institute of Technology, 371 79 .

[3] Shankar, S. I. (2020). Forecasting container throughput with long short-term memory networks. Industrial Management & Data Systems, 120(3), 425-441.

[4] Ferretti, M., Fiore, U., Perla, F., Risitano, M., & Scognamiglio, S. (2022). Deep Learning Forecasting for Supporting Terminal Operators in Port Business Development. Future Internet, 14(221), 1-19. doi:10.3390/fi14080221

[5] Martius, C., Kretschmann, L., Zacharias, M., Jahn, C., & John, O. (2022). Forecasting worldwide empty container availability with machine learning techniques. Journal of Shipping and Trade, 7(19). doi:10.1186/s41072-022-00120-x

[6] Cuong, T. N., You, S.-S., Long, L., & Kim, H.-S. (2022). Seaport Resilience Analysis and Throughput Forecast Using a Deep Learning Approach: A Case Study of Busan Port. Sustainability, 14. doi:10.3390/su142113985

[7] Brands, M. J. (2015). A SIMIO simulatiom model for the evaluation of inter terminal transport systems at Maasvlakte 1 and 2 in 2030. Delft University of Twchnology.

[8] Gowrynathan, J., Chandrakumar, C., & Kulatunga, A. (2016). Selecting the best layout for the container terminal using Modeling and Simulation Techniques. International Conference on Industrial Engineering and Operations Management, Kuala Lumpur, Malaysia. International Conference on Industrial Engineering and Operations Management, Kuala Lumpur, Malaysia.

[9] Razouk, C., & Benadada, Y. (2017). Optimization and simulation approach for empty containers handling. International Journal of Advanced Computer Science and Applications, 11(8), 520-525.

[10] Derse, O., & Göçmen, E. (2018). A Simulation Modeling Approach for Analyzing the Transportation of Containers in a Container Terminal System. International Scientific and Vocational Journal, 2(1), 19-28.

[11] Radifan , H., Gurning, R., & Handani, D. (2019). Analysis of the Container Dwell Time at Container Terminal by Using Simulation Modelling. International Journal of Marine Engineering Innovation and Research, Vol. 5(1), Mar. 2020. 34-43, 5(1), 34-43.

[12] Sadaghi, S. M., & Shivafar, I. (2024). Prediction of Empty Container Demand Using Deep Neural Networks (Case Study: Shahid Rajaee Port). Journal of Transportation Research, 21(2), 177-188. doi: 10.22034/tri.2024.417293.3194

[13] Sadaghi, S. M., & Shivafar, I. (2024). Optimization of Empty Container Operations through Simulation, a case study of Shahid Rajaee Port. *Road*, *32*(118), 61-74. doi: 10.22034/road.2023.423773.2217

[14] Shahid Rajaee Port empty container dataset (2021-2023).

INTERNATIONAL JOURNAL OF
COASTAL, OFFSHORE & ENVIRONMENTAL ENGINEERING IJCOE Vol.9/No. 2/Spring 2024 (53-61)

Available online at: www. Ijcoe.org

Investigation of Evaporate Deposits of Tees area in coastal of Makran zone

Mohyeddin Ahrari-Roudi*

Assistant Professor, Department of Oceanography, Faculty of Marine Science, Chabahar Maritime University, Chabahar, Iran; m.ahrari@cmu.ac.ir

ARTICLE INFO

Article History:
Received:17 April 2023
Accepted: 15 Mar. 2024

Keywords:
Tees
Chabahar
Makran
Evaporate
Sediment
Coastal
Environment

ABSTRACT

The evaporite chemical sedimentary rocks are rare, but extremely important commercially as the raw materials for the chemical industry. As the name suggests, the evaporites consist of a suite of minerals formed from the evaporation of sea water. Tees area was located of the northern coast of the Oman Sea is located in the northern Chabahar in southern Sistan and Baluchestan province. In this research, evaporite deposits of region by used investigation of geochemical, mineralogical and sedimentological and were taken 17 samples of sediments (non-systematic method). The samples analyzed by Geological Survey and Mineral Exploration of Iran. Was calculated Correlation coefficients, cluster and Factor analyses. According to the results of chemical analysis and field observations, the study area is located in Supratidal And are directly affected by sea water. The main source of the basin has been affected by external factors basin (large evaporate and sea water fed) are placed. The amount of Na and chlorine are the maximum amount and the rest less than 1. The amount of B and Li in the sediments show significant correlation (average between 338.8 and 738.5) that the correlation is similarly changed. The extent of these changes can be affected by seasonal rivers of Serkan and Tees by related environmental factors. There are also significant differences between the amount of Li and B (average between 399.7 and 738.5), probably affected by coastal erosion and transport margins have been deposited by flowing water and this makes B from earlier upland areas Na and Li stacked in margins of areas. Evaporite minerals that are mainly halite. In study area for all three categories evaporite minerals Contains of chloride, sulfates and carbonates Of course is in low amount. According to cluster and factor analysis, three sources were identified included biogenic, geogenic (continental) and environment.

1. Introduction

Evaporites are layered crystalline sedimentary rocks that form from brines generated in areas where the amount of water lost by evaporation exceeds the total amount of water from rainfall and influx via rivers and streams. The mineralogy of evaporite rocks is complex, with almost 100 varieties possible, but less than a dozen species are volumetrically important. Minerals in evaporite rocks include carbonates (especially calcite, dolomite, magnesite, and aragonite), sulfates (anhydrite and gypsum), and chlorides (particularly halite, sylvite, and carnallite), as well as various borates, silicates, nitrates, and sulfocarbonates. Evaporite deposits occur in both marine and nonmarine sedimentary successions.

Evaporites are sediments chemically precipitated due to evaporation of an aqueous solution. Common evaporates can be dominated by halite (salt), anhydrite and gypsum. Evaporites may be marine or non-marine. Marine evaporates formed by evaporation of water within an ocean basin with increasing evaporation produce calcite and dolomite (~10% evaporation), gypsum (~80% evaporation), and halite (~90% evaporation). Anhydrite can be precipitated at

temperatures >40ºC. Minerals such as sylvite (KCl), carnalite ($KMgCl_3.6H_2O$) and langbeinite ($K_2Ca_2Mg(SO_4)_{6.H2O}$) are typical minor components of marine evaporites. Restricted ocean basins with limited circulation of sea water and coastal plains (sabkhas) during marine regression are typical depositional environments for marine evaporates. Non-marine evaporites may be dominated by halite, gypsum or anhydrite and also can contain borax ($Na_2B_4O_7.10H_2O$), epsomite ($MgSO_4.7H_2O$), and gaylussite ($Na_2Ca(CO_3)_2.5H_2O$). Non-marine evaporites typically form in arid to subtropical environments in basins with limited fluvial input and output (e.g., playa lakes).

Alteration of evaporites after deposition is common. Anhydrite can replace gypsum by dehydration during burial whilst gypsum can form by hydration of anhydrite by interaction with groundwater. Gypsum and anhydrite can also be found as concretions formed during diagenesis. Halite deposits are capable of flow as diapirs on burial and rise through overlying sedimentary sequences. Anhydrite and gypsum commonly form a cap rock on diapirs due to dissolution of halite. Halite diapirs can extrude at the Earth's surface to form salt glaciers. Evaporites often form important decollement layers in fold thrust belts. Evaporites are often interbedded with other sedimentary rocks such as mudstones, marls and siltstones. Where evaporites have been removed by dissolution but pseudomorphs remain deposits are often termed evaporitic [1, 2].

In warm and arid climates, water evaporating from landlocked, or playa, lakes may result in the development of various minerals. As the lake waters evaporate, they become naturally enriched in the different soluble chemicals carried into them by streams. These chemicals have been obtained through weathering and erosion of nearby rock materials. Continued evaporation concentrates these chemicals to the point where they precipitate and accumulate at the bottom and shores of lakes as a group of distinctive minerals [3].

Considering that so far accurately and evaporate deposits of the southern region of Sistan-Baluchistan province has been less studied and extraction of these deposits, 70 years old, it is necessary be a full scientific study of sediments to the type of minerals, trace elements, their origin and their impact on the environment to be assessed.

Geographical location and access roads to the area

The port of Chabahar is located in the south-east of Iran, north-west of the Indian Ocean, and north-east of the Oman. Chabahar is situated on the Makran Coast of the Sistan and Baluchestan province of Iran. The Port of Chabahar is a seaport in Chahbahar in southeastern Iran. Its location lies in the Gulf of Oman. It is the only Iranian port with direct access to the ocean. The port was partially built by India in the 1990s to provide access to Afghanistan and Central Asia, bypassing Pakistan. Study area in southeast Iran, the extreme south of the coastal Makran region and is part of the city of Chabahar. Because of its establishments and ease of access to ocean as well as Oman Sea and Persian Gulf, long ago it was the center of business, trade and navigation. Chabahar coastal town with an area of 14 square kilometers located in this zone. Chabahar with a population of more than two hundred thousand largest and most active coastal city of Zahedan, Iranshahr Iran by land ways, Nikshahr, Chabahar, Konarak and related Jask. It is also possible air flights from Tehran to Zahedan, Bandar Abbas or Chabahar is possible.

Paleogeographic the oldest deposits in Chabahar belonging to Middle Miocene has been from collection of sandstone, mudstone and Conglomerate (Figure 1).

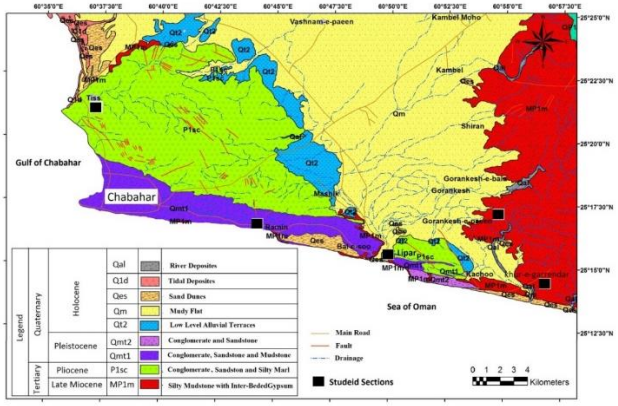

Figure 1. Portion of the Geologic map of the study area

These deposits and the fossils found in them, represent the facies are shallow (intertidal and possibly to 30 meters deeper than the sea) and then the upper Miocene sedimentary Basin in a little deeper and marl unit was deposited in those circumstances lower Pliocene continued [4]. The marl unit also contains large quantities of molluscs shells that can be represented neritic sedimentary environment. Late Pliocene orogenic phase in the performance of a shallow basin become again a set of sandstone and conglomerate deposited in study area. There are primary sedimentary structures in the sediment's signs and high-energy shallow sedimentary environments and is also fast deposition of sediment in it. In early Quaternary deposits and dry environment by advancing sea, the beach for progressive and unconformity deposits has been formed in a coastal part of the study area. The effect next orogenic movements and mild, sediment has formed as marine terraces [4, 5]. Highland's region of east-west trend and often are flat.

Material and Methods

In order to investigate the geochemical and sedimentological and mineral identification evaporation in this area, with the use of reviews Office includes research reports, student theses, scientific papers presented at seminars and publications and so on. Also, geological maps and geochemistry related to

this area were collected and investigated. After the study is to gather research information geological map of the study area, all the information and previous work conducted on the region's geology was investigated. Field studies including repeated visits regional and surface sampling 15 samples of sediment Tees areas, Pozm and park on the northern coast of Chabahar, study the sedimentary structures and institutions of the region. When you navigate in the area of evaporites, formed crystals, morphology, and vegetation, in order to investigate and more precision, photos were taken (Figure 2).

Figure 2. Surface sediments in the region Tees

In order to determine the geographic location of the sampling was used GPS and the results were recorded in Table 1. The samples sent for chemical analysis to laboratories of Geological Survey of Iran in Karaj and results were received. To identify evaporite minerals samples, XRF and XRD studies were performed. To identify evaporite minerals samples, XRF and XRD studies were performed. To analyze the data was used from Excel and $SPSS_{v23}$ software.

Table 1. Geographical location sediment samples with GPS

No.	Longitude	Latitude	Area
At-01-93	E 60° 37' 28"	N 25 18' 16"	Tees
At-02-93	E 60° 37' 32"	N 25 18' 20"	Tees
At-03-93	E 60° 37' 36"	N 25 18' 24"	Tees
At-04-93	E 60° 37' 40"	N 25 18' 28"	Tees
Ap-01-93	E 60° 19' 08"	N 25 27' 14"	Pozm
Ap-02-93	E 60° 19' 12"	N 25 27' 20"	Pozm
Ap-03-93	E 60° 19' 14"	N 25 27' 24"	Pozm
Ap-04-93	E 60° 19' 20"	N 25 27' 30"	Pozm
Ap-05-93	E 60° 19' 24"	N 25 27' 34"	Pozm
Apa-01-93	E 60° 33' 47"	N 25 26' 26"	Parak

Results and Discussion

Evaporite Reserves that with main high thickness have been deposited in marine basins (Jacob). These deposits and the continuation of sedimentation in the region by factors such as weather conditions and changes in static basin, hydrographic and tectonic linked. When the basin is out of equilibrium, evaporates will deposit [6]. Laminated anhydrite and halite will precipitate in the center of the field. Congestion (feeding) of alternating will allow the water mass to be formed thick sequence. If this does not happen, sediments on the basin floor dry and evaporate minerals will come into existence. One sedimentary basin uplift above sea level can again start a new cycle [7, 8, 9]. The average amount of Li in the earth's upper crust is about 70 ppm economic factor to form Li in internal environments (such as pegmatites) and external (e.g., ground salt, Sabkha and clay). In both cases, under certain circumstances, after the deposition of Li is less soluble and can be focused to an economic deposit. Li occurs in a variety of rocks and water but usually low concentrations. Curves and the values of Li and B were measured in the study area (Table 2 and Figure 3).

	AT-01-93	AT-02-93	AT-03-93	AT-04-93	AP-01-93	AP-02-93
Na*	37.00	34.85	36.53	31.62	38.45	39.5
MgO	0.6	1	0.4	1.8	-	< 1
Al_2O_3	0.1	0.6	0.2	0.8	0.1	< 1
SiO_2	0.2	1.9	0.4	2.5	0.2	0.1
SO_3	0.5	1.1	2.2	3.4	0.6	0.1
K*	0.23	0.33	< 1	0.74	< 1	< 1
Cao	0.5	1.6	2.4	0.4	0.6	0.1
ZrO_2	< 1	< 1	0.1	< 1	< 1	-
Cl*	57.44	54.71	56.43	49.41	59.57	60.28
Br	< 1	< 1	< 1	< 1	< 1	< 1
Humidity	3.17	3.09	0.87	5.02	0.22	0.14
CeO_2	0.1	0.2	0.2	0.2	-	-
Fe_2O_3	< 1	< 1	< 1	< 1	< 1	< 1

Table 2. Value measured B and Li

Sample No.	B	Li	Location
At-01-93	3.86	3.34	Tees
At-02-93	2.96	3.33	Tees
At-03-93	0.86	10.01	Tees
At-04-93	6.2	8.46	Tees
Ap-01-93	0.5	8.43	Pozm
Ap-02-93	4.4	2.55	Pozm
Ap-03-93	3.24	3.32	Pozm
Ap-04-93	5.64	4.25	Pozm
Ap-05-93	0.76	6.58	Pozm
Apa-01-93	1.06	23.58	Parak

According to Table 2 and Figure 3, variations B is between 0.1 and 6 and variations Li is between 3

and 24. The highest value of Li is in the area park and the lowest value of that in the area Pozm. The highest value of B is in the area Tees and the lowest value of that in the area Pozm. Figure 4 and 5 shows the amount of B, Li, major elements and Location of samples on map in the study area. According to the map that was drawn with GIS software, has determined that the samples were influenced by seawater and are totally dependent on it. Of course, in the area surrounding the study area is changed to a value indicating not great abundance. The amount of B in the center of the basin will increase, but reduced the amount of that in the margins of the basin indicate that the influence of sea water.

Table 3) XRD analysis of samples

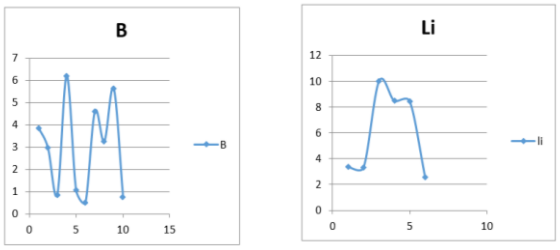

Figure 3. Diagrams B and Li variations

Variations the abundance of elements show that with away from the sea, basin are affected by fresh water river seasonal and the amount of Li will more and the salinity of seawater is more implicated, the amount of B increases in the basin. According to Figures 4 and 5, the region most affected Pozm lowest seasonal rivers, and sea water, thus is provided conditions for the accumulation of B element. Due to seasonal river discharge into the sea, the amount of B is deposited on the margins of the sea. The amount of Li because more weight, the concentration in the upstream. In Pozm area in addition to the amount of B, Li and the number of major elements compared to other regions increasing trend that can be said probably be the origin of environmental pollutants. By using the XRD analysis, 12 kinds of chemical composition (include So_3, Na, SiO_2, Al_20_3, Fe0, Ca_2O_3, MgO, B, Li, K, CL, Br) were identified in studied area. According to Table 3 and figure 6, Halite is the mineral found in sedimentary basins studied (Pozm and Tees). The graph in Figure 6 shows three ranges is the most abundant mineral halite.

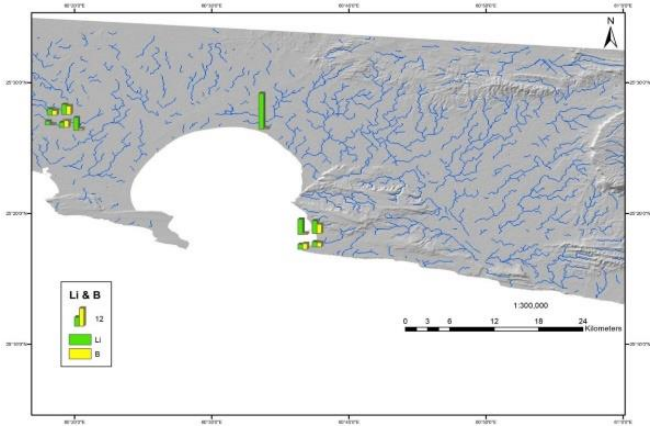

Figure 4. Values of B and Li on map in the study area using GIS software

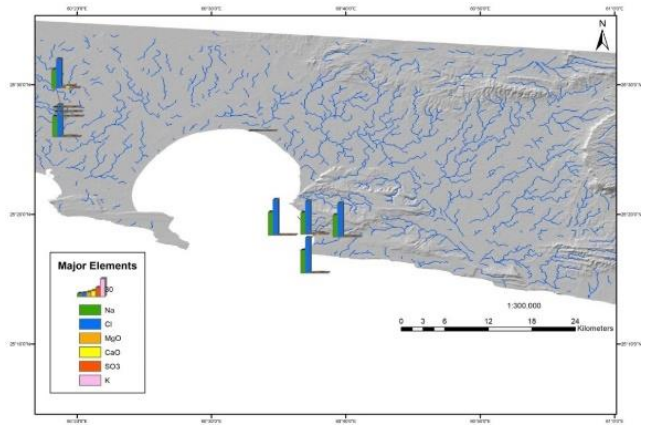

Figure 5. Values of Major Elements on map in the study area using GIS software

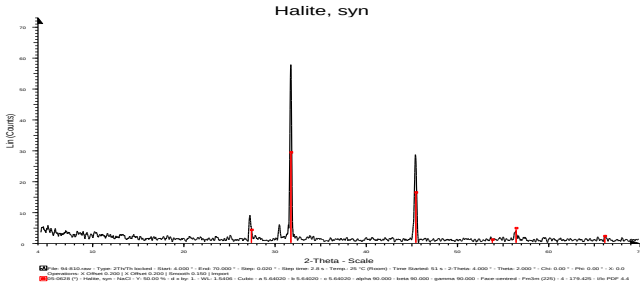

Figure 6. Graph of the results of XRD analysis

Table 4 shows the amount of each element in the six samples analyzed that the following will be discussed to determine the mean, median and variations weight percent the elements. In order to analysis and interpret more, were calculated the correlation coefficient, clustering and factor analyze for samples. The results of elemental analysis shows that the study area, the conditions of the evaporites is formed. But these conditions to prepare for the mineral halite given the amount of Na, Cl. Histograms in figures 7 to 10 shows that the number of elements and their variations P-P. The objective is to determine the effective distribution data. Of course, the median and standard deviation determined above each histogram.

According to the figures 7 to 10, between the median and standard deviation of the data, there is little difference in one point to reach their greatest amount. But at the end of the diagrams can be seen a decreasing trend. These variations increased and then decreased ppm in combination, caused by the effect of external factors (such as erosion and clastic particles entering the basin and the influence of sea water in front of the sea) are on conditions of the sedimentary basin. Though, environmental agents are effective on the basin. Table 5 shows the model of Pearson's the correlation coefficient of elements. Since both elements are included, the effects of the elements can be shown as a numeric value and adaptive coefficient. This amount is always between -1 and +1. In the event that exists positive linear correlation between the two elements, this factor is +1 and in the case of a negative linear relationship exists, this amount is -1 and the relationship between the elements is determined by the numeric value of zero. On the other hand, these factors, meaning that at specified confidence level. In this table, the elements that have the most correlation show with red color and ones that have low correlation with green color and the elements that have lacking in the correlation coefficient do not have any symbols. Therefore, carbonates and chlorides the correlation is significant and is related to the mechanism of their formation. In the region of Pozm, these elements due to the little distance to the coastline and the effect of upstream sediment basin is probably a result of external basin activities.

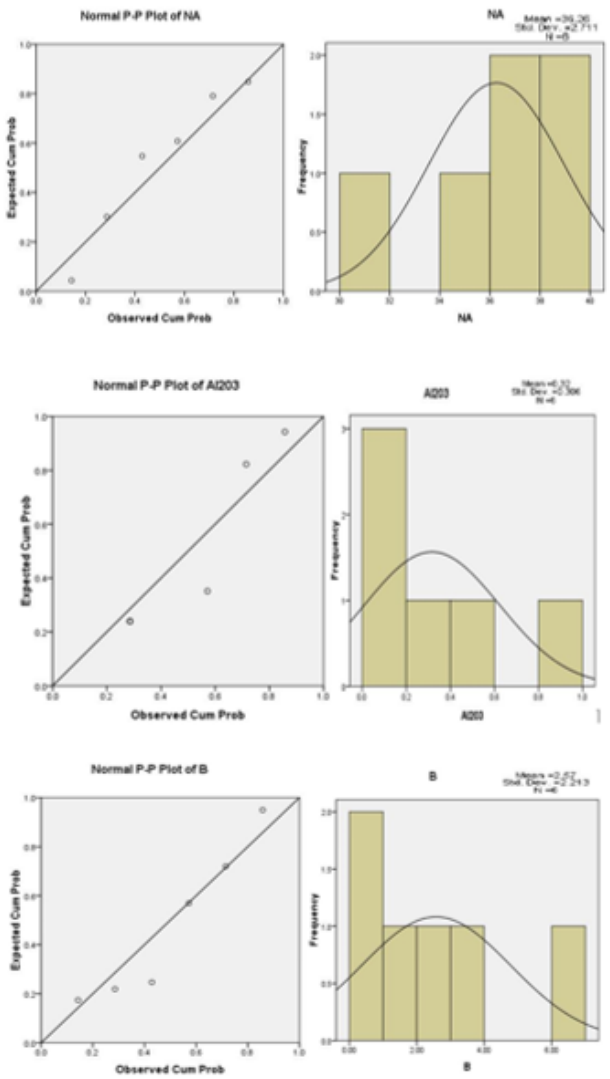

Figure 7. Histograms of B, Na and Al_2O with their variations P-P

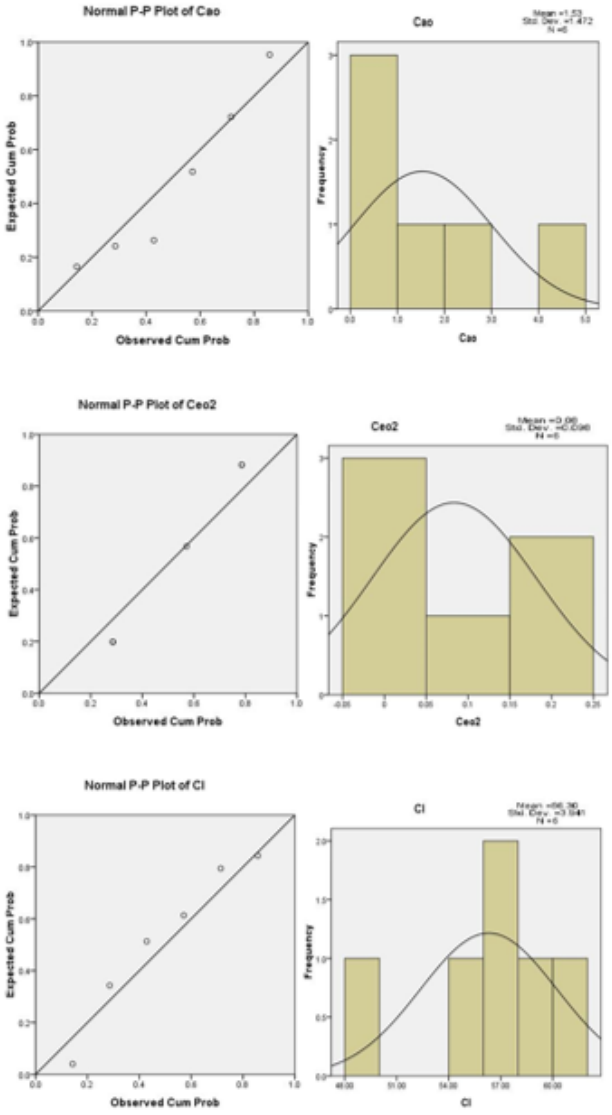

Figure 8. Histograms of Cl, CaO and CeO_2 with their variations P-P

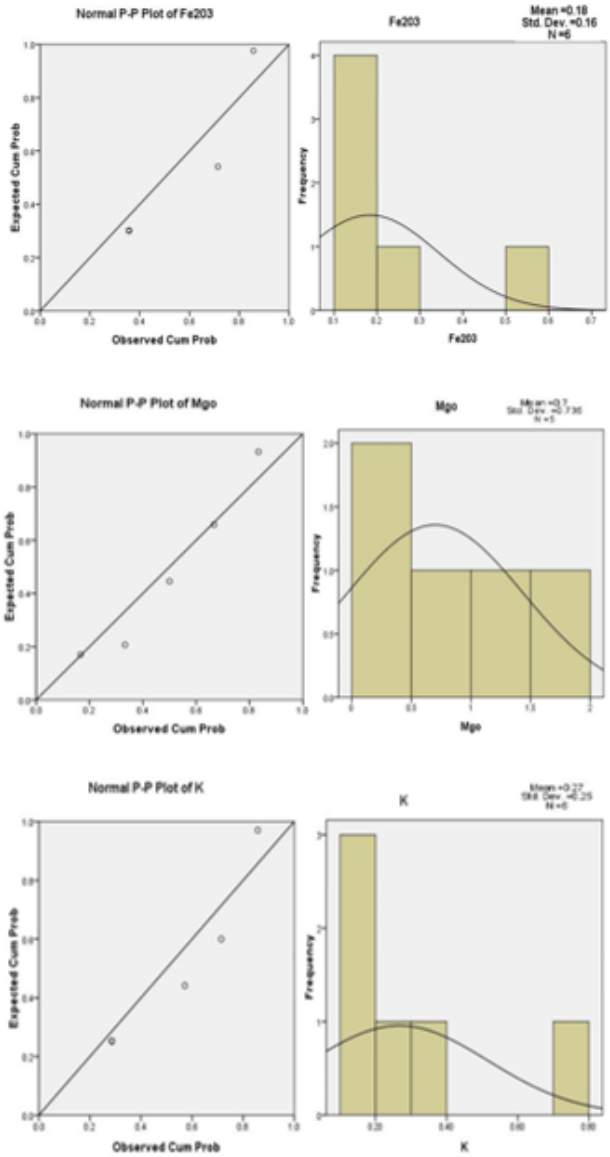

Figure 9. Histograms of K, MgO and Fe_2O_3 with their variations P-P

Cluster Analyses is indicated in Figure 11. The results of these studies (Dendritic) in the study area, shows three groups of elements. The first group: includes elements Na and Cl are highly correlated together and B with lower relationship the origin of this group is within the basin (inner Basin). The second group: includes elements SiO_2, Al_2O_3 and MgO are highly correlated together the origin of this group is Geogenic and by rivers or wind (erosion rocks) have been imported into the basin. The third group: includes elements Fe_2O_3, SO_3, K, B and CaO are highly correlated with each other the origin of this group is biological origin and due to environmental pollution. Of course, Ceo_2 combined with high difference between the second and third groups are linked and also Zro_2 combined with more distance associated with the second and third groups. The evaporative

crystallization of minerals in accordance with the results of chemical analysis are as follows:
Initially carbonates (including $CaCO_3$, Ca SO_4) then chloride (NaCl includes a solid solution with chloride, KCl, $MgCl_2$, B and Mg) and sulfates (including $MgSO_4$, KCl $MgCl_2$ +6H_2O) formed are. Therefore, the necessary conditions for the formation of three groups of evaporite minerals (including chloride, sulfates and carbonate) are available in the study area. But according to the elements Na and Cl, the necessary conditions for the formation of chlorides (especially halite) is much better than in the studied area.

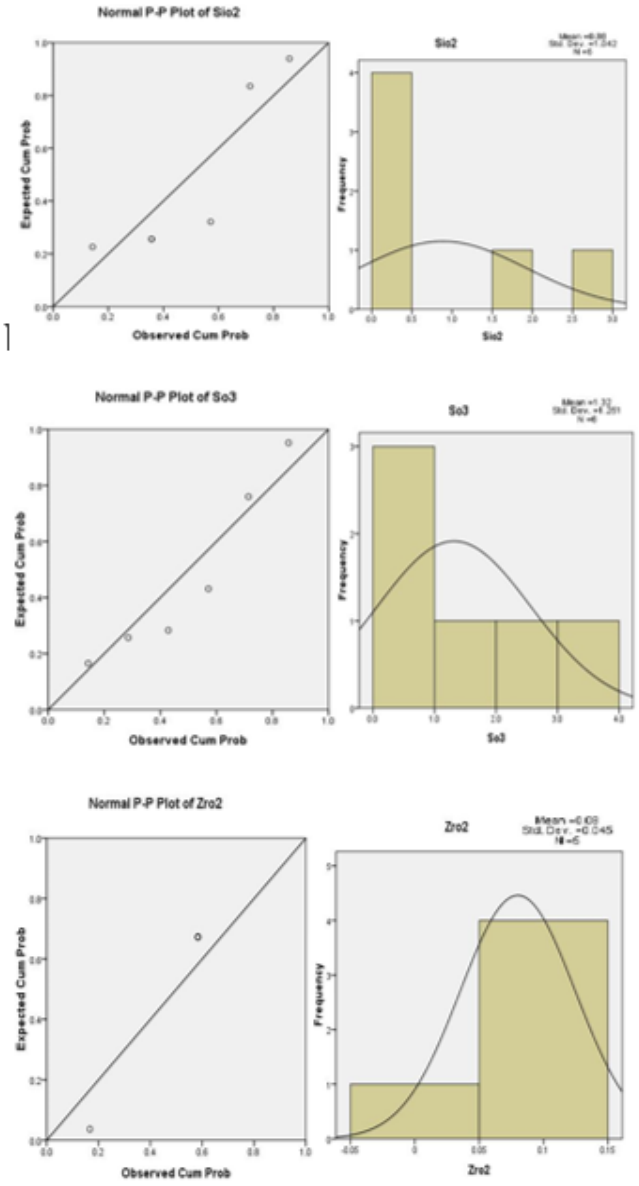

Figure 10. Histograms of ZrO, SO_3 and SiO_2 with their variations P-P

Table 4. The results of elemental analysis by using the software SPSS17

Case Summaries[a]

	S.N	NA	Mgo	Al203	Sio2	So3	K	Cao
	AT-01	37	0.6	.1	.2	.5	.23	.5
	AT02	35	1	.6	1.9	1.1	.33	1.6
	AT-03	37	o.4	.2	.4	2.2	.10	2.4
	AT-04	32	1.8	.8	2.5	3.4	.74	4.0
	AP-01	38	0	.1	.2	.6	.10	.6
	AP-02	39	0.1	.1	.1	.1	.10	.1
N	6	6	6	6	6	6	6	6
Minimum		32	0	.1	.1	.1	.10	.1
Maximum		39	o.4	.8	2.5	3.4	.74	4.0
Mean		36.26		.317	.883	1.317	.2667	1.533
Median		36.79		.150	.300	.850	.1650	1.100

	S.N	Zro2	Cl	Br	Humidity	Ceo2	Fe203	B
	AT-01	O.1	57.44	o.1	3.17	0	.1	3.86
	AT02	0.1	54.71	0.1	3.09	0	.2	2.96
	AT-03	0.1	56.43	0.1	.87	0	.1	.86
	AT-04	0.1	49.41	0.1	5.02	0	.5	6.20
	AP-01	0.1	59.54	0.1	.22	0	.1	1.06
	AP-02	0	60.28	0.1	.14	0	.1	.50
N	6	6	6	6	6	6	6	6
Minimum		0	49.41	0.1	.14	0	.1	.50
Maximum		O.1	60.28	o.1	5.02	0	.5	6.20
Mean			56.3017		2.0850	.08	.183	2.5733
Median			56.9350		1.9800	.05	.100	2.0100

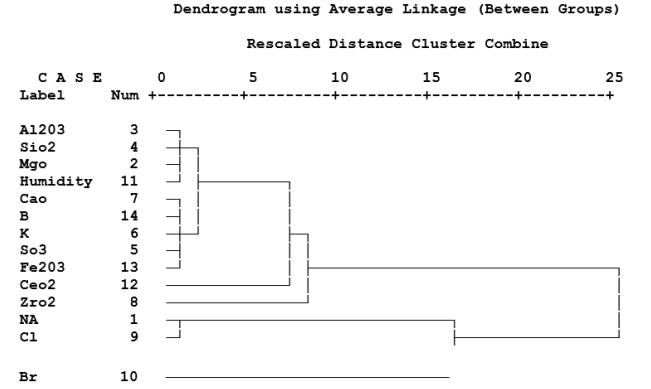

Figure 11. Cluster Analyses of elements in study area

Correlations

		NA	Al203	Sio2	So3	K	Cao	Cl	Humidity	Ceo2	Fe203	B
NA	Pearson Correlation	1	-.945*	-.940*	-.864	-.943*	-.906*	.998**	-.901*	-.511	-.919*	-.869
	Sig. (2-tailed)		.005	.005	.027	.005	.013	.000	.014	.300	.010	.025
	N	6	6	6	6	6	6	6	6	6	6	6
Al203	Pearson Correlation	-.945*	1	.998**	.751	.905*	.820*	-.930**	.805	.543	.904*	.756
	Sig. (2-tailed)	.005		.000	.085	.013	.046	.007	.053	.266	.013	.082
	N	6	6	6	6	6	6	6	6	6	6	6
Sio2	Pearson Correlation	-.940*	.998**	1	.724	.905*	.796	-.922**	.817*	.524	.897*	.769
	Sig. (2-tailed)	.005	.000		.104	.013	.058	.009	.047	.286	.015	.074
	N	6	6	6	6	6	6	6	6	6	6	6
So3	Pearson Correlation	-.864	.751	.724	1	.752	.993**	-.892*	.618	.555	.810	.615
	Sig. (2-tailed)	.027	.085	.104		.084	.000	.017	.191	.253	.051	.194
	N	6	6	6	6	6	6	6	6	6	6	6
K	Pearson Correlation	-.943*	.905*	.905*	.752	1	.793	-.939**	.910*	.217	.977**	.931**
	Sig. (2-tailed)	.005	.013	.013	.084		.060	.005	.012	.680	.001	.007
	N	6	6	6	6	6	6	6	6	6	6	6
Cao	Pearson Correlation	-.906*	.820*	.796	.993**	.793	1	-.927**	.664	.599	.842*	.647
	Sig. (2-tailed)	.013	.046	.058	.000	.060		.008	.150	.209	.035	.165
	N	6	6	6	6	6	6	6	6	6	6	6
Cl	Pearson Correlation	.998**	-.930**	-.922**	-.892*	-.939**	-.927**	1	-.886*	-.507	-.924**	-.860*
	Sig. (2-tailed)	.000	.007	.009	.017	.005	.008		.019	.305	.009	.028
	N	6	6	6	6	6	6	6	6	6	6	6
Humidity	Pearson Correlation	-.901*	.805	.817*	.618	.910*	.664	-.886*	1	.259	.805	.977**
	Sig. (2-tailed)	.014	.053	.047	.191	.012	.150	.019		.620	.053	.001
	N	6	6	6	6	6	6	6	6	6	6	6
Ceo2	Pearson Correlation	-.511	.543	.524	.555	.217	.599	-.507	.259	1	.233	.089
	Sig. (2-tailed)	.300	.266	.286	.253	.680	.209	.305	.620		.657	.866
	N	6	6	6	6	6	6	6	6	6	6	6
Fe203	Pearson Correlation	-.919*	.904*	.897*	.810	.977**	.842*	-.924**	.805	.233	1	.840*
	Sig. (2-tailed)	.010	.013	.015	.051	.001	.035	.009	.053	.657		.036
	N	6	6	6	6	6	6	6	6	6	6	6
B	Pearson Correlation	-.869	.756	.769	.615	.931**	.647	-.860*	.977**	.089	.840*	1
	Sig. (2-tailed)	.025	.082	.074	.194	.007	.165	.028	.001	.866	.036	
	N	6	6	6	6	6	6	6	6	6	6	6

**. Correlation is significant at the 0.01 level (2-tailed).
*. Correlation is significant at the 0.05 level (2-tailed).

Table 5. Results of the correlation coefficient between the elements

Interpret the depositional environment and presenting a model

Arid environments (hot with limited precipitation) are ideal for developing brines. Semiarid playa lakes, sabkhas (supratidal flats), salt pans, estuaries, and lagoons are all environments where brines forms. Evaporites have uneven spacial and temporal distribution, with widespread appearance in broad, shallow basins with minimal competing

sediment flux in arid climates. Although we have no modern analogues, huge evaporate deposits suggest that ancient environments contained large evaporating basins. Because suitable climate conditions are usually between 10° and 30° latitude (a global band of desert), evaporate deposits can assist in reconstructing prehistoric continent positions.

Evaporites in non-marine settings (closed lakes, ephemeral lakes, or playas in arid or semi-arid climates) are most likely to demonstrate a bulls-eye pattern of minerals, with gypsum rims and bitter borate centers. The most common trace minerals are borax, trona, epsomite, gaylussite, and glauberite. Evaporites in shallow marine settings can be divided into supra- and intratidal deposits, and marine shelves. In both instances, the brine is refreshed by seawater and groundwater, and deposits are layered by adjacent facies during as sea level changes adjust shoreline position [10, 11, 12, 13].

Typically, evaporite deposits occur in closed marine basins where evaporation exceeds inflow. The deposits often show a repeated sequence of minerals, indicating cyclic conditions with a mineralogy determined by solubility. The most important minerals and the sequence in which they form include calcite, gypsum, anhydrite, halite, polyhalite, and lastly potassium and magnesium salts such as sylvite, carnallite, kainite, and kieserite; anhydrite and halite dominate. These sequences have been reproduced in laboratory experiments and, therefore, the physical and chemical conditions for evaporite formation are well known.

The outcrops in the area are calcareous mudstone (former marls) and marine terraces and plateaus which are composed of two levels, and the city of Chabahar, is located on them. Silty sand and sandy silt are two sediment types in Chabahar Bay. The sands and silts are dominated by Siliciclastic sediments of quartz, calcite, feldspar, rock and oyster shell fragments. These sediments have a moderate to well sorting, platykurtic kurtosis and positive skewness. Some of shell fragments come from intra-basin and others are clastic. The clastic shell fragments are mostly originated from the upper part of the marine terraces and have been transported into the Bay by the wind or water erosion. The calcite grains are also abundant clastic sediments [15, 16, 17, 18]. The evaporator is a heat transfer system, and is that part of a refrigeration cycle in which liquid refrigerant is evaporated for the purpose of removing heat from the refrigerated space or product [19, 20]. Sabkha is a phonetic translation of the Arabic word for a salt flat. Sabkhas are supratidal, forming along arid coastlines and are characterized by evaporite-carbonate deposits with some siliciclastics. Sabkhas form subaerial, prograding and shoaling-upward sequences [21, 22, 23, 24] that have an average thickness of a meter or less. Sabkha are common in modern supra- and intratidal settings, with evaporites intermixed with siliclastic debris washing down from inshore erosion, and offshore sand tossed up by storms. Sabkha commonly demonstrate chicken wire structure, elongate anhydrite clumps separated by strings of carbonate or siliclastic mud. In the other hand, in the study area, the basin is Sabkha model which is connected by tidal basin and then because of the sand dunes (like a bar) and prevent the return of water. Basin compounds concentrated and after evaporating in the study area are formed evaporites (Figure 12).

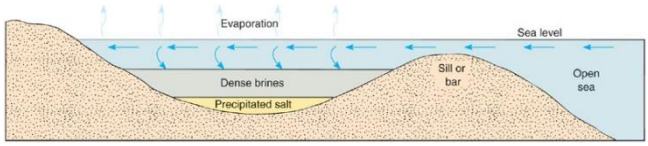

Figure 12. Cross-sectional diagram of a barred basin, illustrating the deposition of evaporates (Depositional model suggested).

Conclusions

The effects of the elements can be shown as a numeric value and adaptive coefficient. This amount is always between -1 and +1. In the event that exists positive linear correlation between the two elements, this factor is +1 and in the case of a negative linear relationship exists, this amount is -1 and the relationship between the elements is determined by the numeric value of zero. On the other hand, these factors, meaning that at specified confidence level. The results of these studies (Dendritic) in the study area, shows three groups of elements. The first group: includes elements Na and Cl are highly correlated together and B with lower relationship the origin of this group is within the basin (inner Basin). The second group: includes elements SiO_2, Al_2O_3 and MgO are highly correlated together the origin of this group is Geogenic and by rivers or wind (erosion rocks) have been imported into the basin.The third group: includes elements Fe_2O_3, SO_3, K, B and CaO are highly correlated with each other the origin of this group is Biological origin and due to environmental pollution. Of course, Ceo_2 combined with high difference between the second

and third groups are linked and also Zro_2 combined with more distance associated with the second and third groups. In the study area, the basin is Sabkha model which is connected by tidal basin and then because of the sand dunes (like a bar) and prevent the return of water. Basin compounds concentrated and after evaporating in the study area are formed evaporites. The evaporative crystallization of minerals in accordance with the results of chemical analysis that is show initially carbonates (including $CaCO_3$, Ca SO_4) then chloride (NaCl includes a solid solution with chloride, KCl, $MgCl_2$, B and Mg) and sulfates (including $MgSO_4$, KCl $MgCl_2$ $+6H_2O$) formed are. Therefore, the necessary conditions for the formation of three groups of evaporite minerals (including chloride, sulfates and carbonate) are available in the study area. But according to the elements Na and Cl, the necessary conditions for the formation of chlorides (especially halite) is much better than in the studied area.

References

[1] Boggs, S., (2006), Principles of Sedimentology and Stratigraphy (4th ed.), Pearson Prentice Hall, Upper Saddle River, NJ, 662p

[2] Aharonson O., et al., (2009), An asymmetric distribution of lakes on Titan as a possible consequence of orbital forcing. Nature Geoscience 2:851–854. Doi: 10.1038/ngeo698.

[3] Adabi, M.H. and Asadi Mehmandosti, E., (2008), Microfacies and geochemistry of the Ilam Formation in the Tang-e- Rashid area, Izeh, Journal of Asian Earth Sciences, V.33, 267-277pp.

[4] Aghanabathi, A., (2010), Geology of Iran, The Geological Survey of Iran, Third Edition, 586p.

[5] Alsharhan, A.S. and Kendall, C.G.St.C, (2008), Holocene coastal carbonates evaporate of the Southern Arabian Gulf and their ancient analogues, earth Science Reviews, V.61, Issues 3-4, 191-143pp.

[6] Ahrari Roudi, M.; Moussavi-Harami, R.; Lak, R.; Mohboubi, A. and Motamed, A., (2012), Using of Ground Penetrating Radar (GPR) AND Sediment Cores As Method Interpretation os Sedimentary Environments the Estuaries of North west oman Sea, Research Journal of Environmental and Earth Sciences, V.4, 500-510pp.

[7] Burwash, R.A., Kupricka, J. and Wijbrans, J.R., (2000), Metamorphic evolution of the Precambrian basement of Alberta; Canadian Mineralogist, v. 38, 423–434pp.

[8] Blatt, H., Middleton, G. and Murray, R.., (1980), Origin of sedimentary rocks, Prentice Hall PUB.Co., 780P.

[9] Barnes J.W., et al., (2011), Organic sedimentary deposits in Titan's dry lakebeds: Probable evaporite.216:136–140.

[10] Tucker, M.E., (1986), Sedimentary Petrology, An Introduction, 5th Ed.

[11] Pettijohn, F.J., (1975), Sedimemtary rocks, Harper Pub. Co., New York, p.434-441

[12] Milner, H.B., (1962), Sedimentary Petrography, Vol. 1, 2nd Ed., The Mac Mollan Co., 643p.

[13] Rahimpour-Bonab, H. and Kalantarzadeh, z., (2005), Origik of secondry Potash deposits:Acase from Miocene evaporates of Central Iran, Journal.ofAsian Erath Sciences,v.25, 157 – 166pp.

[14] Malaska M.J., Hodyss R., (2014), Dissolution of benzene, naphthalene, and biphenyl in a simulated Titan Lake 242:74–81.

[15] Pararas-Garayannis, G., (2006), Potential of tsunami generation along the markan subduction zone in the northern Arabian sea. Case study: the earthquake and tsunami of November 28 1945, Presentation at 3 Tsunami Symposium of Tsunami Society.

[16] Leeder, M.R., (1982), Sedimentary, Process and Products, Umwin, Hymna Pub. Co., 344p.

[17] Jacob, K, H, and Quittmeyer, R.C., (1979), The Markan region of Pakistan and Iran are system with active plate subduction. Geodynamics of Pakistan, 305-318pp.
Doi: 10.1016/j.icarus.2014.07.022.

[18] Edvards, A.C., (2001), Grain size and sorting in modern sands. Jornal of Coastral Research, Vol. 17 (1), 38-52pp.

[19] Warren, J. K., (1999). Evaporites, their evolution and economics, Blackwell, 438p.

[20] Dean, W.E. and Schreiber, B.C, (1978), Marine evaporates, lecture notes for short course, No.4, soc. econ. paleont. Mineral. 188P.

[21] Chan, L.H., Starinsky, A. and Katz, A., (2002), the behavior of Li and its isotopes in oilfield brines; Geochimica ET Cosmochimica Acta, v. 66, no. 4, 615–623pp.

[22] Al-Farraj, A., (2005). An evolutionary model for sabkha development on the north coast of the UAE, Journal of Arid Environments, v. 63, 740p.
Doi: 10.1016/j.icarus.2011.08.022.

[23] Sharma, G.S., (1978), Upwelling off the southwest coast of India, Indian Journal of Marine Science, V.78-19

[24] Renyuan Li, Wenbin Wang, Yifeng. Peng Wang, (2024), Advanced Material Design and Engineering for Water-Based Evaporative Shi, Chang-ting Wang cooling, Vol. 36, Issue12, Hygroscopic Materials, https://doi.org/10.1002/adma.202209460

INTERNATIONAL JOURNAL OF
COASTAL, OFFSHORE & ENVIRONMENTAL ENGINEERING IJCOE Vol.9/No. 2/Spring 2024(62-70)

Available online at: www. Ijcoe.org

Numerical simulation of flow for the improvement of the access channel to the port of Quila (Barranguila) in Colombia by using T form Groyne structure

Mehdi Nezhadnaderi[1], Kiyanoosh Guilaninezhad [2], Mohammad Hossein Vafaee[3], Babak Pordel Maragheh [4], Babak Fazli Malidareh[5], Ali Sheykhbahaei[6], Abolfazl Bagheri[7] and Seyed Mohammad Mousavi[8]

[1] Department of Civil Engineering, Tonekabon Branch, Islamic Azad University, Tonekabon, Iran. (Corresponding Author). mehdi2930@yahoo.com.
[2]Department of Civil Engineering, Tonekabon Branch, Islamic Azad University, Tonekabon, Iran. saman.mohareri@yahoo.com
[3] Assistant Professor, Department of Civil Engineering, Pooyesh Instituteof Higher Education, Qom.Iran. M.h.vafaee2024@gmail.com
[4] Department of Civil Engineering, Ardabil Branch, Islamic Azad University, Ardabil, Iran. civil_babak2005@yahoo.com
[5] Department of Civil Engineering, Babol Branch, Islamic Azad University, Babol, Iran. Fazli.babak@babolia.ac.ir
[6] PhD Candidate in Physical Oceanography at university of Hormozgan/ Iranian National Institute for Oceanography and Atomospheric science, Ali.sheykhbahaei@inio.ac.ir
[7] Department of Civil Engineering, Tonekabon Branch, Islamic Azad University, Tonekabon, Iran. Abolfazl.Bagheri@yahoo.com
[8] Department of Civil Engineering, Tonekabon Branch, Islamic Azad University, Tonekabon, Iran. Mosavi.622@gmail.com

ARTICLE INFO

Article History:
Received: 29 Oct. 2023
Accepted: 13 April 2024

Keywords:
T form Groyne
Flow pattern
Secondary currents
90 Degree bend

ABSTRACT

Barranguila is located on the left bank of the Magdalena River, about 22 km from the outskirts of the mouth. The river flows in the direction of the north to the Caribbean. Measures were taken to create a duct with a width of 150 meters and a depth of 9.2 meters in the river. In this research, the factors affecting the sedimentation and erosion process in terms of structural modifications in the access channel were investigated using numerical methods. In the present study, the numerical results of the effect of non-volumetric spray drift with 90^0 T-shaped spray guns, relative to the external wall of an arch with a length of 15 channel width, on the average velocity distribution and shear stress in a 90^0 gentle arch with a ratio of **R**/**B** = 4, 0.7 m wide and 0.14 m water depth. The results of the study showed that the presence of a spur gear causes uniformity of upstream velocity and high-speed transmission from the outer wall to the middle of the canal to the inner wall. The shear stress of the bed is increased due to the presence of a spray gun but has little effect on the location of the shear stress incidence. As it can be seen, the negative pressure in the outer arc is increased and in the external arc exposed to erosion due to the high forces caused by positive pressure, the reduction of the Groyne is reduced and the conditions for the stabilization of the bed are provided. As can be seen, in the inner arc, after the construction of a Groyne, a negative pressure increases as well, and the ability to precipitate in this area also increases.

1. Introduction

The changes in the bed and banks in the river bend are of great importance from the point of view of morphology and river engineering. One way to stabilize the external bend is to use breakwater structures. The port of Barranquilla is located on the left bank of the Magdalena River, approximately 22 km upstream of its mouth. The river flows in a near-north direction and empties into the Caribbean Sea. Until 1972, the river had only one access channel for navigation, and it accepted vessels with a draft of up to 10 m. From 1970 onwards, adverse morphological changes forced the government to carry out emergency dredging operations. In 1986, the Ministry of Public Works signed a contract with the University of the North and the Hydraulic Laboratory of Las Flores to study the problem and design corrective measures. The project aimed to design arrangements for the creation of a channel 150 m wide and 2.9 m deep. In 1987, a team of engineers from Haskoning and the Delft Hydraulic Institute of the Netherlands joined the Colombian team. Several solutions were identified, such as constructing a non-permeable guide dam, a sand dam, and difficult spots in the river, and removing the recently created fill area. In this research, the factors affecting scour in the conditions of corrective structures in the desired access channel will be investigated using a numerical method.

Breakwaters are usually constructed to protect shores or to provide sufficient depth for navigation purposes. Known by names such as epis, groynes, and cross arms, these structures can be grouped by their shape, such as T-shaped or L-shaped.

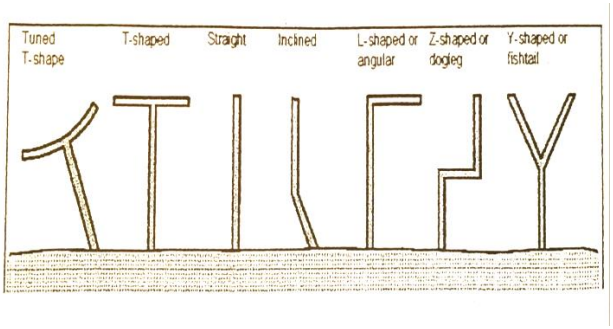

Figure 1 - Types of breakwaters that so far have been built

The most important parameters that should be considered in the design of breakwaters are: breakwater design plan, breakwater length, distance between breakwaters, orientation with the flow path, crest height, slope of the bank, materials used in the breakwater section.

- **Breakwater length**

The length used for the breakwater is usually calculated in the intervals between the committee rate and the maximum flow depth and is usually about a quarter of the average width of the desired bank.

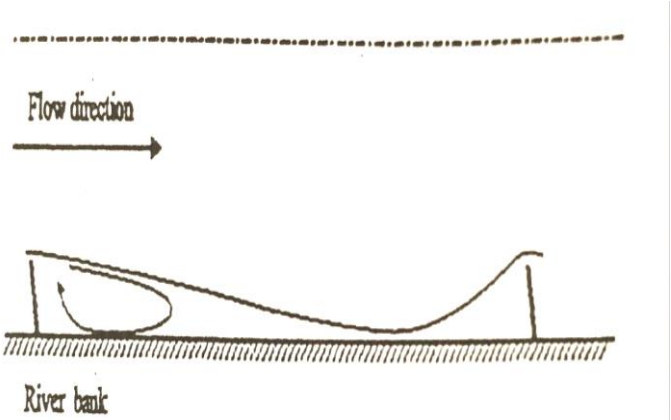

Figure 2- Flow pattern in the field of breakwaters with very small aspect ratio.

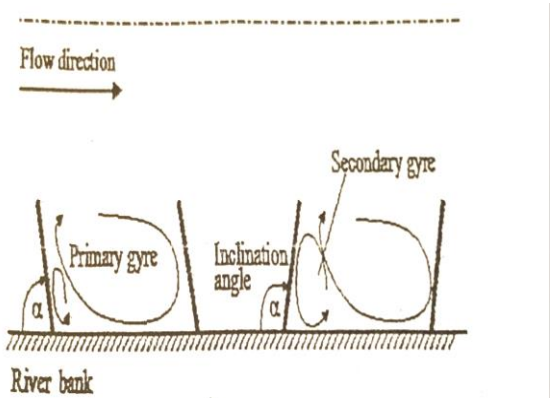

Figure 3- View of breakwaters with different angles and how the flow moves in their area.

In 2013, Div Salar and Mousavi Jahromi studied the effect of increasing the wing length of an L-shaped breakwater on the scour around it in a 90-degree arc.

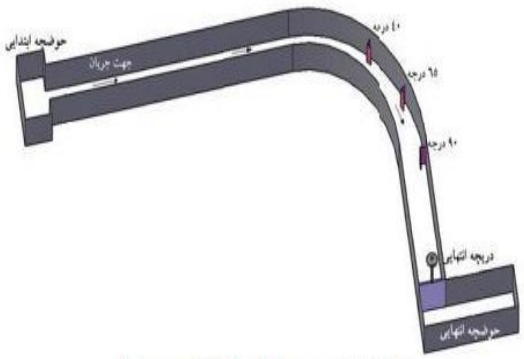

Figure 4- Schematic of the laboratory flume used (Divsalar and Mousavi Jahromi, 2013).

Figure 5- Schematic of the laboratory flume used and the used sluice gate samples (Divsalar and Mousavi Jahromi, 2013).

Figure 6- Example of the experiment (Sluice gate L with wing size 10.5 cm, Q=4.25 liters per second and φ=90 degrees of bed before and after scouring (Divsalar and Mousavi Jahromi, 2013).

In 2009, Vaghefi et al. studied the temporal changes in scour around a T-shaped breakwater in a 90-degree arc.

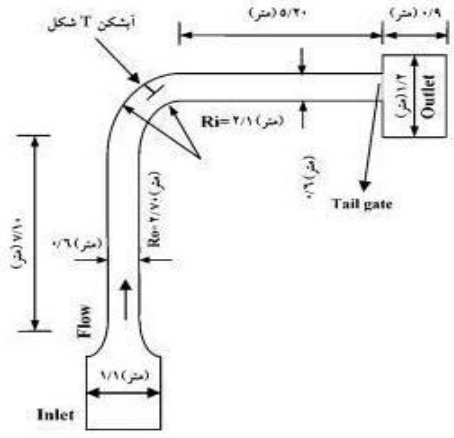

Figure 7- Laboratory sciences used by Vaghefi et al. 2009

In 2015, Vaghefi et al. studied the effect of supporting structures on the flow pattern around T-shaped sluice gates in a 90-degree bend.

In 2015, Vaghefi et al. studied a laboratory study of turbulent flow in a 180-degree bend.

In 2012, Mehrnahad and Ghodsian studied the effect of the parameters of sluice gate length and material diameter on scour around a T-shaped sluice gate located in a 90-degree bend.

In 2009, Ghodsian and Vaghefi studied a laboratory study of scour and flow around a T-shaped sluice gate in a 90-degree bend. Experimental research was conducted to investigate the bed in the bend and its protection using gravel. The experiments were conducted in a 90-degree bend with sediments with an average diameter of 0.34 and 1.18 mm. The results of this study show that the water mainly occurs in the outer arc of 90 degrees of horizontal maximum sedimentation and sedimentation occurs around 30 degrees of the middle section near the concave and convex part. During the downflow, the scour depth increases near the concave bank and its maximum value increases around the 30 degrees section. At further downstream, the scour depth decreases along the section. On the other hand, sedimentation occurs near the lower part of the convex channel from 20 degrees to 60 degrees. There is a transverse slope of the water surface within the section with a higher surface on the concave side. As a result of this transverse slope, the bottom water moves from the concave bank towards the convex focus while the surface water moves from the convex to the section.

In 2012, Vaghefi et al. studied the effect of Froude number on scour around a T-shaped weir in a 90-degree bend. This paper presents the results of experiments on scour around a T-shaped weir located in a 90-degree bend. The effect of the tooth length on the scour rate is investigated. The experiments are repeated in a rectangular channel. The results show that with increasing weir length, the maximum scour depth and the volume and dimensions of the scour hole increase. The location of the maximum scour depth occurs at a distance of about 10 to 20% of the length of the ponds upstream.

In 2009, Hosseini et al. conducted a field study of the condition of water structures in the Ghezel Ozan River [7].

Field visits to the project area show that the agricultural lands on the left bank have been restored and are well cultivated. Therefore, it was suggested that the structures be reviewed to continue protecting the lands in the critical area mentioned. It was also recommended that necessary measures be taken to strengthen the bodies of the apiaries located in the meanders of the arteries in order to prevent serious damage to these structures during floods. It was recommended that the number of river arteries and their meandering nature be examined in the management plans and that a final decision be made based on the morphology of the river. The use of a system of breakwaters and longitudinal embankments to control the river, prevent erosion of the banks, and restore new lands is recommended as a suitable model for managing rivers.

Using the results of field visits and technical and structural assessments of the reorganization plans can be very useful in identifying and reconstructing critical areas and damaged structures, improving the efficiency of the studied plan, and making future plans more effective. Therefore, it is suggested that the executive authorities pay special attention to this issue.

Figure 9- View of a constructed spillway in the Qezel Ozen-Qowijan River

Elyasi et al. (2011), using Flow3D software and applying the RNG k-ε turbulence model, simulated the flow pattern around a single submerged spillway in a straight inclined channel without considering the free surface and compared the results of the numerical model with experimental data. The results of this simulation, without considering the free surface, showed a good agreement with the experimental data. Comparison of the velocity profiles in the numerical model and the experimental results indicates the agreement of these data.

Mosteh and Atma (2004) investigated the effect of spillway length on the circulation zone behind the spillway by considering the scale effect with the Fluent software.

Shahrokhi (2008) prepared a numerical model of the flow pattern around a weir using Fluent software and applied different turbulence models to study the effect of these models on the length of the flow separation zone behind a weir. The most important result of this research shows that the LES turbulence model has the best agreement with the experimental results and this model provides a better prediction of the length of the separation zone behind the weir. Finally, it was suggested that the model be implemented in a wider range of changes in flow parameters, length and angle of installation of the weir.

Akhirya et al. (2011) conducted a numerical simulation of the hydraulic flow and sediment transport around various weirs. The modeling results showed that among the turbulence models, the RNG k-ε and k-ε models were closer to the experimental data, but the RNG k-ε turbulence model showed the best results for simulating the flow field around the weir.

Abbasi-Chenari et al. (2011) simulated the flow pattern around L-shaped breakwaters perpendicular to the shore using the Fluent software and the k-ε turbulence model. In this study, the L-shaped breakwater was impermeable and was placed non-submerged at 5 different angles of the river curve. The results indicate that the flow turbulence, the maximum velocity range, and ultimately the highest bed scouring occur at the breakwater tip. Also, with increasing discharge and Froude number, the maximum flow velocity range near the breakwater tip increases and its shape is stretched in the flow direction. Finally, it was concluded that the k-ε turbulence model has good accuracy in simulating the backflow areas downstream of the breakwater and the location of eddies and flow turbulence around the breakwater.

Ghanadan et al. (2012) numerically simulated the flow over a wide-edge lateral spillway using Fluent software and compared the results obtained from this software with experimental data. The results showed that among the turbulence models available in the software, the RNG k–ε turbulence model has a higher accuracy for simulating the flow over a lateral spillway. Also, using the calibrated model, the effect of changing the height and width of the spillway crest on the discharge passing through the spillway was investigated. Accordingly, it was concluded that the height of the wide-edge lateral spillway crest is more effective on the discharge value of the spillway outlet than the crest width.

2. Methods

The port of Barranquilla is located on the left bank of the Magdalena River, approximately 22 km upstream of its mouth. The river flows in a northerly direction and empties into the Caribbean Sea. Until 1972, the river had only one navigable channel, admitting vessels with a draft of up to 10 m. Since 1970, adverse morphological changes have forced the government to undertake emergency dredging operations. In 1986, the Ministry of Public Works signed a contract with the University of the North and the Las Flores Hydraulic Laboratory to study the problem and design corrective measures. The project aimed to design arrangements for the creation of a channel 150 m wide and 2.9 m deep. In 1987, a team of engineers from Haskoning and the Delft Hydraulic Institute in the Netherlands joined the Colombian team. Several solutions were identified, such as the construction of the Natrava guide dam, a sand dam, and the removal of the recently created embankment. In this study, the factors affecting scour in the conditions of corrective structures in the desired access channel will be investigated using a numerical method. The figures below show the location of the Magdalena River in Colombia.

Figure 10 - Location of the Magdalena River and the port of Barranquilla in Colombia

Figure 11 - Location of protective structures at the beginning of the access channel to the Barranquilla port in Colombia

Figure 12 - Location of the Magdalena River and the port of Barranquilla in Colombia

Figure 13- Location of the Magdalena River and the port of Barranquilla in Colombia

To solve the flow using computational fluid dynamics, the following steps must be performed (Shojaifard and Noorpour Hashtroodi, 1995):

- Selecting the Gambit model to create the geometry
- Selecting the computational model
- Selecting the calculation solution method in the model
- Selecting the basic equations to solve
- Determining the physical characteristics of the materials
- Determining the boundary conditions
- Specifying the problem solving parameters
- Making an initial guess in the entire solution field
- Performing the solution and outputting the calculations.

3. Results and Discussions

In this study, Gambit software version 3.3.2 was used to generate the geometry and mesh it. The mesh pattern was Quad element and map type was used for the surfaces. The existing boundary conditions are velocity input from the left side from the top of the arc and pressure output boundary condition at the bottom of the arc outlet. The simulation results from Fluent software are seen in Figures 14 to 22.

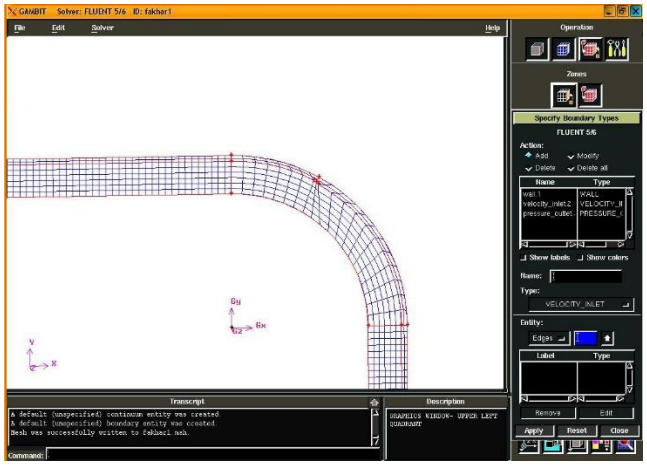

Figure 14 - Mesh pattern in the arch in the presence of a T-shaped breakwater with a length of 15% of the channel width at an angle of 30 degrees to the y-axis.

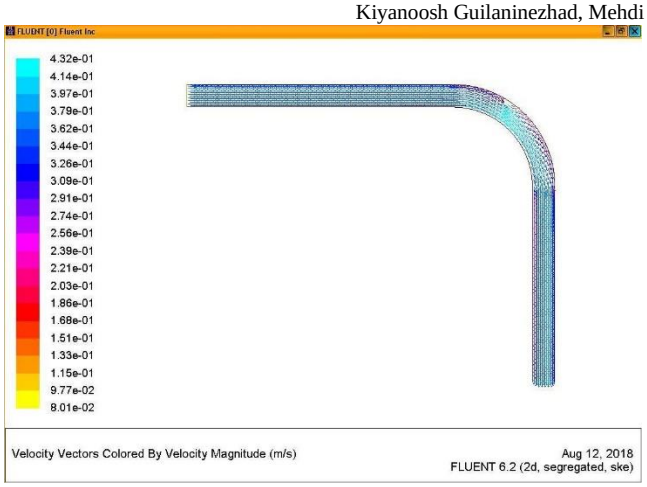

Figure 15- Average velocity distribution pattern in the curve in the presence of a T-shaped breakwater with a length of 15% of the channel width at an angle of 30 degrees to the y-axis.

As can be seen, the velocity in the inner arch increases, and in the outer arch, which has been subject to erosion due to high forces resulting from positive pressure, it decreases with the construction of the breakwater, and conditions are created for bed stabilization.

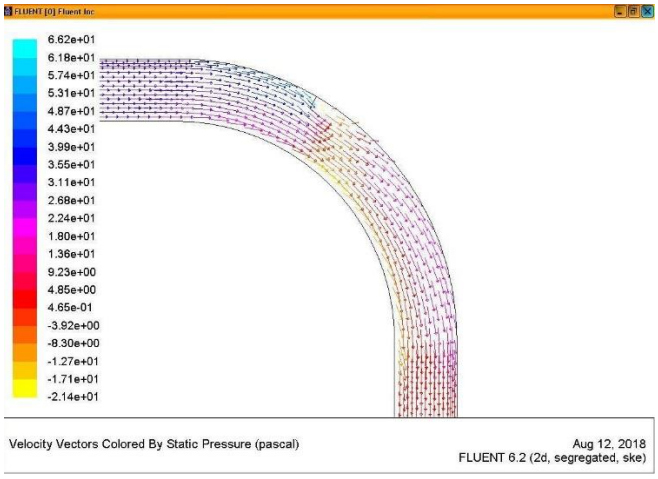

Figure 16 - Pressure distribution pattern in the arch in the presence of a T-shaped breakwater with a length of 15% of the channel width at an angle of 30 degrees to the y-axis.

As can be seen, the negative pressure in the outer arch increases, and in the outer arch, which was exposed to erosion due to high forces caused by positive pressure, it decreases with the construction of the breakwater, and conditions are provided for bed stabilization. As can be seen, the negative pressure in the inner arch also increases after the construction of the breakwater, which also increases the ability to deposit sediment in this area.

Figure 17 - Mesh pattern in the arch in the presence of a T-shaped weir with a length of 15% of the channel width at an angle of 45 degrees to the y-axis.

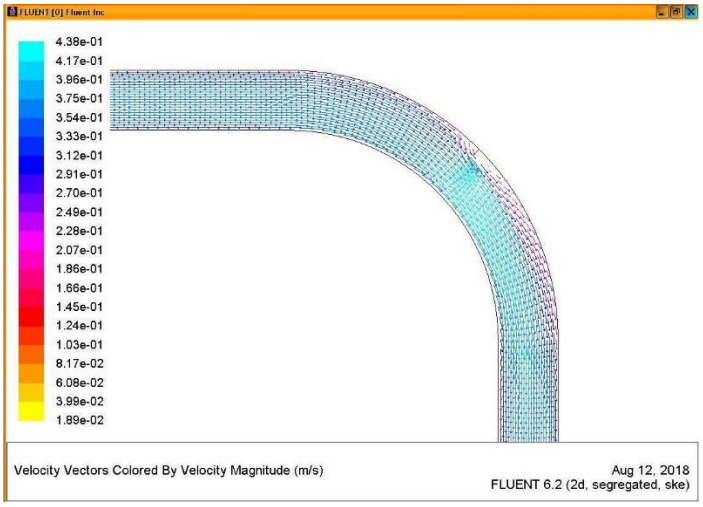

Figure 18 - Velocity distribution pattern in the curve in the presence of a T-shaped breakwater with a length of 15% of the channel width at an angle of 45 degrees to the y-axis.

As can be seen, the velocity in the inner arch increases, and in the outer arch, which has been subject to erosion due to high forces resulting from positive pressure, it decreases with the construction of the breakwater, and conditions are created for bed stabilization.

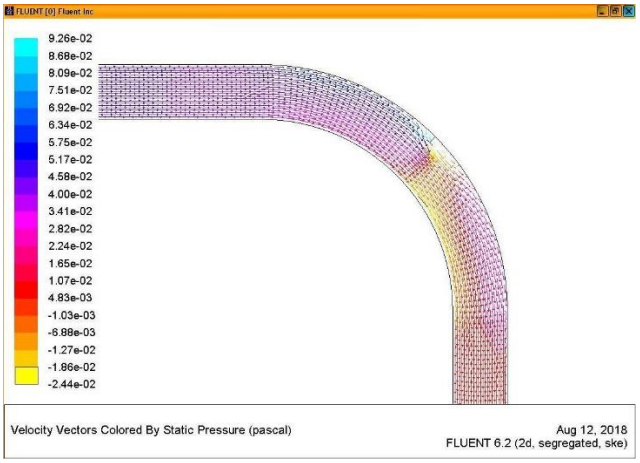

Figure 19- Pressure distribution pattern in the arch in the presence of a T-shaped breakwater with a length of 15% of the channel width at an angle of 45 degrees to the y-axis.

As can be seen, the negative pressure in the outer arch increases and in the outer arch part that has been exposed to erosion due to high forces caused by positive pressure, it decreases with the construction of the breakwater and conditions are provided for bed stabilization. As can be seen, the negative pressure in the inner arch also increases after the construction of the breakwater, which also increases the sedimentation ability in this area.

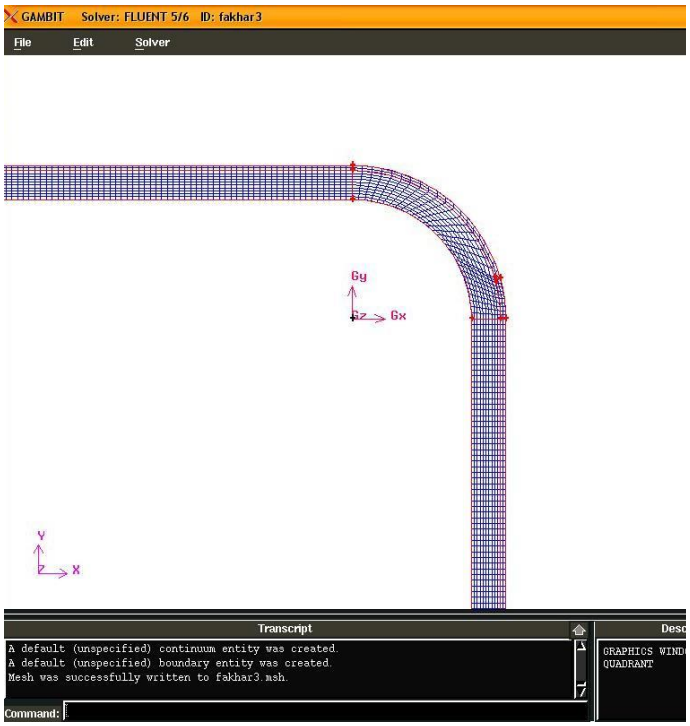

Figure 20 - Pressure distribution pattern in the arch in the presence of a T-shaped breakwater with a length of 15% of the channel width at an angle of 75 degrees to the y-axis.

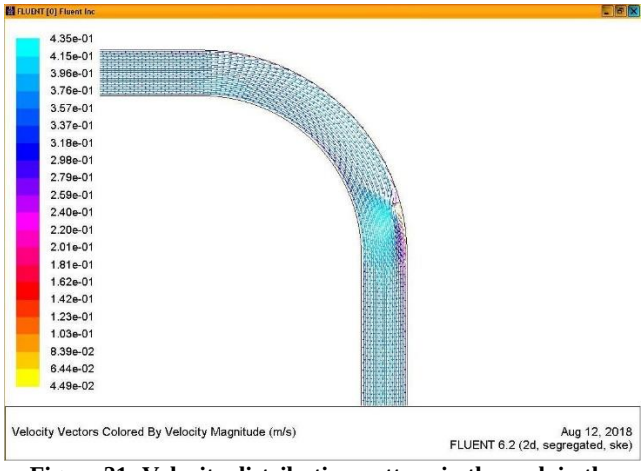

Figure 21- Velocity distribution pattern in the arch in the presence of a T-shaped breakwater with a length of 15% of the channel width at an angle of 75 degrees to the y-axis.

As can be seen, the negative pressure in the outer arch increases and in the outer arch part that has been exposed to erosion due to high forces caused by positive pressure, it decreases with the construction of the breakwater and conditions are provided for bed stabilization. As can be seen, the negative pressure in the inner arch also increases after the construction of the breakwater, which also increases the sedimentation ability in this area.

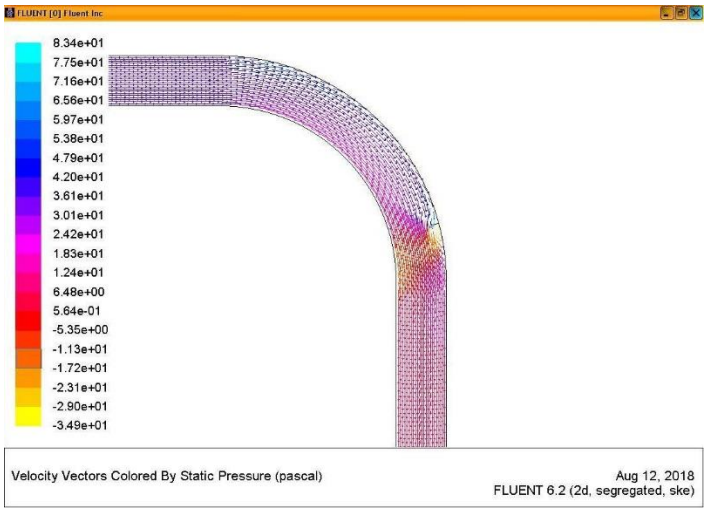

Figure 22- Pressure distribution pattern in the arch in the presence of a T-shaped breakwater with a length of 15% of the channel width at an angle of 75 degrees to the y-axis.

As can be seen, the negative pressure in the outer arch increases and in the outer arch part that has been exposed to erosion due to high forces caused by positive pressure, it decreases with the construction of the breakwater and conditions are provided for bed stabilization. As can be seen, the negative pressure in the inner arch also increases after the construction of the breakwater, which also increases the sedimentation ability in this area.

4. Conclusions

The aim of the present study is to investigate the effect of the presence of a breakwater in the arch on the flow pattern. For this purpose, the data obtained from the two-dimensional velocity acquisition were analyzed. The overall results of this numerical study can be stated as follows: the velocity distribution pattern in the arch indicates the concentration of areas with maximum velocity downstream of the arch and in the vicinity of the outer wall, which indicates the importance of protecting these areas by breakwaters. The use of breakwaters has made the velocity distribution upstream of the breakwater uniform, and also caused the high-velocity area to be transferred to the middle of the channel and the inner wall, but the placement of the breakwater increases the flow velocity in the channel compared to the case of the arch without breakwaters. According to the results in both cases, the main cause of erosion of the outer bank of the arch is the concentration of high-velocity areas in the final third of the arch, which, as can be seen, the placement of the breakwater has effectively prevented the formation of these areas. The speed in the vicinity of the outer bank of the arch is greatly reduced and the placement of the

breakwater causes the dispersion and transfer of the high-speed zone from the outer wall to the middle of the channel and the inner bank. According to Figures 15 to 22, the speed changes in the vicinity of the breakwater noses change rapidly and high speeds are located a short distance from the breakwater noses. This shows that protecting the breakwater noses is inevitable to maintain the stability of the breakwater structure.

According to the velocity distributions presented in Figures 15 to 22, in this case, high-velocity zones dominate over a large area of the arch near the inner wall. Figures 15 to 22 represent the average velocity distribution in the arch in the presence of a breakwater with a length of 15% of the channel width. Considering the shape of the T-shaped breakwaters, they also protect it by moving high-velocity layers away from the outer wall of the arch.

5. References

1. Ghodsian, M., & Vaghefi, M. (2009). Experimental study on scour and flow field in a scour hole around a T-shaped spur dike in a 90° bend. Int. J. Sediment. Res. 24(2): 145-158.
2. Tang, X. L., Chen, Z. C., & Yang, F. (2006). Dynamic large eddy simulation of secondary flow near a groyne. Int. J. Nonlinear. Sci. and Num. Simul. 7(3): 257-262.
3. Vaghefi, M., Akbari, M., & Fiouz, A. R.. (2015). An experimental study of mean and turbulent flow in a 180degree sharp open channel bend: secondary flow and bed shear stress. KSCE J. Civil. Eng. 20 (4):1582-1593.
4. Vaghefi, M., Ghodsian, M., & Adib, A. (2012). Experimental study on the effect of Froude Number on temporal variation of scour around a T-shaped spur dike in a 90 degree bend. App. Mech. and Material 147: 75-79.
5. Vaghefi, M., Ghodsian, M., & Salehi Neyshaboori, S. A. A. (2009). Experimental study on the effect of a T-shaped spur dike length on scour in a 90 degree cannel bend. Arab. J. Sci. and Eng. 34(2B): 337-348.
6. Vaghefi, M., Ghodsian, M., & Salehi Neyshaboori, S. A. A. (2012). Experimental study on scour around a T-Shaped spur dike in a channel bend. J. Hydraul. Eng. 138(5): 471-474.
7. Ahmad, M. (1951). Spacing and protection of spurs for bank protection. Civil Eng. and Public. Rev. 46: 3-7.
8. Vaghefi, M., Mohsenimehr, V. A., & Akbari, M. (2014). Numerical investigation of wing to web length ratios parameter of T-shaped spur dike in a 90 degree bend on scour pattern. J. River. Eng. 2(3): 45-52.
9. Vaghefi, M., Safarpoor, Y., & Hashemi, S. S. (2015). Effects of relative curvature on the scour pattern in a 90° bend with a T-shaped spur dike using a numerical method. Int. J. River. Basin. Manag. 13(4): 501-514.
10. Vaghefi, M., Shakerdargah, M., & Akbari, M. (2014). Numerical investigation of the effect of Froude number on flow pattern around a submerged T-shaped spur dike in a 90° bend. Turk. J. Eng. and Env. Sci. 38(2): 266-277.
11. Yang, S. Q. (2005). Interactions of boundary shear stress, secondary currents and velocity. Fluid. Dynamic. Res. 36: 121-136.
12. Shojaifard, M.J. & Noorpar Hashtroudi, A. S. (translators). 2000. Versteeg, H.K. & Mallalaskara, (1995). Introduction to Computational Fluid Dynamics", Iran University of Science and Technology Publications, Tehran.
13. Div Salar, A., & Mousavi Jahromi, H. (2014). Study of the effect of increasing the wing length of an L-shaped gully on the scour around it in a 90-degree bend. Scientific and Research Journal of Irrigation Sciences and Engineering, 37(3), Pages 53-61.
14. Vaghefi, M., Ghodsian, M. & Salehi Neyshaburi, A. (2009). Study of temporal changes in scour around a T-shaped gully in a

90-degree bend. Journal of Water and Soil Conservation Research, 16(1).

15. Mehrnohad, A., & Ghodsian, M. (2012). Laboratory study of the effect of gully length and material diameter parameters on scour around a T-shaped gully located in a 90-degree bend, Scientific and Research Journal of Iranian Water Resources Research, 8(8).